UNIVERSITY OF LONDON

IMPERIAL COLLEGE OF SCIENCE, TECHNOLOGY AND MEDICINE

Department of Physics

Optics Section

MULTIPHOTON PROCESSES IN INTENSE LASER FIELDS

by

Rajeshree Bhatt

A thesis submitted for the degree of Doctor of Philosophy of the University of London and for the Diploma of Membership of the Imperial College of Science, Technology and Medicine.

August 1989

To my parents, family and Simon

ABSTRACT

This thesis examines two aspects of the interaction of intense laser radiation with matter: the potential scattering of electrons in the presence of a laser field and the photodecay of atomic or ionic bound states.

We present an exact numerical calculation of the potential scattering of electrons in a laser field in one dimension, which is valid at all intensities and frequencies, using the Kramers–Henneberger (KH) transformation to calculate the reflection and transmission coefficients. In the KH reference frame, the simultaneous effect of the potential and laser field on the electron can be described by a static potential 'dressed' by time–dependent components. For the model potential chosen, the number of bound states of the static potential is shown to increase with the laser parameter α_0 which is proportional to the square root of the intensity and inversely proportional to the square of the frequency. The exact results show evidence of resonances caused by these new bound states. We compare the results of the exact calculations with those obtained using an approximation scheme suggested by Gavrila and Kaminski and discuss the validity of this approximation.

We also study the decay of atomic or ionic bound states to a structured continuum of states by means of photon absorption, and examine the modifications to the traditional description of the decay process brought about by the threshold of the continuum. Exact numerical results for the energy spectrum and the time–evolution of the bound state population show that under strong field conditions, the decay of the bound state is incomplete. This effect is interpreted both in terms of the exact eigenstates of the whole system and, by diagonalising only the sub–system of the bound states, in terms of the dressed states. It is found that the decay of the lower bound state is suppressed when the separation of the dressed states causes the energy of the lower state to move below that of the threshold.

ACKNOWLEDGMENTS

I am pleased finally to be in a position to acknowledge all the help, support and guidance I have received from my college supervisor Professor P. L. Knight. I am greatly indebted to Dr. B. Piraux, with whom I had a close and fruitful collaboration. I would also like to thank my CASE supervisor, Dr. P. T. Greenland for his contributions, Dr. K. Burnett for valuable discussions, Dr. M. A. Lauder and Dr. F. A. M. de Oliveira for advice on various computing matters and Mr. I. McCoy for assisting in the preparation of this thesis. I am grateful to all the friends I have made at Imperial College who have made my years there so enjoyable. My special thanks are due to Dr. S. Buckle for his support and encouragement.

Finally I would like to thank the S.E.R.C. and the United Kingdom Atomic Energy Authority, Harwell for the provision of a CASE studentship.

CONTENTS

CHAPTER 1

INTRODUCTION

In this thesis, we are concerned with the interaction of atoms and electrons with intense radiation e.g. that from a laser. Specifically, we present a theoretical and computational analysis of two types of processes:

(i) the laser–assisted scattering of an electron by a potential schematically representing an atom. The presence of the potential allows the electron to absorb and emit photons, leading to significant modifications to the radiation–less scattering behaviour. Many approximation schemes have been devised to calculate the modified scattering cross–sections, but these are inadequate for high laser frequencies and intensities. We present exact numerical results for a one–dimensional model over a wide range of laser frequencies and intensities.

(ii) the decay of atomic or negative ionic bound states due to photon absorption. We focus on the deviations from the exponential decay law which occur at high intensities when effects due to the lower bound, or threshold, of the photoelectron continuum become important. Exact numerical results for the energy spectrum of the photoelectron and the time–evolution of the bound state population are presented.

§1.1 *Thesis Plan*

Section 1.2 sets the scene for the detailed calculations which follow by describing the various intensity regimes which determine the nature of the effects of

the radiation–matter interaction and by linking these to some of the theoretical approaches and key experimental results in this area.

In Chapter 2, we examine the properties of the Kramers–Henneberger[1] [2] transformation which we shall use to solve the scattering problem discussed in Chapter 3. The transformation introduces a new reference frame oscillating at the same frequency as the incident radiation field. Applying this transformation to the problem of interest for us, the Hamiltonian for an electron moving in a model one–dimensional potential in the presence of a laser field, we find that the combined effect on the electron is equivalent to a different static potential dressed by time–dependent components. We show that the static potential can support more bound states than the original unperturbed potential and discuss the implications of these new states.

In Chapter 3, building on the foundations laid in Chapter 2, we consider the scattering of an electron in such a model. Gavrila and Kaminski[3] have developed a scheme in which the static potential is treated exactly and the time–dependent components are treated as perturbations. This treatment is not adequate under all conditions: it is a high frequency approximation. We solve the one dimensional problem exactly and find indications that the new bound states discussed in Chapter 2 appear as resonances in the transmission and reflection coefficients which are the one–dimensional analogues of the scattering cross–section. As a comparison, we also solve the problem using the Gavrila–Kaminski approximation and discuss the validity of their scheme in the light of our exact results.

In Chapter 4, we change direction and consider the coupling by a laser field of a bound atomic state to a continuum of states via an intermediate bound state. The continuum extends to infinity in one direction only and the intermediate bound state

is assumed to lie close to its lower limit, thereby introducing threshold effects. This models the photo–ionisation of an atom, although the exclusion of Rydberg states makes it more suitable as a description of the photo–detachment of a negative ion. The problem is analysed using three different methods, each highlighting a particular aspect of the threshold effects.

In Chapter 5, we summarise the main conclusions from this work and make suggestions for further work.

§*1.1.1 Labelling convention*

Within each chapter, equations are labelled first by chapter number and then by equation number. Figures are labelled similarly first by chapter number and then by figure number. For referring to an equation or figure, the chapter number is only used if the equation or figure lies in a different chapter; otherwise only the equation or figure number is used. Appendices follow the relevant chapter as does the list of references. Equations in appendices are labelled by the appendix letter suffixed by the equation number and are always referred to by the whole label.

§*1.2 Background*

The interaction between atoms and intense radiation at optical frequencies has been studied extensively since the early sixties, when it was given impetus by the development of the laser. The signature of the high intensity field is the occurrence of induced multiphoton transitions between some (as yet unspecified) initial and final states. These transitions fall into three categories: bound–bound, bound–free and free–free transitions, although these are not mutually exclusive in that the transition

between given initial and final states could involve intermediate transitions of more than one kind.

In Fig 1 we illustrate typical levels of laser intensity at which various effects come into play. Bound–bound transitions and bound–free transitions (photo –ionisation) may, however, be observed at lower intensities than those shown on the diagram, while a combination of the two resulting in resonantly enhanced multiphoton ionisation may be observed starting at around 10^9 W/cm^2. Above Threshold Ionisation (ATI) which involves transitions between continuum states of the atom is only seen to occur at intensities of around 10^{12} W/cm^2 or higher at optical or infra–red frequencies. These transitions are called continuum–continuum transitions, whilst the name free–free transitions is generally used to refer to inelastic collisions in laser–assisted electron scattering. At higher intensities, when the ponderomotive energy of an electron (the energy that a 'free' electron has by virtue of its oscillation in an electromagnetic field), becomes comparable to the photon energy, the probability of higher order processes is enhanced over that of lower order ones and the phenomenon of peak–switching occurs. Although this effect is understood qualitatively, theories giving quantitative agreement with experiment have yet to be developed. At still higher intensities, around 10^{16} W/cm^2, the atomic unit of intensity is approached and the radiation field is stronger than the Coulomb force binding the electron to the nucleus. The atomic structure is then so distorted that traditional approaches relying on an expansion in a basis set composed of the unperturbed atomic eigenstates must be abandoned. It is this type of problem, but in the context of electron scattering rather than ionisation, that we address in Chapters 3 and 4. Beyond this, relativistic effects become increasingly significant, but these lie outside the scope of this thesis.

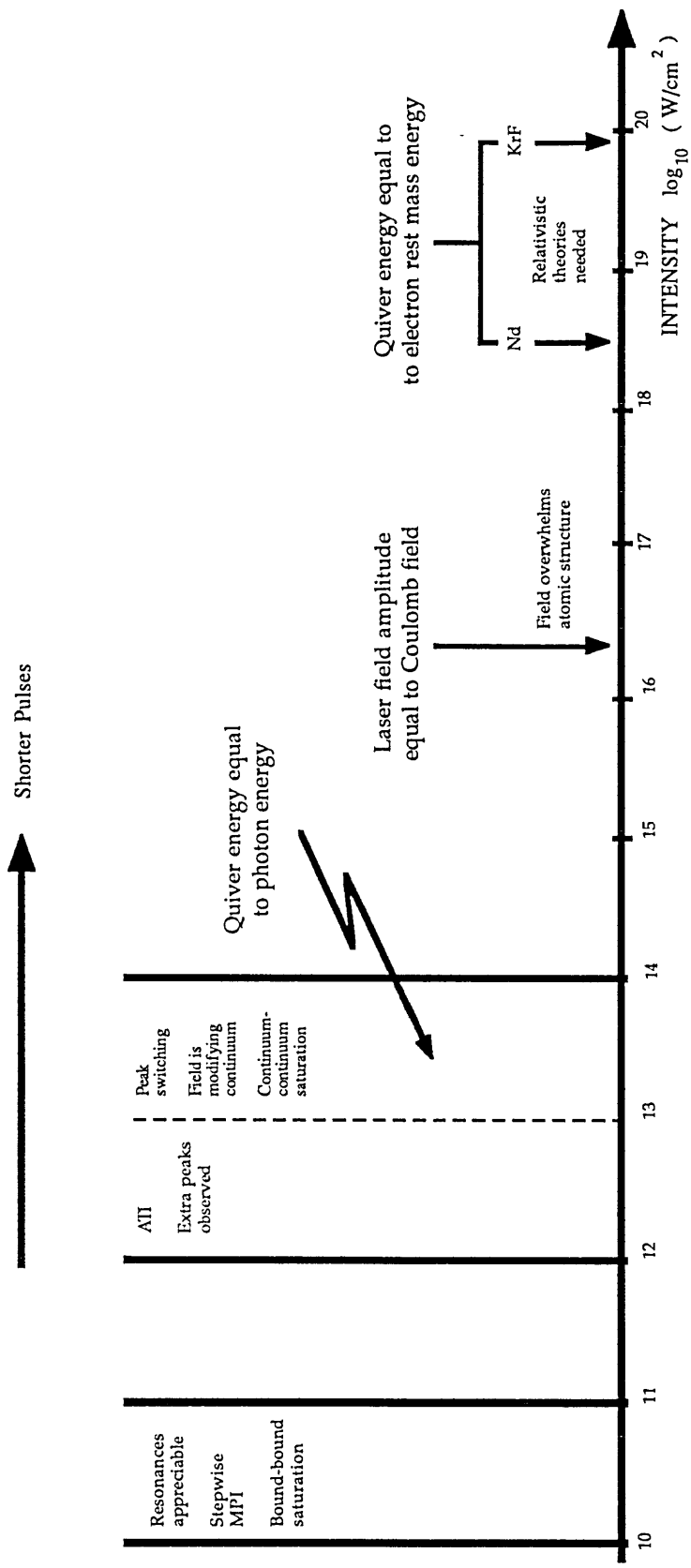

Figure 1.1 Interaction of ultrashort, high-intensity pulses with atoms.

§1.2.1 Perturbation Theory

Standard time–dependent perturbation theory[4] at the nth order yields the following expression for the transition rate for an n–photon process between the ground state $|g\rangle$ and a final state $|f\rangle$:

$$R_n = \frac{2\pi}{\hbar}\left[\frac{2e^2}{\varepsilon_0 c}\right]^n I^n \left| \sum_{i\ldots k} \frac{\langle g|r|i\rangle \langle i|r|j\rangle \ldots \langle k|r|f\rangle}{(E_g + \hbar\omega - E_i)(E_g + \hbar\omega - E_j)\ldots..} \right|^2 \tag{1.1}$$

where $|i\rangle$, $|j\rangle$, ... $|k\rangle$ are the intermediate atomic states with energy E_i ,..., E_k ; I is the intensity and ω the frequency of the radiation. E_g and E_f are the energies of the ground and final states respectively. If $|f\rangle$ is a bound state, a factor $\delta(E_g + \hbar\omega - E_f)$ must be included on the RHS. The generalised cross–section is an intensity independent parameter that depends only on atomic quantities and is defined by

$$\sigma_n = R_n/I^n. \tag{1.2}$$

The calculation of the generalised cross–section for high order processes is itself an immense task, involving (n–1) summations over the complete set of eigenstates of the atom, and requiring knowledge of the atomic wavefunctions. Various approximations to simplify the task have been proposed and employed with different degrees of agreement with experiment[5].

The simple power law shown in Eq (1) is not, however, adequate for describing multiphoton processes under all circumstances:

Firstly, it does not take into account the shift in the energy of the states caused by the interaction with the radiation. At the lowest order, this shift, known as

the ac Stark shift, is due to two–photon transitions with zero net absorption or emission and is linear in the intensity. The denominator in Eq (1) therefore becomes intensity dependent, thus changing the overall intensity dependence of the transition rate.

Secondly, perturbation theory also breaks down if intermediate states in the n–photon process are m–photon resonant with the initial state since one of the denominators in Eq (1) will vanish. In this case, the population of the initial state does not decay at a constant rate, but oscillates between the resonant states at the Rabi frequency[6] which is proportional to the square root of the intensity.

Thirdly, in intense fields, higher order contributions to the nth order cross–section become important. It is therefore no longer meaningful to define a rate as in Eq (1). One then needs a treatment that includes the field to all orders. A commonly used technique is to identify the 'essential states' of the problem and solve the Schrodinger Equation in the reduced set of basis states, by means of, for example, Laplace or Fourier Transforms. In this method, which we use in Chapter 4, the initial and final states are assumed to be the atomic eigenstates, unperturbed by the laser field. Other theories have attempted to include the distortion of the atomic states from the outset. In charged particle scattering, for instance, the radiation field is incorporated exactly in the wavefunction of the incoming and outgoing particle far from the scattering centre[7] (see § 3.2.1). This type of wavefunction describes a Volkov state[8] which is also the basis for a theory proposed by Keldysh[9], in which the final states for multiphoton ionisation are Volkov states. The Kramers–Henneberger transformation has also been used in an attempt to include part of the electron–radiation interaction in the initial state in multiphoton ionisation calculations[2] (see Chapter 2).

§1.2.2 Radiative Scattering Experiments

In order to demonstrate the kind of intense field effects that are observable and to highlight some of the problems that theorists are tackling at present we shall now describe some past experiments in multiphoton physics. The first experiment that we consider is the laser assisted electron scattering one of Weingartshofer *et al*[10 11]. The geometry of the experiment is shown in Fig 2. The gas beam consists of

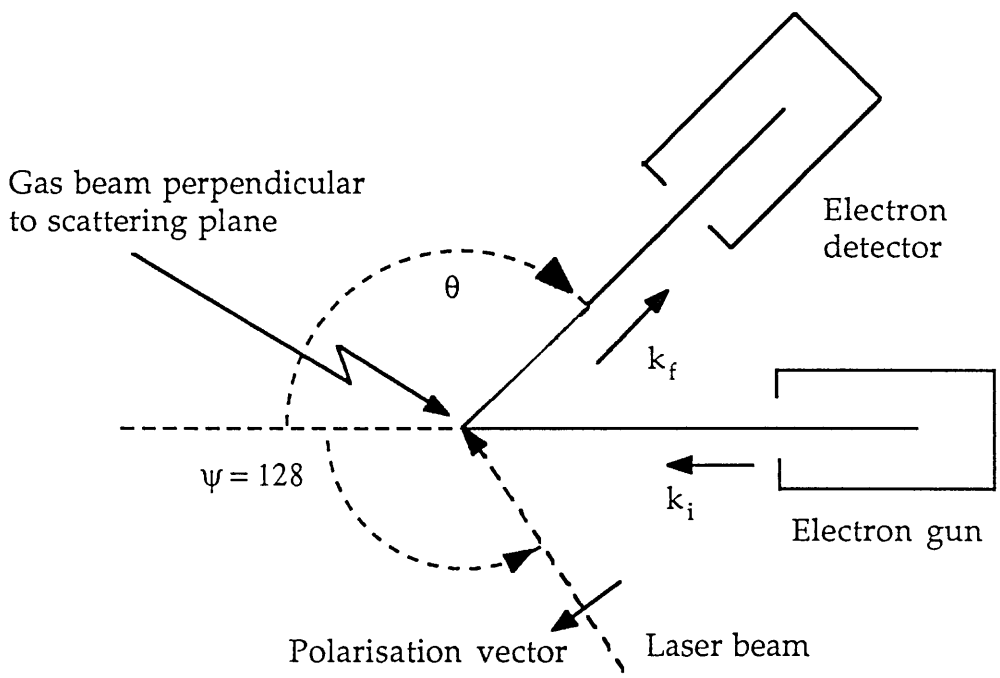

Figure 1.2 Geometry of the laser assisted scattering experiment. (From Ref 11)

argon atoms and is perpendicular to the plane defined by the incoming and detected outgoing electron beams. A pulsed CO_2 laser (photon energy 117 meV) polarised linearly in the scattering plane is used. An electron spectrometer of resolution better than 40 meV detects the outgoing electrons. Measurements of electron counts are made at different incident energies, scattering angles and laser intensities ($10^6 - 10^8$ W cm^{-2}). A typical electron spectrum is shown in Fig 3.

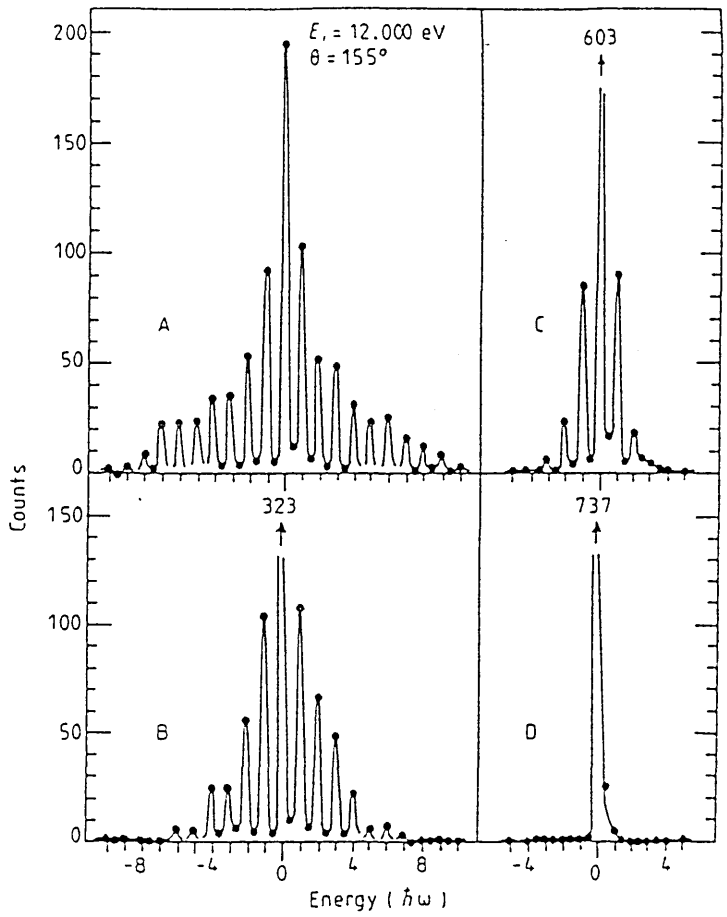

Figure 1.3 Free-free electron energy spectra for e-Ar scattering with incident electron energy $E_i = 12$ eV and scattering angle $\theta = 155^\circ$. The spectra show the number of scattered electrons with the laser intensity decreasing from about 10 W/cm^2 in A to zero in D. The polarisation vector is parallel to the scattering plane. (From Ref. 11)

Multiphoton absorption and emission are clearly seen: up to 11 photons are exchanged during the scattering process. As the photon energy is much smaller than the incident energy of the electron, the low–frequency theory of Kroll and Watson, described in Section 3.2.2, should suffice as a description of the experiment.

However, the theory assumes that the laser is continuous wave, and if the laser is pulsed, then, as Kruger and Jung[12] have pointed out, detailed characteristics of the temporal and spatial pulse shape must be known before quantitative comparison of experiment with theory may be made. This information was not available in sufficient detail, but qualitative agreement is very good. This will be discussed further in Chapter 3, after a summary of the Kroll–Watson approximation.

The difficulty of making accurate measurements in this type of experiment is indicated by the fact that only recently has the group of Wallbank *et al.*[13] been able to present quantitative measurements of differential cross–sections for free–free transitions. The experimental cross–sections show some agreement with theoretical models, but the data also shows new structure which is not understood at present. The theoretical models employ either a single–mode or chaotic description for the laser neither of which fits the laser used in the experiment, which operated on only a few modes. A more realistic model for the laser is required for the interpretation of the data.

Scattering experiments in high frequency laser fields such that the low–frequency approximation no longer holds have yet to be carried out, although multiphoton ionisation experiments using radiation with photon energies of 5 eV and 6.5 eV [14] [15] have already been reported. A major motivation for the work presented here is the relative lack of theoretical work in this area.

§1.2.3 Multiphoton Ionisation

Early experiments on multiphoton ionisation were devoted almost entirely to the measurement of the rate of production of ions. Since the development of high resolution electron energy spectrometers, the emphasis has changed over the last 10

years or so to the spectrum of the photoelectron as it leaves the atom. Some experiments[16] had observed electrons with kinetic energy higher than the difference between the energy of the minimum number, N, of photons required for the ionisation and the ionisation potential. The first clear evidence that electrons absorb more photons than the minimum necessary came from an experiment performed in 1979 by Agostini *et al.*[17] in Xenon atoms. Since then several experiments have been reported in which the photoelectron spectrum consists of a series of peaks spaced apart by the photon energy $\hbar\omega$ (Fig 4)[18]. This effect was at first thought to be due to the outgoing electron undergoing inverse bremsstrahlung in the field of neighbouring ions. Measurements of the amplitudes of the peaks at various atomic densities showed a linear dependence rather than the quadratic dependence that would be expected for bremsstrahlung. Hence the absorption of excess photons by the electron was shown to be a single atom process, and has been termed Above Threshold Ionisation or Excess Photon Ionisation.

At low intensities (less than around 10^{12} W/cm^2), the heights of the peaks decrease monotonically with S, the number of excess photons. The intensity dependence of each peak has been found to follow the perturbative law Eq (1) in this regime. For example, in the recent experiment of Lompré *et al.*[19], the order of nonlinearity, κ_n, defined by

$$\kappa_n = d(\log_{10} R_n)/ d(\log I) \tag{1.3}$$

for the above threshold ionisation of Xenon at 1064 nm (N = 11) was measured. It was found that $\kappa_{N+S} \simeq N + S$ at intensities below the saturation intensity (1.2×10^{13} W/cm^2) for a pulse duration of 30 ps. At 200 ps, the orders of non–linearity become identical to N = 11, thus showing that the transition rate is dominated by the N–photon ionisation, and continuum–continuum transitions are

saturated for longer pulses. The long pulse results are in agreement with those obtained by Kruit *et al*[18].

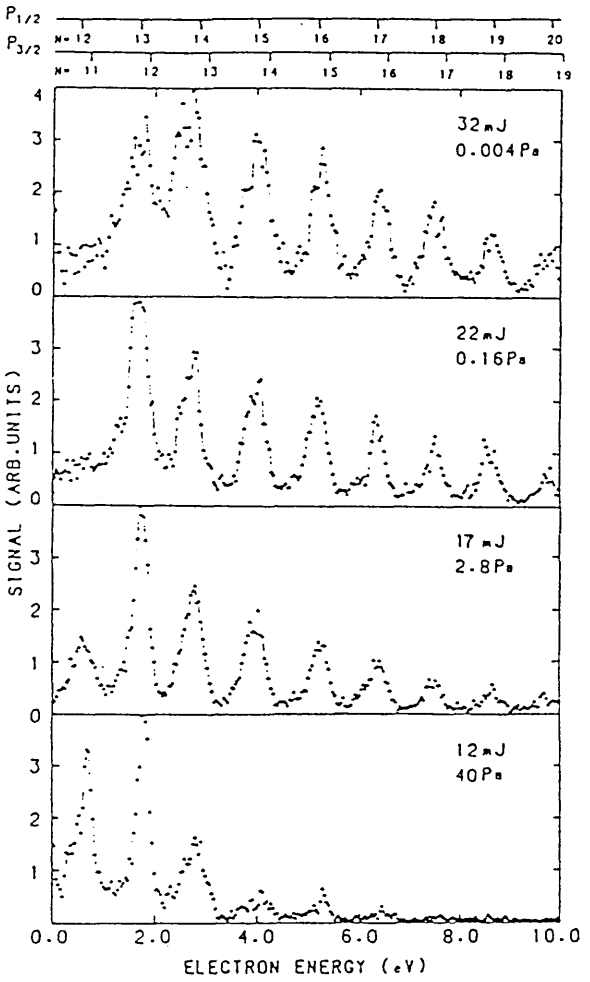

Figure 1.4 Electron energy spectra from multiphoton ionisaton of xenon at 1064 nm($\hbar\omega$ = eV) a) $I \simeq 2.4\ 10^{13}$ W/cm^2, b) $I \simeq 3.4\ 10^{13}$ W/cm^2, c) $I \simeq 4.4\ 10^{13}$ W/cm^2, d) $I \simeq 6.4\ 10^{13}$ W/cm^2. The scale at the top shows the number of photons absorbed from the two possible states $^2P_{3/2}$ and $^2P_{1/2}$.(From Ref.18).

At intensities greater than around 10^{13} W/cm^2, a new, non–perturbative phenomenon occurs: peak suppression. As the intensity of the laser is increased, the

S = 0 peak becomes smaller than the S = 1 peak, then the S = 1 peak becomes smaller than the S = 2 peak and so on. When a long wavelength laser is used, for example a CO_2 laser, although the individual peaks cannot be resolved, the effective number of peaks suppressed is around 2000 in Xenon[20]. There are two different points of view regarding peak suppression. One explains the effect in terms of an increase in the ionisation potential[21] of the atom due to the ac Stark shift of the high–lying states. The ground state which feels the electrostatic force more strongly than the electromagnetic, is shifted only slightly by comparison. The shift of the ionisation potential is approximately given by

$$\Delta = \frac{e^2 \mathcal{E}_0^2}{4m\omega^2} \tag{1.4}$$

where e and m are the electronic charge and mass, ω the frequency of the laser and $\mathcal{E}_0$ the field amplitude. The minimum number of photons required for ionisation is therefore increased. However, no downward shift in the photoelectron energy spectrum is seen because Δ is exactly the energy that the electron gains on leaving the laser focus by being accelerated by the ponderomotive potential [see Ref 22 and Section 3.2] and the position of the peak where the electron has absorbed N + S photons remains unaltered.

According to the second point of view[19], the change in the ionisation potential is too small (or even negative) to account for the peak suppression. The alternative explanation is that the electron, having absorbed N photons, during the ionisation process then absorbs a further S photons while still in the presence of the ionic potential. The 'half–collision' is not bremsstrahlung in the usual sense since the interaction is with the parent ion and not external atoms. The dependence on the atomic density is therefore linear. While the electron is still within the laser focus,

part of the excess energy is absorbed in the form of the ponderomotive energy which is regained as drift energy on leaving the laser focus as above. Thus the position of the peak is not downshifted. Which of the two mechanisms described here more accurately describes the effect still remains to be determined, possibly by accurate measurements of the shift in the ionisation potential.

References

1 H. A. Kramers in *Rapport et Discussions, Solvay Congress* (Stoops, Belgium, 1948) p241.

2 W. C. Henneberger Phys. Rev. Lett. 21 (1968) 838.

3 M. Gavrila and J. Z. Kaminski, Phys. Rev. Lett. 52 (1984) 613.

4 F. H. M. Faisal, *Theory of Multiphoton Processes* (Plenum, New York, 1987) pps 29–51.

5 J. Morellec, D. Normand and G. Petite, Adv. At. Mol. Phys. 18 (1982) 97.

6 P. L. Knight and P. W. Milonni, Phys. Reports 66 (1980) 21.

7 N. M. Kroll and K. M. Watson, Phys. Rev. A 8 (1973) 804.

8 J. H. Eberly in *Progress in Optics* (North–Holland, Amsterdam, 1969) Vol VII, p361.

9 L. V. Keldysh, Soviet Phys. JETP 47 (1964) 1307.

10 A. Weingartshofer, J. K. Holmes, G. Caudle, E. M. Clarke and H. Kruger, Phys. Rev. Lett. 39 (1977) 269. A. Weingartshofer, E. M. Clarke, J. K. Holmes and C. Jung, Phys. Rev. A 19 (1979) 2371.

11 A. Weingartshofer, J. K. Holmes, J. Sabbagh and S. L. Chin, J. Phys. B 16 (1983) 1805.

12 H. Kruger and C. Jung, Phys. Rev. A 17 (1978) 1706.

13 J. Wallbank, J. K. Holmes and A. Weingartshofer, J. Phys. B 20 (1987) 6121.

14 U. Johann, T. S. Luk, H. Egger and C. K. Rhodes, Phys. Rev. A 34 (1986) 1084.

15 T. S. Luk, T. Graber, H. Jara, U. Johann, K. Boyer and C. K. Rhodes, J. Opt. Soc. Am. B 4 (1987) 847.

16 E. A. Martin and L. Mandel, Appl. Opt. 15 (1976) 2378.

17 P. Agostini, F. Fabre, G. Mainfray, G. Petite and N. K. Rahman, Phys. Rev. A 42 (1979) 1127.

[18] P. Kruit, J. Kimman, H. G. Muller and M. J. van der Wiel, Phys. Rev. A 28 (1983) 2.

[19] L.A. Lompré, G. Mainfray, C. Manus and J. Kupersztych, J. Phys. B 20 (1987) 1009.

[20] P. Agostini and G. Petite, Contemp. Phys. 29 (1988) 57 and references therein.

[21] H. Muller and A. Tip, Phys. Rev. A 30 (1984) 3039.

[22] T. W. B. Kibble, Phys. Rev. 150 (1966) 1060.

CHAPTER 2

THE KRAMERS–HENNEBERGER TRANSFORMATION AND INTENSITY–DEPENDENT POTENTIALS

§2.1 *Introduction*

The Kramers–Henneberger Transformation (KHT) has had a long and not uncontroversial history in the study of quantum and semi–classical electrodynamics. The original introduction of this transformation has been attributed to Kramers[1] who used it to remove divergences in non–relativistic quantum–electrodynamics. His derivation of the transformation of the quantum–mechanical Hamiltonian consists of first transforming the canonical variables of the classical Lagrangian in the dipole approximation and then promoting them to quantum operators. Using a similar transformation, Welton[2] derived an expression for the Lamb shift based on the calculation of the mean square amplitude of oscillation of an electron coupled to the zero–point fluctuations of the electromagnetic field.

The use of the KHT in semi–classical multiphoton theory was first proposed by Henneberger[3]. Previous calculations relying on perturbative techniques had yielded ionisation cross–sections that were too low and threshold intensities that were too high compared to the experimental results of the time. It was claimed that perturbation theory was being applied beyond the limits of its validity and ignored the effect of intense radiation on the initial state of the atom. Motivated by this apparent failure of perturbation theory to account for the experimental results, Henneberger performed a unitary transformation of the Hamiltonian in the non–relativistic dipole approximation. His aim was twofold:

(i) to obtain a new Hamiltonian such that the eigenstates of the time–independent part could be calculated exactly. The ground state of this would represent an improvement over the unperturbed ground state as the initial state for ionisation calculations by already taking into account part of the shift due to the interaction with the radiation field.

(ii) to obtain a time–dependent part which could be expanded in a perturbation series that would converge faster than the ordinary perturbation series.

We shall see later how this worked in practice. Henneberger's derivation of the KHT is different from that of Kramers'. As intense laser fields were to be considered, he employed a classical description of the radiation field and, hence, a time–dependent unitary transformation of the Schrodinger Equation. In this picture, divergences due to the coupling to vacuum fluctuations are not present. Since we use this version of the KHT in this thesis, we reproduce his derivation here.

§2.2 *The Kramers-Henneberger Transformation*

We start with the semi–classical minimal–coupling Hamiltonian, H, for an electron in an electromagnetic field in the Coulomb gauge:

$$H = \frac{p^2}{2m} + \frac{e}{m}\,\underline{p}.\underline{A}(\underline{r},t) + \frac{e^2}{2m}\,\underline{A}^2(\underline{r},t) + V(\underline{r}). \qquad (2.1)$$

where $\underline{A}$ is the vector potential and $V(\underline{r})$ is the atomic potential. The electromagnetic field is represented as an infinite plane wave, linearly polarised and in the dipole approximation. We therefore write the vector potential as

$$\underline{A}(\underline{r},t) = \underline{A}(\underline{r}=0,t) = \underline{A}_0 \cos \omega t \tag{2.2}$$

where ω is the frequency of the laser. The Schrodinger Equation for the electron is

$$i\hbar \frac{\partial \Psi(\underline{r},t)}{\partial t} = H\Psi(\underline{r},t) \tag{2.3}$$

We now introduce the new wavefunction $\Phi(\underline{r},t)$ given by

$$\Phi(\underline{r},t) = U_1 U_2 \Psi(\underline{r},t) \tag{2.4}$$

where

$$U_1 = \exp\left\{ \frac{i e^2}{2m\hbar} \int_{-\infty}^{t} d\tau \, \underline{A}^2(\tau) \right\} \tag{2.5}$$

$$U_2 = \exp\left\{ \frac{i e}{m\hbar} \int_{-\infty}^{t} d\tau \, \underline{A}(\tau).\underline{p} \right\} \tag{2.6}$$

U_1 is simply a phase transformation which removes the $\underline{A}^2$ term from Eq (1). This term is of no interest in the dipole approximation since its only effect is to shift the energy of all states by an equal amount, and therefore does not alter the dynamics of the system. The appearance of the momentum, $\underline{p}$, in the definition of U_2 means that it is a displacement operator, causing a time–dependent shift in the position. U_2 is written more simply as

$$U_2 = \exp(\underline{\alpha}.\underline{\nabla}) \tag{2.7}$$

where

$$\underline{\alpha} = \underline{\alpha}_0 \sin \omega t = \frac{e}{m} \int_{-\infty}^{t} d\tau \, \underline{A}(\tau) \tag{2.8}$$

$$\underline{\alpha}_0 = e\underline{A}_0/m\omega \tag{2.9}$$

Its effect is to remove the $\underline{p}.\underline{A}$ term from the Schrodinger Equation and transfer all the information about the radiation field into a time and intensity–dependent potential. The new wavefunction satisfies the following equation

$$i\hbar \frac{\partial \Phi(\underline{r},t)}{\partial t} = \left\{ \frac{-\hbar^2}{2m} \underline{\nabla}^2 + V\left[\underline{r}+\underline{\alpha}(t)\right] \right\} \Phi(\underline{r},t) \tag{2.10}$$

Note that exactly the same transformation may be achieved by simply replacing $\underline{r}$ in Eq (3) with $\underline{r}+\underline{\alpha}(t)$ and deriving the equation of motion for $\Phi(\underline{r},t) = \Psi(\underline{r}+\underline{\alpha}(t),t)$. The transformation is therefore also known as the "space–translation" transformation. This immediately indicates the physical interpretation of the KHT. It is a transformation to a frame of reference that is oscillating at frequency ω and amplitude α_0 in the dipole approximation. The quantity $\underline{\alpha}(t)$ describes the oscillation that a classical free electron with zero initial velocity executes in an electromagnetic field. The Lorentz force on such an electron is

$$m\ddot{\underline{r}} = -e\frac{d\underline{A}}{dt} = e\underline{E}_0 \sin \omega t \tag{2.11}$$

where we have used Eq (2) and the Maxwell Equation $\underline{E} = -\partial\underline{A}/\partial t$ where $\underline{E}$ is the electric field. There is, of course, no magnetic term in Eq (11) because in the dipole approximation, the magnetic field given by $\underline{\nabla} \times \underline{A}$ is zero. Integrating Eq (11) with respect to time gives

$$\underline{r}(t) = -\int_{-\infty}^{t} \frac{e}{m} \underline{A}(\tau) \, d\tau = -\underline{\alpha}(t) \tag{2.12}$$

In the KH reference frame which is the rest frame of this electron, the potential $V(\underline{r})$ appears to be oscillating according to Eq (12). The importance of the KHT is that it decouples the fast oscillation, the jitter or quiver motion, from the motion described by the 'average position'[4]. The decoupling is most clearly demonstrated by the solution to Eq (10) for a free electron in a radiation field. With $V(\underline{r}) = 0$, the solution is simply a plane wave:

$$\Phi_{free}(\underline{r},t) = \exp\left[\frac{-i\hbar^2 k^2}{2m}t + i\underline{k}.\underline{r}\right] \tag{2.13}$$

where $\underline{k}$ is the electron wavevector. Transforming back to the $\underline{p}.\underline{A}$ gauge, we get the well–known Volkov[5] [6] solution for a non–relativistic free electron in a radiation field in the dipole approximation,

$$\Psi_{free}(\underline{r},t) = U_1^{-1}U_2^{-1}\Phi_{free}(\underline{r},t)$$

$$= \exp\left\{\frac{-i\,e^2}{2m\hbar}\int_{-\infty}^{t} d\tau\, \underline{A}^2(\tau) - i\underline{k}.\underline{\alpha}_0 \sin\omega t\ \frac{-i\hbar^2 k^2}{2m}t + i\underline{k}.\underline{r}\right\} \tag{2.14}$$

We shall discuss the Volkov solutions in greater detail in Chapter 3 since they are the asymptotic states for scattering in laser fields.

In the above, we have considered the KHT in a semi–classical context where the dynamics of the laser field does not appear in the Hamiltonian. Kramers' original transformation acted upon the fully quantum–mechanical Hamiltonian in which the external field is also quantised:

$$H_q = \frac{p^2}{2m} + \frac{e}{m}\underline{p}.\underline{A}(\underline{r},t) + \frac{e^2}{2m}\underline{A}^2(\underline{r},t) + V(\underline{r}) + H_{rad} \tag{2.15}$$

where H_{rad} is the Hamiltonian for the free field. In this case the transformation is

$$U_2 = \exp\left[\frac{ie\,\underline{p}.\underline{Z}}{\hbar m}\right] \tag{2.16}$$

Here, $\underline{Z}$ is the Hertz vector, related to the vector potential by $\underline{A} = \dot{\underline{Z}}$ and obeying the commutator relation

$$[H_{rad}, \underline{Z}] = -i\hbar\underline{A} \tag{2.17}$$

The transformed Hamiltonian may be written to order e^2 as

$$H_{new} = U_2 H_q U_2^{-1}$$

$$\simeq \frac{\underline{p}^2}{2m_{obs}} + \frac{e^2}{2m_{obs}} \underline{A}^2(\underline{r},t) + V(\underline{r} + e\underline{Z}/m) + H_{rad} \tag{2.18}$$

where m_{obs} is the observable, renormalised mass[7], $m_{obs} = m + \frac{e^2}{3\pi^2\varepsilon_0 c^2}\int d\underline{q}$, the integration being over all the mode wavevectors.

It is also interesting to consider the KHT as the zeroth order approximation of a transformation that incorporates fully the interaction of the electron with both the potential and the laser field as has been done recently by Janjusevic and Hahn[8]. The solution $\Psi(\underline{r},t)$ of the semi–classical Schrodinger Equation (3) in the $\underline{p}.\underline{A}$ gauge is related to the solution $v(\underline{r},t)$ of the same equation without the laser field by a transformation U:

$$\Psi(\underline{r},t) = U\, v(\underline{r},t) \tag{2.19}$$

Here, $v(\underline{r},t)$ is a solution of

$$i\hbar \frac{\partial v(\underline{r},t)}{\partial t} = H_0\, v(\underline{r},t) \tag{2.20}$$

with

$$H_0 = \frac{\underline{p}^2}{2m} + V(\underline{r}) \tag{2.21}$$

Eqs (3), (19) and (20) may be combined to show that U satisfies a differential equation whose formal solution is

$$U = \exp\left[\frac{-i}{\hbar}\int_{-\infty}^{t} d\tau\, \{H'(\tau) - [UH_0U^{-1} - H_0]\}\right] \tag{2.22}$$

where H' represents the electron–laser interaction:

$$H' = \frac{e}{m}\,\underline{p}.\underline{A}(\underline{r},t) + \frac{e^2}{2m}\,\underline{A}^2(\underline{r},t) \tag{2.23}$$

The implicit equation (22) for U may be solved iteratively, the zeroth order term being obtained by neglecting the first two terms on the RHS. The resulting expression will be recognised as the inverse KHT. At this order, $\Psi(\underline{r},t)$ contains the effects of both the potential and the laser field, but not the coupling between them and so the processes in which real photons are exchanged are not accounted for. These require further iterations, the first of which is described in Ref (8).

Proceeding with Henneberger's scheme, we expand the time–dependent potential $V(\underline{r}+\underline{\alpha}(t))$ in a Fourier series.

$$V(\underline{r}+\underline{\alpha}(t)) = \sum_{n=-\infty}^{\infty} V_n(\underline{\alpha}_0;\underline{r})\, e^{-in\omega t} \tag{2.24}$$

with

$$V_n(\underline{\alpha}_0;\underline{r}) = \frac{1}{T} \int_{-T/2}^{T/2} V(\underline{r}+\underline{\alpha}(t))\, e^{-in\omega t}\, dt; \quad T = \frac{2\pi}{\omega} \tag{2.25}$$

The above expression may be written, after some algebraic manipulation [Ref 9, Eq 8.940.1], as

$$V_n(\underline{\alpha}_0;\underline{r}) = \frac{i^n}{\pi} \int_{-1}^{1} V(\underline{r} + \underline{\alpha}_0 u)\, T_n(u)\, (1-u^2)^{-\frac{1}{2}}\, du. \tag{2.26}$$

where $T_n(u)$ is a Tchebychev polynomial:

$$T_n(\cos\phi) = \cos n\phi \tag{2.27}$$

Therefore, we also have that $V_n = V^*_{-n}$. Eq (26) also provides a convenient expression for computing V_n because the integral in it may be expressed as a sum [Ref 10, Eq 25.4.38]:

$$V_n(\underline{\alpha}_0;\underline{r}) \simeq \frac{i^n}{m} \sum_{j=1}^{m} \cos n\left[\frac{2j-1}{2m}\pi\right] V\left[\underline{r} + \underline{\alpha}_0 \cos\left[\frac{2j-1}{2m}\pi\right]\right] \tag{2.28}$$

Here, m, the upper limit of the sum, is chosen to be high enough so that the required precision in $V_n(\underline{\alpha}_0;\underline{r})$ is achieved.

Henneberger's idea was to consider the zeroth order component, V_0, which is the time–averaged part of $V(\underline{r}+\underline{\alpha}(t))$ as an effective binding potential. This results in the Hamiltonian

$$\tilde{H}_0 = \frac{p^2}{2m} + V_0(\underline{\alpha}_0;\underline{r}) \tag{2.29}$$

whose eigenstates we denote by $|E_n\rangle$. Since V_0 depends on α_0, the states $|E_n\rangle$ are already dressed to some extent by the laser field. The other components of $V(\underline{r}+\underline{\alpha}(t))$ induce transitions between the $|E_n\rangle$ and it was claimed by Henneberger that this part of the interaction may be treated using standard time–dependent perturbation theory.

Although the full program as proposed by Henneberger has not yet been carried out, a number of groups have used the idea of splitting up the interaction into static and time–dependent parts to calculate energy shifts for atoms in intense radiation fields. The first among these were Choi *et al.*[11] who calculated the ground state wavefunctions of $\tilde{H}_0$ for Hydrogen and Helium using a variational method. Their intention was to use these states as the initial states for future calculations of multiphoton transition rates. They found that the ground state energy increases with α_0 and interpreted this as a reduction in the ionisation potential with increasing α_0, an observation that was consistent with the experimental results. Subsequent debate[12 13] on the validity of the KHT has raised the following questions:

(i) Is it sufficient to calculate energy shifts and transition rates in the KH picture without transforming initial and final states?

(ii) Can the difference in energy between the ground states of $V(\underline{r})$ and $V_0(\underline{r})$ be interpreted as the full shift of the atomic states in the presence of the field?

(iii) Is it justifiable to use the ground state of $V_0(\underline{r})$ as the initial state for multiphoton ionisation?

It is clear in view of the unitary nature of the transformation that any physical quantity calculated in the KH picture must be the same as that calculated using the minimal coupling Hamiltonian. This is true provided that one transforms the wavefunctions as well as the Hamiltonian before calculating matrix elements. If the wavefunctions are not transformed, but the Hamiltonian is, it has been shown[3 14] using perturbation theory, that at least up to order e^2, matrix elements for one– and two–photon transitions between resonantly connected initial and final states as well as energy shifts are the same when calculated in the two pictures. However, incorrect[15 16] use of this so–called hybrid procedure where the Hamiltonian is transformed but not the wavefunction, leads to the conclusion that the transformation is valid only in the high frequency regime. This erroneous conclusion was reached, as pointed out by Lambropoulos *et al.*[17] and by Knight[18], because only part of the interaction, namely the time–independent part, V_0, had been employed in the calculation of the shifts. Similarly, it is misleading to interpret the difference in energy between the states $|E_n\rangle$ and the bare atomic states as the full radiative shift of the atoms because it is only part of the shift. This is because the states $|E_n\rangle$ are themselves dressed by the time dependent part of $V(\underline{r}+\underline{\alpha}(t))$, thus inducing further shifts. Taking these into account leads to the same shifts as calculated using standard perturbation theory in the $\underline{p}.\underline{A}$ picture. The use of V_0 only is justified when the further dressing is negligible and this occurs when the interaction is oscillating so fast that the electron feels only its time–average. Under these circumstances, the KHT can offer a definite calculational advantage as will be seen in Chapter 3.

Since the original work of Choi *et al.*[11], the KHT has not been used for the calculation of multiphoton transition rates, possibly because further experimental results showed that the enhancement in multiphoton ionisation noted above was actually due to the multi–mode nature of the ionising laser[19] – something that had not been taken into account in previous calculations. Gavrila[20] has recently

developed a theory for atomic structure and multiphoton ionisation in this regime using the KHT and has shown that at sufficiently high frequency, an atom in a laser field becomes immune to ionisation independent of the intensity of the field. Its structure becomes strongly distorted and large shifts in the ionisation potential are predicted[21 22]. At the next order in $1/\omega$, multiphoton ionisation becomes possible, and expressions for the n–photon ionisation amplitude have been given, assuming that the initial state of the atom in the field is the ground state of V_0. As with the older works mentioned before, the calculation of ionisation rates in the KH picture is bound to raise further problems of interpretation.

§2.3 *Application to a Model Potential*

In the next Chapter, we shall consider the problem of an electron scattered by a potential in the presence of an intense laser field, one of the aims of the work being to discover the importance of the V_n $(n \neq 0)$ relative to the zero order component V_0. The potential to be considered is the polarisation potential which is of the form (in atomic units so that the Bohr radius $a_0 = e = m = \hbar = 1$)

$$V(\underline{r}) = \frac{-A}{(\beta^2 + r^2)^2} \tag{2.30}$$

where A is a measure of the strength of the potential and β is an arbitrary non–zero constant that imposes a cutoff at the origin. This is the potential that is felt by an electron at large distances from a neutral atom. Since we shall restrict our analysis in Chapter 3 to one dimension, we shall now change the notation slightly and replace $\underline{r}$ by x and assume that the incident light beam is polarised along the x–axis. For the case of the polarisation potential V(x), it is possible to derive analytical expressions for the components $V_n(\alpha_0;x)$. These formulae, although complicated in general are

useful in deriving, for instance, asymptotic formulae.

By inserting (27) and (26) into (30) and making the change of variable $u = \cos \phi$, we get

$$V_n(\alpha_0;x) = -A \frac{i^n}{\pi} \int_0^{\pi} d\phi \frac{\cos\ n\phi}{[\beta^2 + (x + \alpha_0\ \cos\ \phi)^2]^2} \tag{2.31}$$

which, by treating β as a continuous variable may be rewritten as

$$V_n(\alpha_0;x) = \frac{A\, i^n}{2\pi} \frac{\partial}{\partial \beta} \int_0^{\pi} d\phi \frac{\cos\ n\phi}{[\beta^2 + (x + \alpha_0\ \cos\ \phi)^2]} \tag{2.32}$$

The denominator of the integrand is expanded to give

$$[\beta^2 + (x + \alpha_0 \cos\phi)^2]^{-1} = \frac{1}{2\beta} \left[[\beta + i(x + \alpha_0 \cos\ \phi)]^{-1} + [\beta - i(x + \alpha_0 \cos\ \phi)]^{-1}\right] \tag{2.33}$$

and substitution of this into (32) yields

$$V_n(\alpha_0;r) = \frac{-A}{2\beta} \frac{\partial}{\partial \beta} \int_0^{\infty} dt \left[e^{-(\beta+ix)t} + (-1)^n\, e^{-(\beta-ix)t}\right] J_n(\alpha_0 t) \tag{2.34}$$

where J_n is a Bessel function of order n. In writing down (34), we have used the relation [Ref 10, Eq 9.1.21]

$$\int_0^{\pi} d\phi \frac{\cos n\phi}{\beta \pm i(x + \alpha_0 \cos \phi)} = i^n \pi (\mp)^n \int_0^{\infty} dt\, e^{-(\beta+ix)t} J_n(\alpha_0 t) \tag{2.35}$$

The integral over t in (35) may be evaluated to give [Ref 9, Eq 6.611.1]:

$$g(\beta) = \int_0^{\infty} dt \left[e^{-(\beta+ix)t} + (-1)^n e^{-(\beta-ix)t} \right] J_n(\alpha_0 t)$$

$$= \frac{\alpha_0^{-n} \left[\sqrt{(\beta+ix)^2 + \alpha_0^2} - (\beta+ix) \right]^n}{\sqrt{(\beta+ix)^2 + \alpha_0^2}} \tag{2.36}$$

Finally, we get

$$V_n(x;\alpha_0) = \frac{A}{2\beta} i^n (-1)^{\frac{n}{2}} \frac{\partial}{\partial\beta} \mathrm{Re}\,\{g(\beta)\} \qquad n = 0, \text{ even} \tag{2.37}$$

$$V_n(x;\alpha_0) = \frac{A}{2\beta} i^n (-1)^{\frac{n+1}{2}} \frac{\partial}{\partial\beta} \mathrm{Im}\,\{g(\beta)\} \qquad n \text{ odd} \tag{2.38}$$

When n=0, we obtain the time–averaged potential, $V_0(x;\alpha_0)$. In this case Eq (37) simplifies to

$$V_0(x;\alpha_0) = \frac{-A}{2\beta} \mathrm{Re} \left[\frac{2\beta^2 - x^2 + \alpha_0^2 + 3i\beta x}{[(\beta + ix)^2 + \alpha_0^2]^{3/2}} \right] \tag{2.39}$$

In the limit that α_0 tends to 0, Eq (39) reduces to the original unperturbed potential Eq (30). Asymptotically, as $|x| \to \infty$, we find that for any n

$$V_n(\alpha_0;x) = \frac{-A\ \alpha_0{}^n\ (-2i)^n}{n!\ x^{4+\,|n|}} \qquad |x| \gg \alpha_0 \tag{2.40}$$

By putting n = 0 in Eq (40), we see that $V_0(\alpha_0;x) = -A/x^4$ as $x \to \infty$ *i.e.* at large distances from the origin, it is identical to the unperturbed potential. The three–dimensional scattering calculations of Van de Ree *et al.*[23] (see Chapter 3 for more details) show that forward scattering appears to be unaffected by the laser field. Since electrons scattered in the forward direction correspond to large impact parameters, it is clear that the dressing of the original potential by the field is negligible at large distances from the centre of the potential. Fig 1 shows V_0 as a

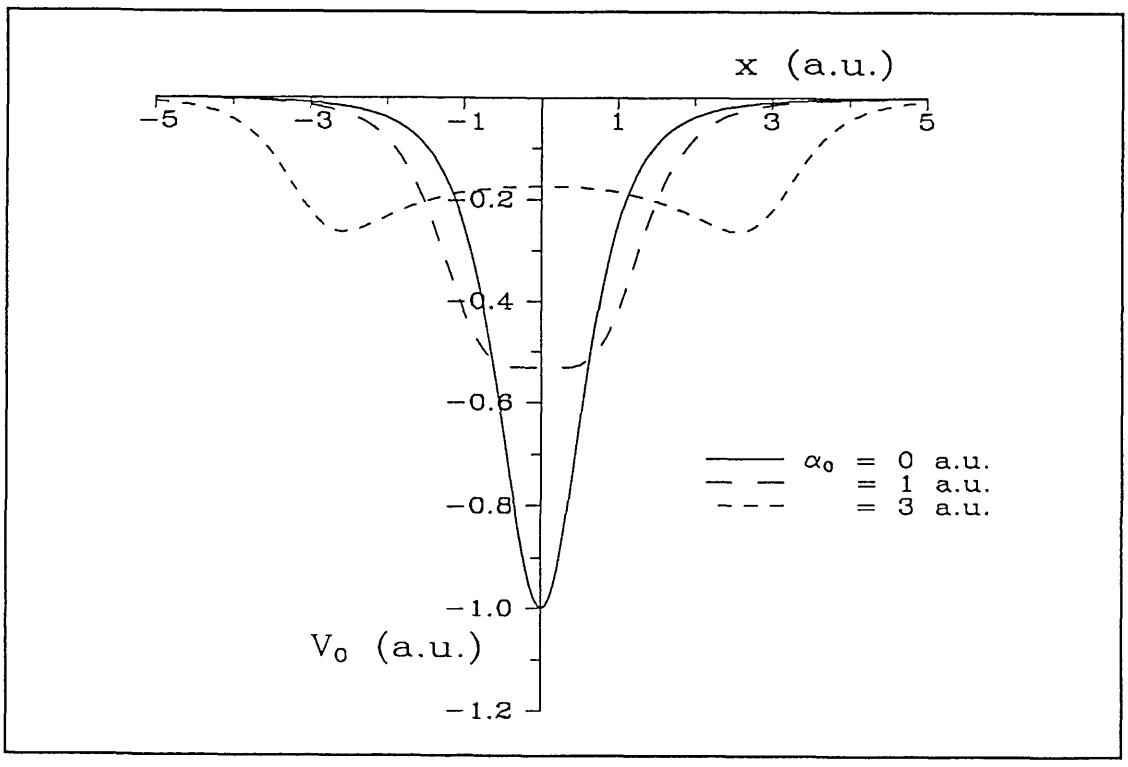

Figure 2.1 The static potential $V_0(x)$ as a function of x for various values of α_0. A = 1 a.u., β = 1 a.u.

function of x for different values of α_0 and with A and β equal to 1 a.u. The effect of the field on the time–averaged potential is to reduce its depth and enhance its range. The presence of the two minima at $x \simeq \pm\alpha_0$ reflects the fact that classically the charge assumed to be responsible for the unperturbed potential (30) appears to oscillate in the KH picture with an amplitude α_0, staying longer at the end points than in the middle where it gives rise to a weaker potential. The double–well feature of $V_0(\alpha_0;x)$ has an interesting consequence: in the KH frame, the wavefunction of the ground state which is peaked strongly at $x = 0$ when $\alpha_0 = 0$, splits into two peaks as α_0 becomes large, as illustrated in Fig 2.

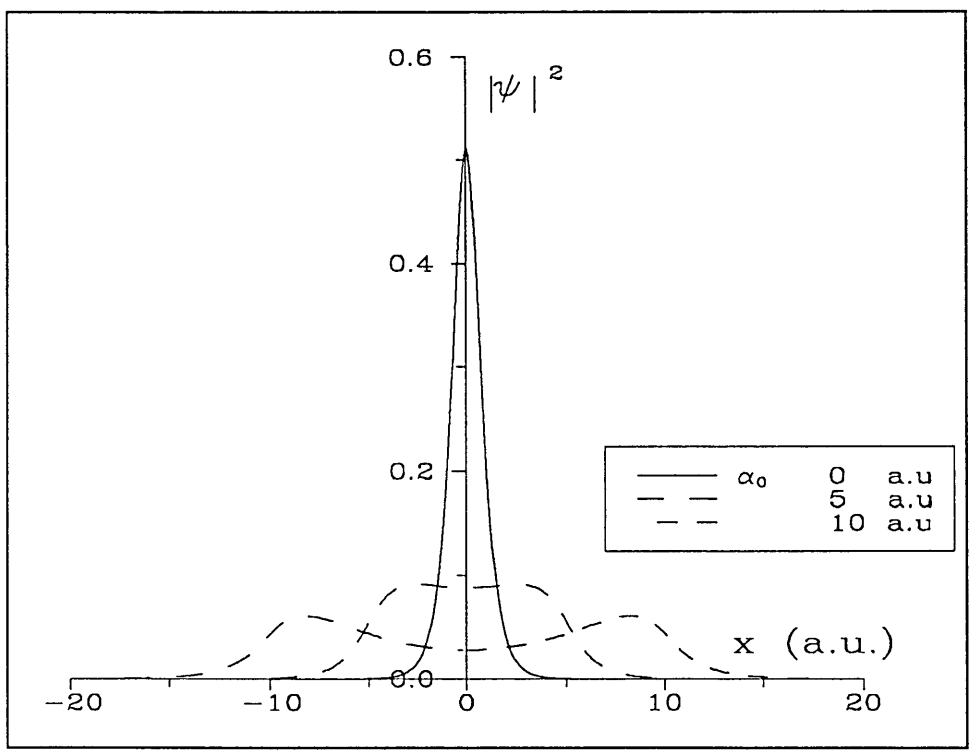

Figure 2.2 The splitting of the wavefunction of the ground state of $V_0(x)$ as α_0 increases. A = 1 a.u., β = 1 a.u.

Because the potential V_0 has been the basis for approximation in a large number of works in multiphoton physics, it would be interesting to discover, in the results of an exact calculation, features that can be ascribed uniquely to V_0. The most obvious way of doing this is to see if the bound states of V_0 induce resonances in scattering cross–sections, for example. To this end, we have obtained the bound state energy levels of the V_0 by numerically calculating the function $\psi(x)$ from

$$\left[\frac{d^2}{dx^2} - 2V_0(x) + 2E\right]\psi(x) = 0 \tag{2.41}$$

and counting the nodes of the function. The ground state wavefunctions depicted in Fig 2 have been obtained by a similar calculation. The energy levels are plotted as functions of α_0 in Figs 3a (A = β = 1 a.u.) and 3b (A = 0.2 a.u., β = 1 a.u.). For the

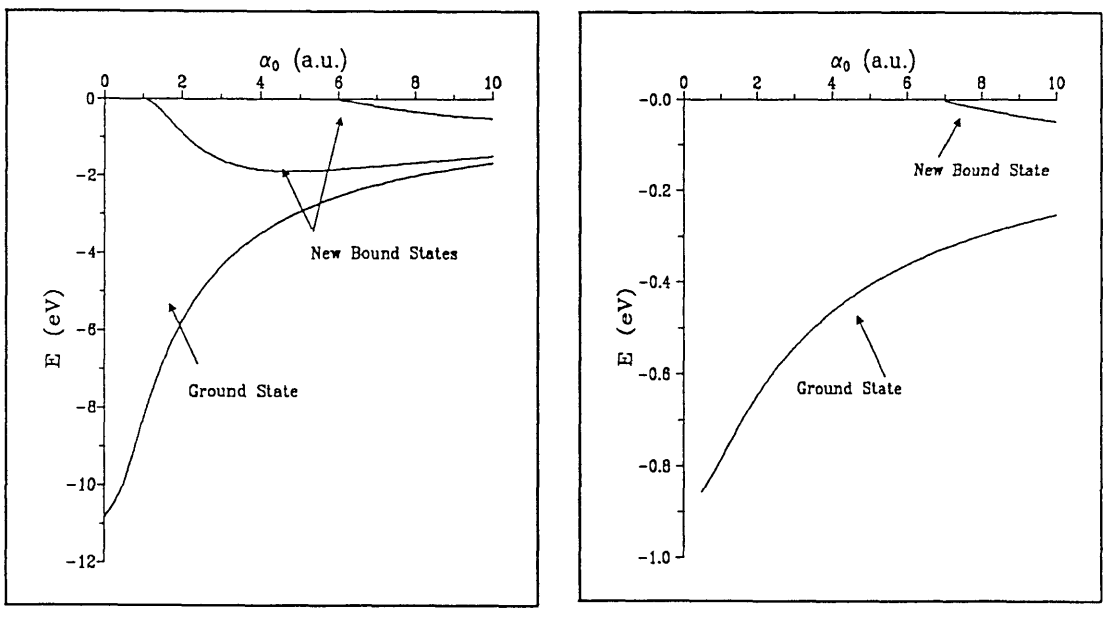

Figure 2.3 The bound state energies of V_0 for β = 1 a.u. and a) A = 1 a.u. and b) A = 0.2 a.u.

value $\alpha_0 = 0$ *i.e.* the field–free case, there is only one bound state in each case. As α_0 increases, this bound state becomes less strongly bound, as expected, since V_0 becomes more shallow. This also agrees with the findings of other workers[11 21 22 24] who have computed the energy levels of V_0 for the Coulombic case. A totally new feature is that new bound states appear from the continuum[25] when α_0 increases. The energy of these states *decreases* initially with α_0 before increasing as for the ground state. Although the appearance of the new bound states may seem surprising at first sight, given that the depth of V_0 decreases with α_0, it must be remembered that the number of bound states a potential can support depends not only on its depth but also its range. To illustrate this, if we approximate V_0 by a square well of depth $V_0(x=\alpha_0)$ and width $2\alpha_0$, the number, N, of bound states is given[26] approximately by the inequality

$$N\pi/2 < \alpha_0 \sqrt{2mV_0(x=\alpha_0)}/\hbar \leq (N + 1)\pi/2 \qquad (2.42)$$

For $\alpha_0 \gg \beta$, $V_0(x=\alpha_0) \sim 1/\alpha_0^{\frac{1}{2}}$ and so it is clear that as α_0 increases, the number of bound states will also increase.

The importance of these new bound states is that if resonances due to them are observed, they will have the added interest of being *entirely* laser–induced resonances. Of course, since we are including only part of the electron–potential –laser interaction, it is not clear that the new states will lead to any physically observable features. Nevertheless, at high frequencies, we might expect their influence to dominate. A calculation which takes the time–dependent parts fully into account will tell us under what conditions the dressing of the unperturbed potential is adequately described by V_0.

It has recently been suggested[27] that these new bound states are, in fact, quasi bound states of the original field–free potential and that their appearance here is an artifact of the neglect of the interchannel coupling. This has been shown not to be the case in two different calculations. In one of these, using the polarisation potential[28], it has been found that the width of the new bound states becomes infinite in the limit $\alpha_0 \to 0$, *i.e.* they are not bound states of the original potential. The second calculation, by Bardsley and Comella[29], has revealed new discrete states in the case of a Gaussian potential, $V(x) = -A \exp(-x^2/\beta^2)$, in the presence of a laser field. Their method was to calculate the quasi energies, W_n, of the Floquet states in the

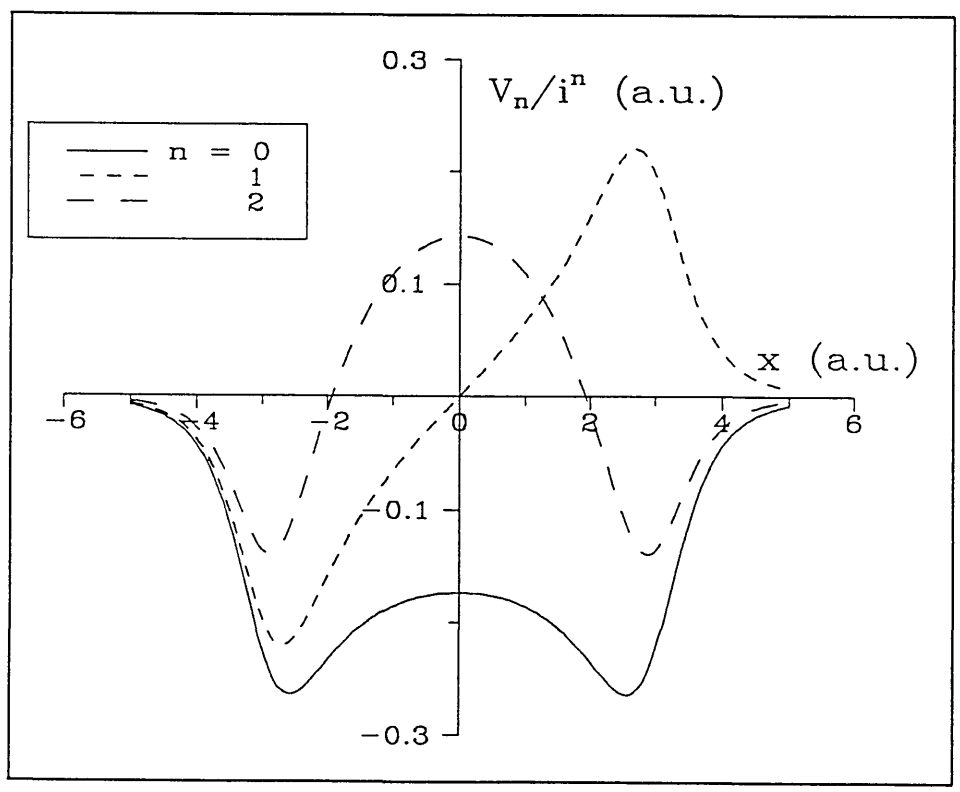

Figure 2.4 The higher order components $V_n(x)$ as a function of x for A = 1 a.u., β = 1 a.u.

p.A gauge. The Floquet states are not stationary states of V_0 alone, but they include the time–dependent interaction as well, and so the energies W_n are complex. The real part of the quasi energy representing the binding energy of the states has been found to follow a similar behaviour to that shown in Fig 3, while the complex part which represents the width is found to decrease with increasing α_0, confirming the results of the calculation with the polarisation potential.

In Fig 4, we compare $V_0(x)$ with $V_n(x)/i^n$ (n=1,2) for $\alpha_0 = 3$ a.u. From this figure, it is obvious that the magnitude of the higher order components is similar to that of V_0 at small and intermediate distances from the origin. In carrying out a scheme which involves treating the time–dependent parts as perturbations to $\tilde{H}_0$, one must be extremely cautious and not make the assumption that for $n \neq 0$, $V_n \ll V_0$. In Chapter 3, we shall address ourselves to the points raised here regarding the splitting up of the interaction in the Kramers–Henneberger picture into static and time–dependent parts.

References

1 H. A. Kramers in *Rapport et Discussions, Solvay Congress*, (Stoops, Belgium, 1948) p241.

2 T. Welton, Phys. Rev. 74 (1948) 1157.

3 W. C. Henneberger Phys. Rev. Lett. 21 (1968) 838.

4 C. Cohen–Tannoudji, J. Dupont–Roc and G. Grynberg, *Photons et Atoms*, (Interedition/ Editions du CNRS, 1987) p279.

5 E. A. Power, *Introductory Quantum Electrodynamics*, (Longman, London, 1964).

6 D. M. Volkov, Z. Physik 94 (1935) 250.

7 J. H. Eberly in *Progress in Optics* (North–Holland, Amsterdam, 1969) Vol VII, p361.

8 M Janjusevic and Y. Hahn (submitted to Phys. Rev. Lett.).

9 I. S. Gradshteyn and I. M. Ryzhik, *Table of Integrals, Series and Products*, (Academic Press, New York, 1980).

10 M. Abramowitz and I. A. Stegun, *Handbook of Mathematical Functions*, (Dover, New York, 1964).

11 C. K. Choi, W. C. Henneberger and F. C. Sanders, Phys. Rev. A 9 (1974) 1895.

12 S. K. Vermani and B. L. Beers, Phys. Rev. A 12 (1975) 715.

13 C. K. Choi, W. C. Henneberger, S. N. Mian and F. C. Sanders, Phys. Rev. A 12 (1975) 719.

14 E. A. Power and T. Thirunamachandran, Am. J. Phys. 46 (1978) 370. Also, E. A. Power in *Multiphoton Processes*, eds. P. Lambropoulos and J. Eberly, (Wiley,1978) p11.

15 R. F. O'Connell, Phys. Rev. A 12 (1975) 1132.

16 G. W. Ford and R. F. O'Connell, Phys. Rev. A 13 (1976) 1281.

17 P. Lambropoulos, E. A. Power and T. Thirunamachandran, Phys. Rev. A 14 (1976) 1910.

[18] P. L. Knight, Phys. Lett. A 60 (1977) 182.

[19] C. Lecompte, G. Mainfray, C. Manus and F. Sanchez, Phys. Rev. Lett. 32 (1974) 265.

[20] M. Gavrila, *Atoms in Unusual Situations*, ed J. P. Briand , NATO ASI Ser. B, Vol 143 (Plenum, New York, 1987) p255.

[21] M. Pont and M. Gavrila, Phys. Lett. A 123 (1987) 469.

[22] M. Pont, N. R. Walet, M. Gavrila and C. W. McCurdy, Phys. Rev. Lett. 61 (1988) 939.

[23] J. Van de Ree, J. Z. Kaminski and M. Gavrila, Phys. Rev. A 37 (1988) 4536.

[24] J. I. Gersten and M. H. Mittleman, J. Phys. B 9 (1976) 2561.

[25] R. Bhatt, B. Piraux and K. Burnett, Phys. Rev. A 37 (1988) 98.

[26] E. Merzbacher, *Quantum Mechanics*, (Wiley, 1970) p108.

[27] R. M. Potvliege and R. Shakeshaft, Phys. Rev. A 38 (1988) 6190.

[28] B. Piraux and N. Elander, ECAMP Conference, Bordeaux, April 1989.

[29] J. N. Bardsley and M. J. Comella, Phys. Rev. A 39 (1989) 2252.

CHAPTER 3

POTENTIAL SCATTERING OF ELECTRONS IN THE PRESENCE OF INTENSE LASER FIELDS

§3.1 *Introduction*

The scattering of charged particles in intense electromagnetic fields has been the object of much interest in the last two decades. If the scattering occurs in the presence of the electrostatic field of an atom or an ion, the charged particle can absorb or emit radiation. In intense electromagnetic fields, this may involve induced multiphoton transitions between the continuum states of the system. These free–free transitions (stimulated and inverse bremsstrahlung) are of importance in the heating of plasmas by lasers, as well as the cause of the opacity of the sun and cooler stars in the infrared. In atomic physics, interest in scattering in laser fields arises because of the possibility of observing laser–induced resonances.

This interest has stimulated a large amount of theoretical work particularly as the laser intensities considered are too high to allow a perturbative expansion in the projectile–laser interaction. Generally, the projectile is taken to be an electron, and its interaction with the atomic or ionic target is modelled by a potential. This assumption eliminates the possibility of exciting or ionising the target; in other words, its internal degrees of freedom are neglected. Moreover, this procedure is unable to take account of exchange effects between the incoming and target electrons. A recent perturbative calculation[1] of laser assisted electron–atom scattering has shown quite considerable modifications to the scattering cross–section when the effect of the laser field the on internal structure of the atom is included. Even the

simplified case where the atom is modelled by a potential has not been treated exactly except with further simplifications such as the use of a separable potential[2], or circularly polarised light[3].

The most well–known approximation in laser assisted scattering is the Kroll–Watson approximation[4] which, for strong fields and scattering potentials, is an expansion in the laser frequency ω, hence it is a low frequency approximation. However, the domain of validity has not yet been clearly established and a calculation with the Yukawa potential has shown that it may extend to higher frequencies and intensities than previously thought[5]. The approximation is described in Section (3.3), by way of introducing some of the concepts involved in radiative scattering, but before we do that, it is necessary to examine in some detail the states of a free electron in a laser field.

§3.2 Asymptotic States

One of the main differences between field–free and radiative scattering is the choice of asymptotic states. We may represent a typical experiment as follows. The space in which the electron moves is divided into five regions. In the first, the electron moves freely and enters the laser focus adiabatically. In the second region, the electron is under the influence of the laser field, and the simultaneous interaction with the potential and the laser field takes place in the third region. After the collision, the electron enters the fourth region where again only the laser field acts upon it. It then exits the laser focus adiabatically into the fifth region. This picture may be justified because typically, in an experiment, the laser focus has a diameter of the order of microns, while the target is of atomic dimensions.

In the above we have assumed a short range force (short range is assumed to

mean one that goes to zero faster than 1/r at large r) so that at distances far from the center of force and away from the laser field, i.e. in the first and fifth regions, the electron wavefunction is simply a plane wave:

$$\Psi(\underline{r},t) = \exp \frac{i}{\hbar}(\underline{p}'.\underline{r}-Et) \tag{3.1}$$

with

$$E = \frac{p'^2}{2m}. \tag{3.2}$$

If the potential is long range e.g. if it is Coulombic, then Eq (1) is not adequate to describe the wavefunction far from the centre of the potential because the effect of the potential cannot be ignored. For a Coulombic potential, a logarithmic phase factor must also be included[6a]. However, the potential due to polarisation effects outside an atom falls off faster than a Coulombic potential, and it is therefore realistic within the limitations of the work presented in this thesis to assume that such phase factors can be ignored. In the second and third regions, the electron wavefunction is given by the solution of the following Schrodinger Equation:

$$i\hbar \frac{\partial \Psi(\underline{r},t)}{\partial t} = \left\{ \frac{(\underline{p} + e\underline{A})^2}{2m} \right\} \Psi(\underline{r},t). \tag{3.3}$$

This solution is the Volkov function that we introduced in Chapter 2 and that we shall now denote by $\zeta_k(\underline{r},t)$ for clarity:

$$\zeta_k(\underline{r},t) = \exp \left\{ \frac{-i e^2}{2m\hbar} \int_{-\infty}^{t} d\tau\, \underline{A}^2(\tau) - \frac{ie}{m} \int_{-\infty}^{t} d\tau\, \underline{A}(\tau).\underline{k} - \frac{i\hbar k^2 t}{2m} + i\underline{k}.\underline{r} \right\} \tag{3.4}$$

with

$$\underline{k} = \underline{p}/\hbar. \tag{3.5}$$

As discussed in Chapter 2 the $\underline{A}^2$ term is not of interest here so we remove it by applying the transformation U_1 [Eq (2.5)]. The new wavefunction $\zeta'_k(\underline{r},t)$ is

$$\zeta'_k(\underline{r},t) = \exp\left\{ -i\underline{\alpha}_0.\underline{k} \sin \omega t - iEt/\hbar + i\underline{k}.\underline{r}\right\} \tag{3.6}$$

where we have assumed a sinusoidally oscillating laser field. Using the generator for the Bessel functions

$$e^{i z \sin\theta} = \sum_{n=-\infty}^{\infty} e^{in\theta} J_n(z), \tag{3.7}$$

Eq (6) may be written as

$$\zeta'_k(\underline{r},t) = \sum_{n=-\infty}^{\infty} J_n(\underline{\alpha}_0.\underline{k}) \exp(i\underline{k}.\underline{r} - i(E + n\hbar\omega)t/\hbar). \tag{3.8}$$

This expression shows that under the influence of the laser field, the electron absorbs and emits virtual photons of energy $\hbar\omega$. These transitions are virtual since a free electron cannot absorb or emit radiation and satisfy energy and momentum conservation at the same time. It is important to note that $\underline{k}$ in Eqs (4–8) is related to the *canonical* momentum by Eq (5).

In principle, the solution (4) is valid only if there are no spatial variations in the vector potential, $\underline{A}$. However, if the variation is sufficiently small over some region, then the electron wavefunction in that region is given by (4). Thus, the

wavefunction of an electron entering a laser field adiabatically will deform from the plane wave (1) to the corresponding Volkov state. Such an electron conserves its total kinetic energy, but behaves as if subject to a conservative force[7] derived from a scalar potential $V_{pond} = e^2A_0^2/2m$ with the momenta inside and outside the field related through

$$\langle p'^2 \rangle = \langle p^2 \rangle + \langle e^2A_0^2 \rangle \tag{3.9}$$

where the angle brackets denote a cycle average. On entering the field, some of the kinetic energy of the electron is converted to the jitter motion that a charged particle executes in an electromagnetic field. In the absence of a potential, this energy is regained as drift kinetic energy on leaving the field. This is the origin of one of the most striking aspects of experiments on Above Threshold Ionisation – the so called peak switching effect[8] which was discussed in Chapter 1. In scattering calculations, the asymptotic states are usually assumed to be the Volkov states. Electron detectors are always located outside the laser field, and so to make contact with experiment, one must relate the Volkov states in the second and fourth regions to electron states in the first and fifth regions. As long as the entry into and exit from the laser focus are adiabatic in the sense that the total kinetic energy of the electron is conserved, then one can simply replace the Volkov state by the plane wave solution with the momentum $\underline{p}'$ given by Eq (9). It is then adequate to work with the Volkov solutions only.

§3.3 *The Born and Kroll-Watson Approximations*

In the low–frequency limit, it is possible to derive rather simple expressions for the scattering cross–sections, which treat the field to all orders *i.e.* they are non–perturbative as far as the laser field is concerned. Standard time–dependent

scattering theory[6b] is used but with the Volkov states as the asymptotic states. The Schrodinger Equation (1.1) is formally solved by means of the retarded Green's function, $G^+(\underline{r},t;\underline{r}',t')$ for a free electron in an electromagnetic field defined by

$$\left[i\hbar\frac{\partial}{\partial t} + \frac{\hbar^2}{2m}\underline{\nabla}^2 + \frac{ie\hbar}{mc}\underline{A}.\underline{\nabla}\right] G^+(\underline{r},t;\underline{r}',t') = \delta(r-r')\,\delta(t-t') \tag{3.10}$$

where the A^2 phase factor is assumed to have been removed by the transformation U_1 [Eq (2.5)], since it affects all the states equally. The Green's function may be expressed in terms of the Volkov states (Eq 6) as follows

$$G^+(\underline{r},t;\underline{r}',t') = \frac{-i}{\hbar}\exp[-\varepsilon(t-t')]\,\Theta(t-t')\,(2\pi)^{-3}\int d\underline{k}\,\zeta_k(\underline{r},t)\,\zeta_k^*(\underline{r}',t') \tag{3.11}$$

dropping the primes on the Volkov functions for convenience. Here, Θ is the Heaviside step–function which together with the limit $\varepsilon \to 0^+$ in the exponential factor ensures that the Green's Function is retarded. The scattering solution $\Psi_k(\underline{r},t)$ of (2.3) is then

$$\Psi_k(\underline{r},t) = \zeta_k(\underline{r},t) + \int_{-\infty}^{t} dt' \int d\underline{r}'\, G^+(\underline{r},t;\underline{r}',t')\, V(\underline{r})\, \Psi_k(\underline{r}',t') \tag{3.12}$$

where we have imposed the boundary condition that the incoming electron is in a Volkov state with wavevector $\underline{k}$. Eq (12) may be solved iteratively to give

$$\Psi_k(\underline{r},t) = \sum_{n=0}^{\infty} [G^+V]^n\, \zeta_k(\underline{r},t) \tag{3.13}$$

which is substituted into the expression of the scattering matrix element for the transition $k_i \to k_f$[6b]

$$S_{k_f k_i} = \frac{-i}{\hbar} \langle \zeta_{k_f} | V | \Psi_{k_i} \rangle \qquad (3.14)$$

where the angle brackets denote integration over all time and space. This yields the Born series for the scattering matrix

$$S_{k_f k_i} = \frac{-i}{\hbar} \sum_{n=0}^{\infty} \langle \zeta_{k_f} | V[G^+V]^n | \zeta_{k_i} \rangle. \qquad (3.15)$$

Performing the integral over time gives

$$S_{k_f k_i} = -2\pi i \sum_{n=0}^{\infty} \sum_{j=-\infty}^{+\infty} \delta(E_{k_f} - E_{k_i} - j\hbar\omega)\, T^n_{k_f k_i}(j) \qquad (3.16)$$

where

$$E_{k_a} = \hbar^2 k_a^2 / 2m\hbar^2, \qquad a = f, i \qquad (3.17)$$

and the nth order contribution to the transition matrix element is

$$T^n_{k_f k_i}(j) = \langle \zeta_{k_f} | V[G^+V]^n | \zeta_{k_i} \rangle. \qquad (3.18)$$

with the bracket denoting a space integration only. Using Eqs (16) and (17) and the definition

$$T_{k_f k_i}(j) = \sum_{n=0}^{\infty} T^{n}_{k_f k_i}(j) \tag{3.19}$$

we obtain the differential cross–section[6c] for scattering accompanied by the exchange of j photons:

$$\frac{d\sigma}{d\Omega}(j,\underline{k}_f\underline{k}_i) = \frac{k_f(j)}{k_i}\left[\frac{m}{2\pi\hbar^2} T_{k_f k_i}(j)\right]^2 \tag{3.20}$$

where

$$k_f(j) = \frac{1}{\hbar}\sqrt{2m(E_{k_f} - E_{k_i} - j\hbar\omega)}\,. \tag{3.21}$$

Limiting the sum in (19) to just one term gives the first Born approximation for the differential cross–section:

$$\frac{d\sigma^1}{d\Omega}(j,\underline{k}_f\underline{k}_i) = \left[\frac{m}{2\pi\hbar^2}\right]^2\left[1 - \frac{j\hbar\omega}{E_{k_i}}\right]^2 |\tilde{V}(\Delta\underline{k})|^2 J_l^2(\Delta\underline{k}(j).\underline{\alpha}_0) \tag{3.22}$$

where

$$\tilde{V}(\Delta\underline{k}) = \int d^3r\, V(r)\, e^{-i\Delta\underline{k}.\underline{r}}, \quad \Delta\underline{k} = \underline{k}_f - \underline{k}_i \tag{3.23}$$

and $\Delta\underline{k}(j)$ is defined in a similar manner using Eq (21). The low–frequency approximation is obtained by assuming that the energy transfer $j\hbar\omega$ is small compared to the kinetic energy, hence

$$\frac{d\sigma^1}{d\Omega}(j,\underline{k}_f\underline{k}_i) \simeq J_l^2(\Delta\underline{k}(j).\underline{\alpha}_0)\,\frac{d\sigma^1}{d\Omega}(\underline{k}_f\underline{k}_i). \tag{3.24}$$

The second factor on the RHS is the first Born approximation for the differential

cross–section in the absence of the laser. Extending the analysis to the second and higher Born orders the following result is obtained in the low frequency limit

$$\frac{d\sigma}{d\Omega}(j,\underline{k}_f,\underline{k}_i) = \frac{k_f(j)}{k_i} J_j^2(\Delta\underline{k}(j).\underline{\alpha}_0) \frac{d\sigma}{d\Omega}(\underline{k}'_f,\underline{k}'_i) + O(\omega^2). \tag{3.25}$$

where $\frac{d\sigma}{d\Omega}(\underline{k}'_f,\underline{k}'_i)$ is the exact field free cross–section evaluated at the shifted momenta

$$\underline{k}'_a = \underline{k}_a + \frac{m j \omega \underline{\alpha}_0}{\hbar \underline{\alpha}_0 . \Delta\underline{k}}, \qquad a = f, i. \tag{3.26}$$

If the j dependence of $k_f(j)$ on the RHS of Eq (24) is neglected, the following cross–section sum rule may be obtained

$$\sum_{j=-\infty}^{\infty} \frac{d\sigma}{d\Omega}(j,\underline{k}_f,\underline{k}_i) = \frac{d\sigma}{d\Omega}(\underline{k}'_f,\underline{k}'_i) + O(\omega^2). \tag{3.27}$$

Eq (25) is the Kroll–Watson result[4]. It tells us that in the low frequency approximation, the scattering is modified in a basically very simple way by the laser field, being related to radiation–less scattering by the presence of the Bessel functions. This is because the electron–laser interaction is neglected in the intermediate states, and is only taken into account in the asymptotic states. This decoupling of the two different interactions is possible because the electron, having a high kinetic energy, spends a longer time in the initial and final states than in the intermediate states. For this reason, the Kroll–Watson result does not give any new information about the scattering process. The experimental results of Weingartshofer

et al[9]. have been shown to be in qualitative agreement with Eq (24); quantitative comparison is not possible because it is necessary to include the effects of the temporal and spatial shapes of the laser pulse[10] which were not known. The results are also consistent with the sum rule (27).

In deriving Eq (24), an expansion in powers of jω has to be made, therefore at high intensities and low incident energies when the number of photons exchanged is expected to be large, the theory is not valid. It is also not capable of describing scattering resonances. Recently, however, extensions to the Kroll–Watson result have been made in order to enable high laser intensity scattering to be treated[11]. The exact numerical calculations in one–dimension in the p.A gauge performed by Jung and Taylor[12] show that a Kroll–Watson type of low–frequency approximation suitably modified to treat resonances[13] shows good agreement at low photon energy and moderate intensity.

§3.4 *The Gavrila-Kaminski scheme*

In the low frequency approximation discussed above, the photon energy is much smaller than the incident energy of the electron, but with work on the development of VUV and X–ray lasers, when this condition would not be satisfied, the high photon energy case is becoming of more interest. A non–perturbative theory dealing with scattering in the presence of intense high–frequency laser fields has been presented by Gavrila and Kaminski[14] (GK). This is based on the Kramers–Henneberger transformation and uses an iterative procedure to calculate scattering amplitudes for inverse bremsstrahlung. They have derived formulae for the scattering amplitude at the two lowest orders in the high frequency limit (to be discussed further in the next section). Preliminary calculations indicate that when these high frequency conditions are satisfied, these two amplitudes dominate the scattering and

the scattering in the elastic channel (no photons absorbed or emitted) reduces to that from the time–averaged potential $V_0(\underline{\alpha}_0;\underline{r})$ discussed in Chapter 2. The scattering amplitude then exhibits large deviations from the field–free case.

The aim of the work presented in the remainder of this Chapter is to test this hypothesis by solving the problem exactly in the KH picture over a range of parameters, both in the high and low frequency regimes. We also consider some more general aspects of potential scattering, for example, the influence of the bound states of V_0 on the scattering amplitudes. Because an exact solution can only be obtained numerically, a complete solution in three–dimensions would be very complex and expensive in computer resources since the problem involves the solution of an infinite system of differential equations in which states of different angular momentum as well as different energy are coupled by the interaction with the potential and the field. We have therefore confined ourselves to a one–dimensional treatment where an exact solution is both possible and feasible, with the understanding that the lessons learnt from this will be valuable in tackling the full three–dimensional problem. In particular, it should provide information about the number of equations that must be taken into account.

§3.4.1 *Basic Formalism*

In the remainder of this chapter, we use atomic units unless otherwise stated. We start by considering the transformed Schrodinger Equation for the electron in one dimension, Eq. (2.10) and substitute into it the Fourier series for $V(x + \alpha_0 \sin \omega t)$:

$$i \frac{\partial \Phi(x,t)}{\partial t} = \left\{ -\frac{1}{2}\frac{d^2}{dx^2} + \sum_{n=-\infty}^{+\infty} V_n(\alpha_0;x)\, e^{-in\omega t} \right\} \Phi(x,t). \tag{3.28}$$

Since the potential is a periodic function of time, we invoke the Floquet theorem and seek a solution of the form

$$\Phi(x,t) = e^{-iE_i t} \sum_{n=-\infty}^{+\infty} \phi_n(x)\, e^{-in\omega t} \tag{3.29}$$

where E_i is the kinetic energy of the incident electron. Inserting Eq. (29) into Eq. (28), we get an infinite system of coupled differential equations for the components $\phi_n(x)$,

$$-\frac{1}{2}\frac{d^2}{dx^2}\phi_n + [V_0 - (E_i + n\omega)]\,\phi_n + \sum_{\substack{m=-\infty \\ (m\neq n)}}^{+\infty} V_{n-m}\,\phi_m = 0. \tag{3.30}$$

We shall refer to the components ϕ_n as channel functions. Their physical meaning is as follows. Each channel function ϕ_n corresponds to an electron state that has kinetic energy $E_n = E_i + n\omega$ as $x \to \pm\infty$. The boundary conditions of the problem are a flux of particles of energy E_i and momentum $k_i = \sqrt{2E_i}$ in the incoming channel and a flux of scattered particles of energy E_n and momentum $k_n = \sqrt{2E_n}$ in the outgoing channel n, with $n = 0, \pm1, \pm2, \ldots$. When $E_n > 0$, the outgoing channel is open *i.e.* the incident electron can make a transition to this channel and leave the interaction region with energy E_n while if $E_n \leq 0$, the channel is closed and the electron cannot leave the region. In fact, because the flux must be conserved in our model, the electron is not trapped forever, but absorbs enough photons so that its total energy becomes positive. The likelihood of the electron leaving the region with momentum k_n is indicated by the reflection and transmission amplitudes, R_n and T_n respectively.

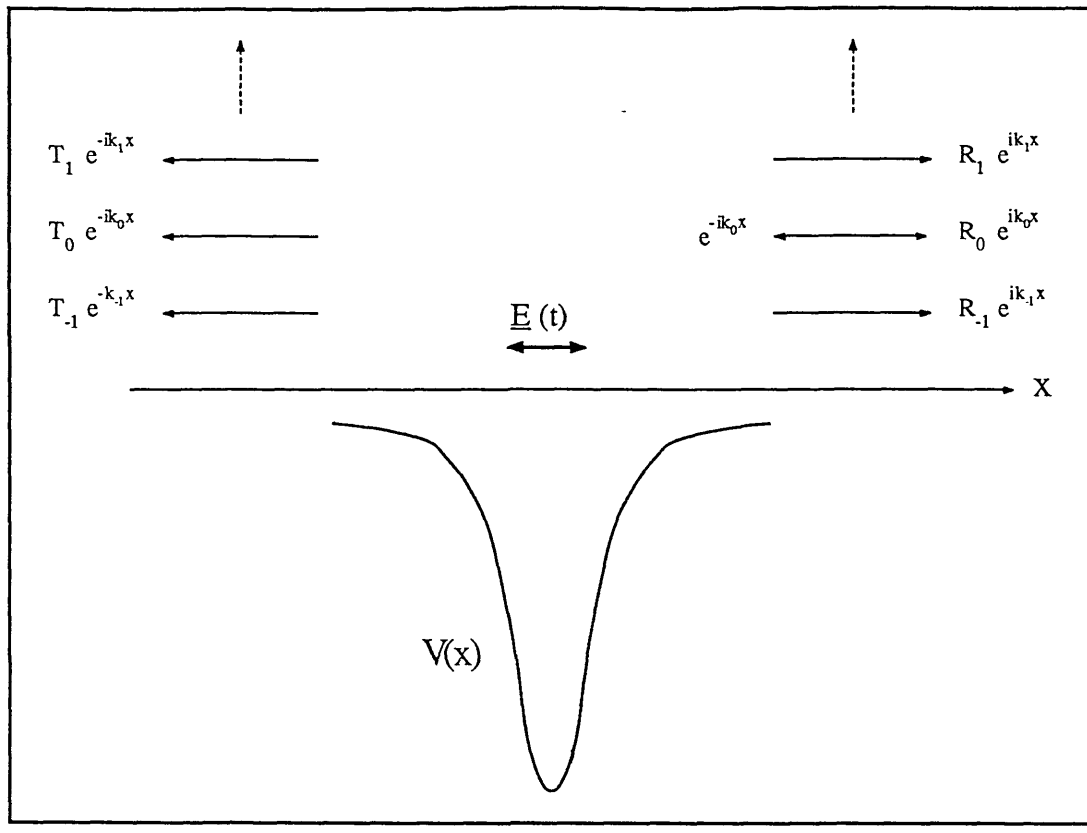

Figure 3.1 Geometry of the scattering problem.

The geometry of the problem is illustrated in Fig 1. The incident electron moves from the right ($x = +\infty$) towards the left ($x = -\infty$). In addition, we assume that all the Fourier components $V_n(x)$ of the potential $V(x + \alpha \sin \omega t)$ [see Eq. (2.40)] tend to zero faster than $1/x$ for large values of x. Under these conditions, the asymptotic behaviour is

$$\left.\begin{aligned} \phi_0(x) &\xrightarrow[x\to+\infty]{} e^{-ik_0x} + R_0\, e^{ik_0x} \\ \phi_0(x) &\xrightarrow[x\to-\infty]{} T_0\, e^{-ik_0x} \end{aligned}\right\} \qquad (3.31)$$

for the elastic channel and

$$\left.\begin{aligned} \phi_n(x) &\xrightarrow[x\to+\infty]{} R_n\, e^{ik_n x} \\ \phi_n(x) &\xrightarrow[x\to-\infty]{} T_n\, e^{-ik_n x} \end{aligned}\right\} \quad n \neq 0 \tag{3.32}$$

for the inelastic channels.

An analytic solution of system (30) does not exist, therefore we must resort either to some approximation or to numerical calculations. In the following, we shall describe one particular approximation scheme, that of GK as well as a method for obtaining the exact numerical solution. We shall then compare the results from the two methods.

§3.4.2 The High Frequency Approximation

In order to derive an iterative solution of system (30), we begin by introducing the retarded Green's operator $G^{(+)}(E)$:

$$G^{(+)}(E) = (E - \tilde{H}_0 + i\varepsilon)^{-1} \tag{3.33}$$

where $\tilde{H}_0$ has been defined in Eq (2.29) and ε is a small positive number. Note the difference between this operator and the one defined by Eq (10). While the latter includes the full interaction of the electron with the electromagnetic field and none of the electrostatic interaction V(x), the former includes a part of both interactions in the form of V_0. Formally, the channel functions ϕ_n are given by

$$|\phi_n\rangle = |\psi^{(+)}_{k0}\rangle \delta_{n0} - G^{(+)}(E_n) \sum_{\substack{m=-\infty \\ (m\neq n)}}^{+\infty} V_{n-m}\, |\phi_m\rangle \tag{3.34}$$

where $\psi^{(+)}_{k0}$ is the solution of

$$\tilde{H} \, |\psi_{k0}\rangle = \tfrac{1}{2}k_0^2 \, |\psi_{k0}\rangle \tag{3.35}$$

and satisfies the boundary conditions (31) with reflection and transmission coefficients R and T respectively. In Appendix A of this chapter, we show that R_n and T_n may be expressed as

$$R_n = R\,\delta_{n0} - (1-\delta_{n0})\frac{1}{ik_n}\left\{\langle\psi^{(-)}_{-k_n} \mid V_n \mid \psi^{(+)}_{k0}\rangle + \sum_{\substack{l \\ l\neq n}}\sum_{\substack{m \\ m\neq l}} \langle\psi^{(-)}_{-k_n} | V_{n-l}\, G^{(+)}(E_l)\, V_{l-m} \, |\phi_m\rangle\right\} \tag{3.36}$$

$$T_n = T\,\delta_{n0} - (1-\delta_{n0})\frac{1}{ik_n}\left\{\langle\psi^{(-)}_{+k_n} \mid V_n \mid \psi^{(+)}_{k0}\rangle + \sum_{\substack{l \\ l\neq n}}\sum_{\substack{m \\ m\neq l}} \langle\psi^{(-)}_{+k_n} | V_{n-l}\, G^{(+)}(E_l)\, V_{l-m} \, |\phi_m\rangle\right\} \tag{3.37}$$

Here, $\psi^{(-)}_{\pm -k_n}$ are solutions of (35) such that the 'incident' electron is moving away from the origin. They are related to $\psi^{(+)}_{\pm -k_n}$ by

$$\psi^{(-)}_{\pm -k_n} = \psi^{(+)*}_{\mp k_n} \tag{3.38}$$

An expansion for the R_n and T_n may be derived by repeatedly inserting (34) into (36) and (37). Gavrila and Kaminski[14] claim that successive terms will decrease rapidly and the first non–vanishing term of (36) and (37) represent a good

approximation to the exact result if the following conditions are met:

$$\omega \gg |E(\alpha_0)| \tag{3.39a}$$

$$\alpha_0^2\omega \gg 1 \tag{3.39b}$$

$$\omega \gg E_i \tag{3.39c}$$

where $E(\alpha_0)$ is the ground state energy of the static potential V_0. These conditions hold for high frequency, high intensity lasers. They were later revised to exclude (b) thus removing the restriction to intense lasers, while retaining the high frequency requirement. For $\alpha_0 \ll 1$ *i.e.* when the classical excursion amplitude of the electron in the field is much less than a Bohr radius, the usual perturbation theory result is recovered for large enough ω. At high intensities, the condition (a) becomes easier to satisfy if the frequency is held fixed since $|E(\alpha_0)| \to 0$ as $\alpha_0 \to \infty$ (see Fig 2.4). If both the conditions (a) and (c) are satisfied, it appears that the electron feels only the time–averaged potential V_0. It follows that R_n, T_n $(n \neq 0) \ll R_0$, T_0 since R_0 and T_0 represent the exact solution of the potential scattering problem with V_0 and hence must satisfy the condition $|R_0|^2 + |T_0|^2 = 1$. Note that the inequality (c) excludes the possibility of free–free emission while (a) and (c) together exclude the possibility of free–bound emission, the latter exclusion implying that the theory is unable to account for possible resonances due to transitions via bound states of either $V(x)$ or $V_0(x)$.

We have calculated numerically the lowest order terms contributing to R_n and T_n, the first non–vanishing terms of Eqs (36) and (37). In this approximation, we are essentially neglecting all inter–channel couplings, except those to the elastic (incoming) channel. The wavefunctions $\psi^{(-)}_{\pm k_n}$ and $\psi^{(+)}_{\pm k_n}$ were calculated by solving Eq (35) using a second–order Runge–Kutta method (NAG routine D02BBF) while the integral along the x–axis implied by the angle brackets in Eqs (36) and (37) was

carried out using a Gaussian quadrature method (with weights and abscissae obtained using NAG routine D01BCF). The results will be presented in Section (3.5).

To the best of our knowledge, the only other existing numerical calculations using the GK method are those that have been carried out by researchers working in collaboration with Gavrila and Kaminski[15–17]. These have concentrated on scattering in the elastic channel only (in three dimensions) and have not calculated the amplitudes for multiphoton transitions. In the first two of these, the cross–section for scattering from the angle–average of the potential $V_0(\underline{r})$ was calculated. More recently, J. Van de Ree *et al.*[17] have calculated the scattering amplitude in the elastic channel without carrying out the angle–average on $V_0(\underline{r})$, for the case where V(r) is a Coulomb potential. They have found that at zero scattering angle the amplitude coincides with the field–free case. As the angle is increased, large oscillations in the ratio of the two amplitudes are observed. The potential $V_0(\underline{r})$ behaves like a Coulomb potential, V_c, at large r (cf. Eq (2.40)) with a strong distortion for $r <\sim \alpha_0$. The oscillation has been interpreted by Van de Ree *et al.* as being due to interference between scattering from the original unperturbed Coulomb potential, V_c and that from a field induced potential, $V_0 - V_c$.

§3.4.3 *Exact calculations*

In this section we describe the procedure adopted to calculate the reflection and transmission coefficients exactly. We start by considering the set of equations (30) which for numerical purposes must be truncated to N equations with N given by

$$N = n_e + n_a + 1 \tag{3.40}$$

where $-n_e$ (≤ 0) and n_a (> 0) are the lower and upper limits in the sum over m. In the

following, we shall, for clarity, label the channel functions by Greek indices which will run from 1 to N instead of $-n_e$ to n_a.

From the theory of differential equations, the homogeneous system (30) has a set of 2N linearly independent solutions. Consequently, the channel function ϕ_β is a linear combination of 2N functions, each of which we denote by $\chi_{\beta,j}$ $(1 \le j \le 2N)$. These $\chi_{\beta,j}$ satisfy the following equation:

$$\frac{d^2}{dx^2}\chi_{\beta,j} = \sum_\sigma E_{\beta,\sigma}\,\chi_{\sigma,j}, \quad 1 \le j \le 2N \tag{3.41}$$

where $E_{\beta,\sigma}$ is given by

$$E_{\beta,\sigma} = 2\{V_{\beta-\sigma} - \delta_{\beta\sigma}\,[E_i - (n_e - \beta + 1)\omega]\}\,. \tag{3.42}$$

In terms of the functions $\chi_{\beta,j}$ the general solution may be written in matrix form as

$$\Phi(x) = \begin{bmatrix} \chi_{1,1} & \cdots & \chi_{1,N} \\ \vdots & & \vdots \\ \chi_{N,1} & \cdots & \chi_{N,N} \end{bmatrix} \underline{A} + \begin{bmatrix} \chi_{1,N+1} & \cdots & \chi_{1,2N} \\ \vdots & & \vdots \\ \chi_{N,N+1} & \cdots & \chi_{N,2N} \end{bmatrix} \underline{B} \tag{3.43}$$

where $\underline{A}$ and $\underline{B}$ are constant NxN matrices. Using this notation, the set of equations (30) becomes

$$\underline{I}\,\frac{d^2}{dx^2}\,\underline{\Phi}(x) = \underline{E}(x)\,\underline{\Phi}(x)\,. \tag{3.44}$$

$\underline{I}$ is the identity matrix and the elements of $\underline{E}$ are given by (42). The asymptotic behaviour corresponding to the expressions is described in this notation by

$$\underline{\Phi}(x) \underset{x \longrightarrow -\infty}{\longrightarrow} \begin{bmatrix} e^{-ik_1 x} & & 0 \\ & e^{-ik_2 x} & \\ & & \vdots \\ 0 & & e^{-ik_N x} \end{bmatrix} \underline{T} = \underline{K}^{-} \underline{T}, \tag{3.45}$$

$$\underline{\Phi}(x) \underset{x \longrightarrow +\infty}{\longrightarrow} \begin{bmatrix} e^{-ik_1 x} & & 0 \\ & e^{-ik_2 x} & \\ & & \vdots \\ 0 & & e^{-ik_N x} \end{bmatrix} \underline{J} +$$

$$\begin{bmatrix} e^{ik_1 x} & & 0 \\ & e^{ik_2 x} & \\ & & \vdots \\ 0 & & e^{ik_N x} \end{bmatrix} \underline{R} = \underline{K}^{-} \underline{J} + \underline{K}^{+} \underline{R}. \tag{3.46}$$

The wave vector k_n is defined by

$$k_n = \sqrt{2E_n}, \qquad E_n > 0 \tag{3.47}$$

for an open channel and

$$k_n = i\sqrt{|2E_n|}, \qquad E_n < 0 \tag{3.48}$$

for a closed channel. The elements of the J matrix are given by

$$J_{ij} = \delta_{n_e+1\ i}\, \delta_{n_e+1\ j}, \tag{3.49}$$

reflecting the fact that the only incoming flux occurs is the channel corresponding to the energy E_i. $\underline{R}$ and $\underline{T}$ are the reflection and transmission matrices respectively. We define the reflection and transmission coefficients in channel λ as follows:

$$r_\lambda = \frac{k_\lambda}{k_{n_e+1}} \left| R_{\lambda\, n_e+1} \right|^2, \tag{3.50}$$

$$t_\lambda = \frac{k_\lambda}{k_{n_e+1}} \left| T_{\lambda\, n_e+1} \right|^2. \tag{3.51}$$

Note that R_n and T_n in Eq (36) and (37) are equal to $R_{\lambda\ n_e+1}$ and $T_{\lambda\ n_e+1}$ respectively. With this normalisation, the conservation of probability is expressed as

$$\sum_\lambda (r_\lambda + t_\lambda) = 1, \tag{3.52}$$

where the sum over λ includes the open channels only.

In order to solve the set of equations, (44), numerically, we adopt the following procedure: First, we divide the x axis into three intervals, $I_1 = (-\infty, -x_t)$, $I_2 = (-x_t, x_t)$ and $I_3 = (x_t, +\infty)$. The cutoff, x_t is a positive number is chosen such that the solution $\underline{\Phi}(x)$ in the intervals I_1 and I_2 is given to a good approximation by the expressions (45) and (46). This will be the case when $|V_0| \ll |E_n|$ so that the matrix $\underline{E}$ defined by Eq (42) is approximately diagonal. From Eq (2.40) we see that x_t is essentially dependent on α_0 for given A; the larger α_0 is, the larger x_t will have to be.

Having determined the form of the solution at $x = x_t$, we may use that as a starting point for calculating the solution in the interval I_2. The problem is that the matrix $\underline{T}$ is unknown at this stage. The way we get around this is to replace it by a constant, arbitrary but non zero matrix $\underline{D}$. From now on, in order to maintain a distinction between the 'true' solution and the numerical one, we shall replace $\underline{\Phi}$ by $\underline{S}$ whenever we wish to refer to the numerical solution. Thus, our starting solution is

$$\underline{S}(x = -x_l) = \underline{K}^{-}\underline{D}. \tag{3.53}$$

This is merely a renormalisation of (45) i.e. there is some constant matrix $\underline{C}$, such that

$$\underline{D} = \underline{T}\,\underline{C}^{-1}, \tag{3.54}$$

and multiplying (53) by $\underline{C}$ regains (45). The solution at any point in I_2 may be calculated from Eq (41) using Eq (53) by means of some suitable integration algorithm. The algorithm used in the present calculation is based on the de Vogelaere method[18] which is detailed in Appendix C.

Having obtained the numerical solution, $\underline{S}(x)$, and its derivative with respect to x, $\underline{S}'(x)$, at $x = x_t$, we may extract the reflection and transmission matrices by matching them to the boundary condition (46) and its derivative. In doing this, we must remember to take account of the normalisation of the wavefunction. Therefore, instead of matching the numerically computed solution $\underline{S}(x_l)$ with (46), we must first multiply it by the matrix $\underline{C}$, so that

$$\underline{S}(x_l)\,\underline{C} = \underline{K}^{-}\underline{J} + \underline{K}^{+}\underline{R}, \tag{3.55}$$

The derivatives are matched in a similar way

$$\underline{S}'(x_l)\,\underline{C} = \underline{K}^{-}{}'\underline{J} + \underline{K}^{+}{}'\underline{R}, \tag{3.56}$$

where $\underline{K}^{+}{}'$ and $\underline{K}^{-}{}'$ are the first derivatives of $\underline{K}^{+}$ and $\underline{K}^{-}$ respectively. Equations (55) and (56) are easily solved for $\underline{R}$ and $\underline{C}$ to give

$$\underline{R} = (\underline{S}'^{-1}\,\underline{K}^{+\prime} + \underline{S}^{-1}\,\underline{K}^{+})^{-1}\,(\underline{S}^{-1} - \underline{S}'^{-1})\underline{K}^{-}\underline{J}\,, \tag{3.57}$$

$$\underline{C} = \underline{S}^{-1}\,(\underline{K}^{-}\underline{J} + \underline{K}^{+}\underline{R})\,. \tag{3.58}$$

Thus we see that this procedure uniquely determines the reflection matrix $\underline{R}$ as well as the matrix $\underline{C}$ and hence the transmission matrix $\underline{T}$ given by Eq (54). It is obviously convenient to choose $\underline{D} = \underline{I}$, in which case $\underline{T}$ is obtained directly from Eq (58).

§3.5 *Results and Discussion*

In this section, we present the results of our numerical calculations of the reflection and transmission coefficients using both the GK approximation and the exact method. The tests used to check the results are described briefly in appendix B. The plan of the section is as follows. We begin with a short discussion of some technical aspects of the exact numerical calculation. Then we present some exact results, and compare them to the field–free case. This is followed by an assessment of the validity of the GK approximation in various regimes.

§3.5.1 *Number of channels*

Since an exact numerical solution of the Schrodinger Equation for a realistic situation is feasible only if the size of the system is not too large, we begin by discussing the number of channels that must be taken into account. In other words, we need to know the smallest number, N, at which we may truncate the system of differential equations (30) and still obtain an accuracy of the order of, say, 1%. Ideally one should check this for each point in the parameter space which includes, in our one–dimensional case, the laser intensity and frequency, the incident energy

of the electron and the constants A and β that appear in the definition of the polarisation potential. Clearly, this is difficult if not impossible to achieve in practice and therefore it would be useful to uncover some general trends by studying a few cases. We shall discuss three particular cases in detail; of these, two violate the GK conditions (39a) and (39c). The parameters relevant to the three cases, which we shall refer to as A, B and C are displayed in Table 1. In Figs (2) to (4), we present results for $E_i = 0.1$ eV which satisfies the condition $E_i \ll \omega$.

CASE	A (a.u.)	ω (eV)	α_0 (a.u.)	$\lvert E_0 \rvert$ (eV)
A	1.0	1.8	3.0	4.4
B	1.0	10.0	2.0	5.8
C	0.2	6.0	10.0	0.25

Table 1: Parameters for the cases A, B, and C.

Each figure consists of a reflection or transmission coefficient plotted against the total number of channels, N_T, included in the calculation for that point. N_T is increased so that it starts at 1, *i.e.* the elastic channel, then (reverting to the original notation for the channel functions) n = 1 is included, followed by n = –1, n = 2, n = –2, and so on. Note that the N_T = 1 case corresponds to purely elastic scattering from the static potential $V_0(\alpha_0;x)$. It must be emphasised that although the number of equations is truncated, the system is solved exactly in the sense that the coupling V_{n-m} between the channels n and m ($-n_e \le n,m \le n_a$) is treated exactly. We discuss in Appendix B what happens if some of these couplings are neglected.

It is expected that when the scattering may be described to a good approximation in terms of V_0 only, inclusion of more than one channel should make only a small difference to the coefficients. This could occur, for example, when the

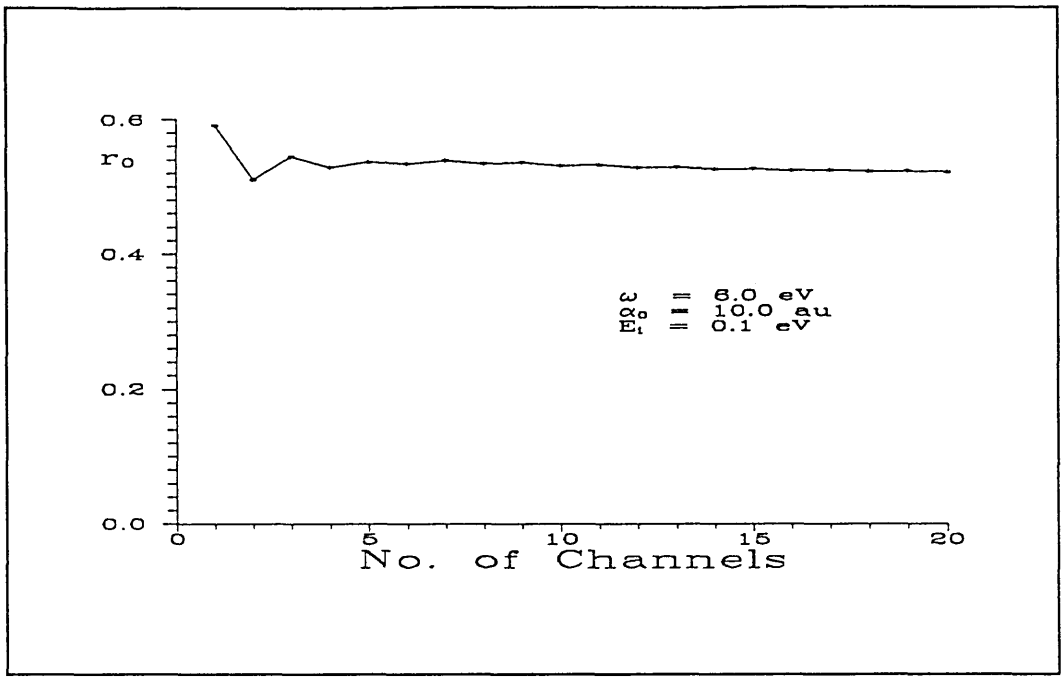

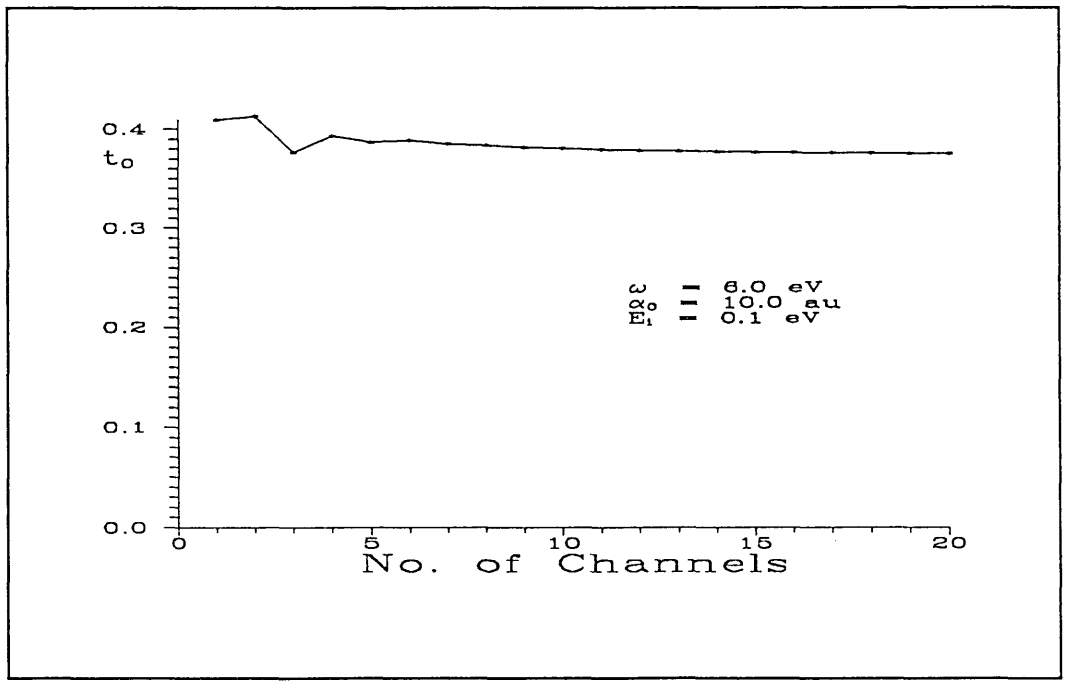

Figure 3.2 Reflection and transmission coefficients r_0 and t_0 in the elastic channel for case C vs total number of channels included in the exact calculation. A = 0.2 a.u., β = 1 a.u.

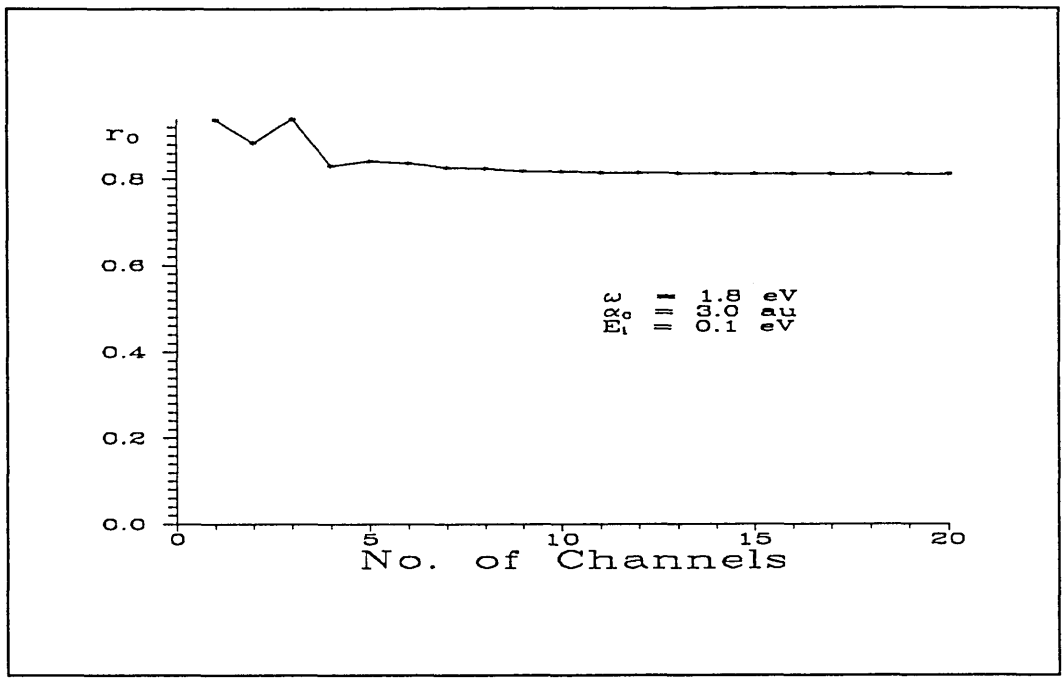

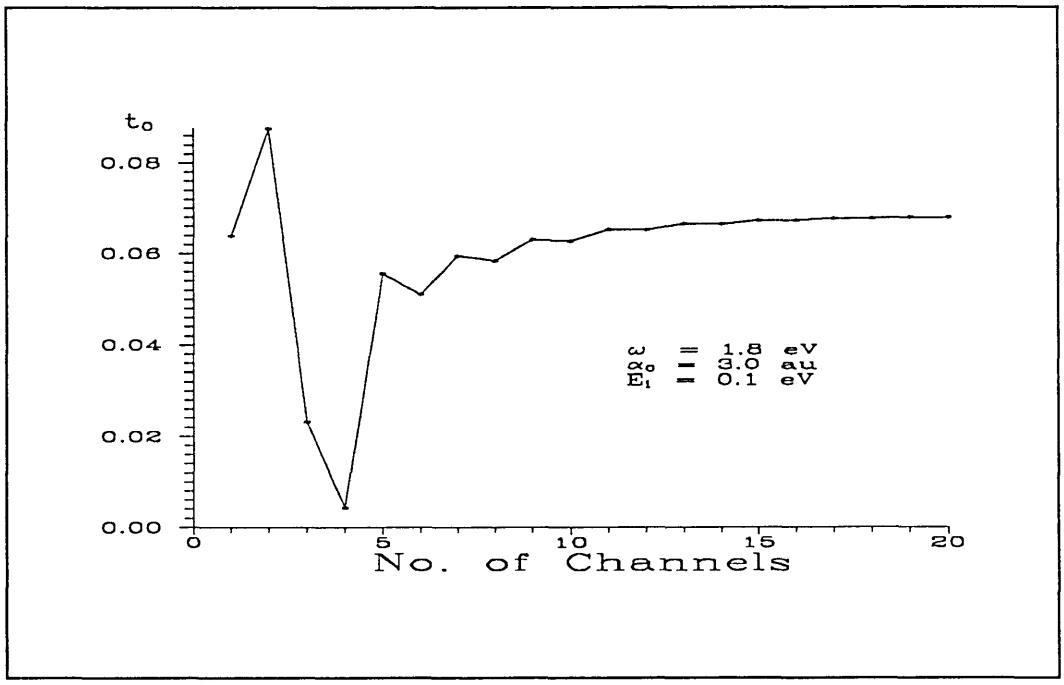

Figure 3.3 Reflection and transmission coefficients r_0 and t_0 in the elastic channel for case A vs total number of channels included in the exact calculation. A = 1 a.u., β = 1 a.u.

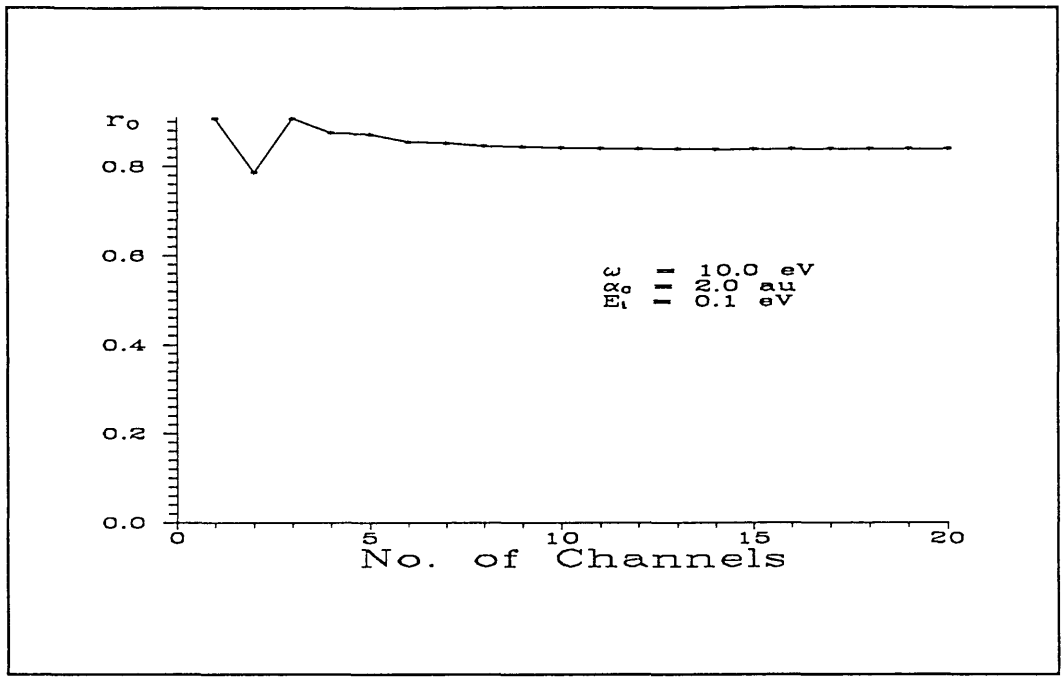

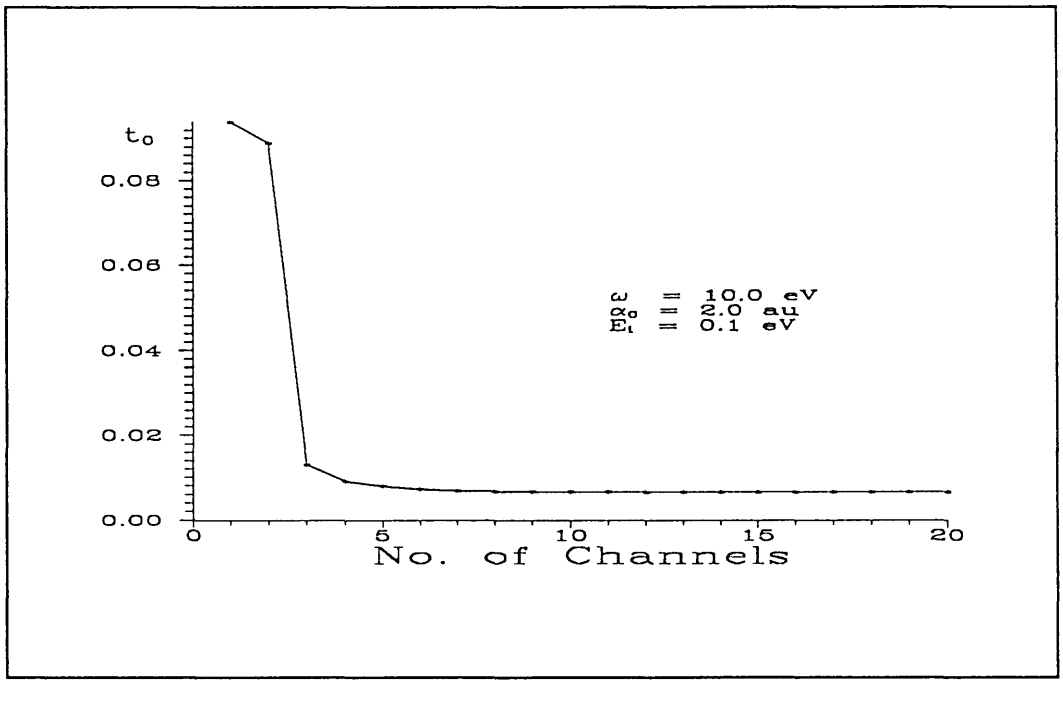

Figure 3.4 Reflection and transmission coefficients r_0 and t_0 in the elastic channel for case B vs total number of channels included in the exact calculation. A = 1 a.u., β = 1 a.u.

GK conditions are satisfied, as in case C for small enough incident energy. We see from Fig (2) that is indeed true – inclusion of each additional channel causes a fractional change in both r_0 and t_0. The behaviour in cases A (Fig 3) and B (Fig 4) is quite different. In case A, t_0 fluctuates considerably with N_T before stabilising when N_T is greater than around 17. The value at $N_T = 1$ is not very different from that at $N_T = 20$, but this is not true in general for any value of E_i and, in fact, we shall see later that large deviations from scattering purely by V_0 do occur.

By contrast, in case B, t_0 exhibits a dramatic drop from its value at $N_T = 1$ to that at $N_T = 3$ after which it stabilises relatively quickly. This implies that the coupling

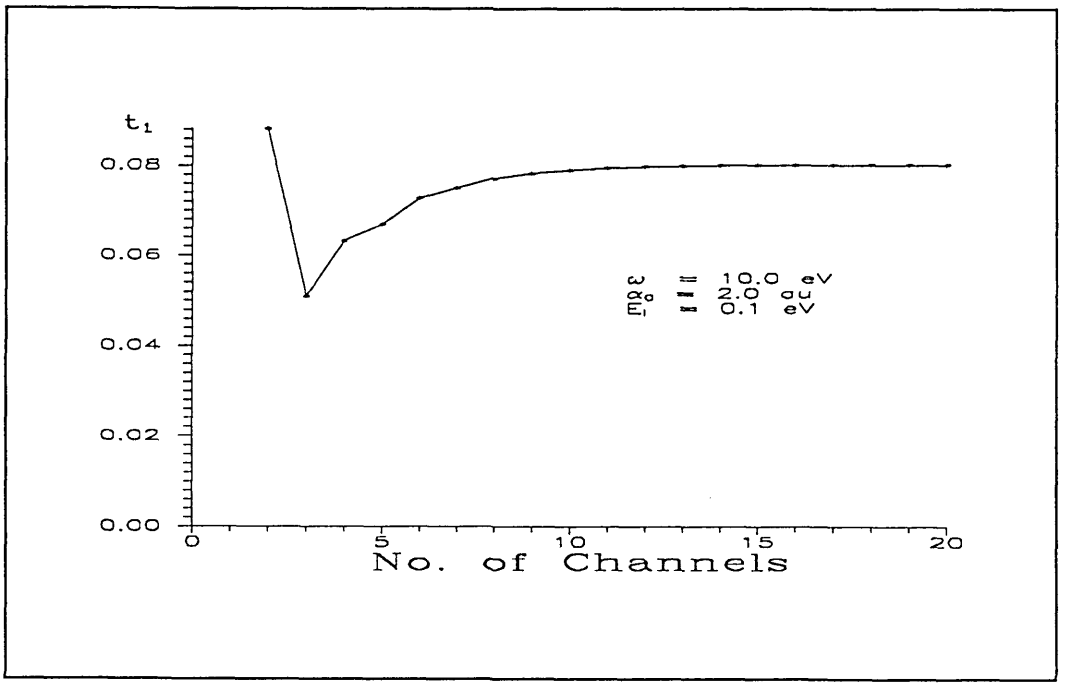

Figure 3.5 Transmission coefficient t_1 with one photon absorbed for case B vs total number of channels included in the exact calculation. A = 1 a.u., β = 1 a.u.

between the channel functions ϕ_{-1}, ϕ_0 and ϕ_1 is particularly strong. The reason for this may be the occurrence of a bound state of V(x) at energy E = –10.88 eV which is almost one–photon resonant with the incoming electron. Resonant enhancement of multi–photon transitions via this state could explain the fact that the biggest drop is seen when the channel ϕ_{-1} is introduced, allowing the emission of one photon by the incoming electron. In Fig (5), we see that the introduction of the channels ϕ_{-2} and ϕ_{-3} also causes a significant change (around 5–10%) in t_1; this is remarkable because these channels correspond to energies well below the bound state of both V(x) and $V_0(x)$, but the reason for this is not clear.

It should be noted that the trends described above occur not only in the elastic channel, but also in the inelastic ones. As n, the number of photons exchanged, increases, the number of channels required for r_n and t_n to stabilise also increases. However, for the purposes of this thesis, we are mainly concerned with values of n that are rather small, which in the regimes we consider represent the dominant channels. Therefore 15–20 channels are sufficient in general to achieve an acceptable accuracy.

§3.5.2 *Dependence on Incident Energy*

Fig 6 illustrates the reflection and transmission coefficients r_0 and t_0 as a function of the energy of the incident electron for case A. For comparison we have also included the coefficients for radiation–less scattering from V(x) as well as from $V_0(x)$ alone. These will be referred to as r_n' and t_n' and r_n^{GK} and t_n^{GK} respectively. the most striking feature about the exact solution is the presence of cusps, which are more apparent in t_0 than r_0. These are separated by the photon energy E_L (= ω in a.u. or 27.2 × ω in eV) and they correspond to the opening up of new channels. In other words, the nth cusp corresponds to the incident electron having enough kinetic

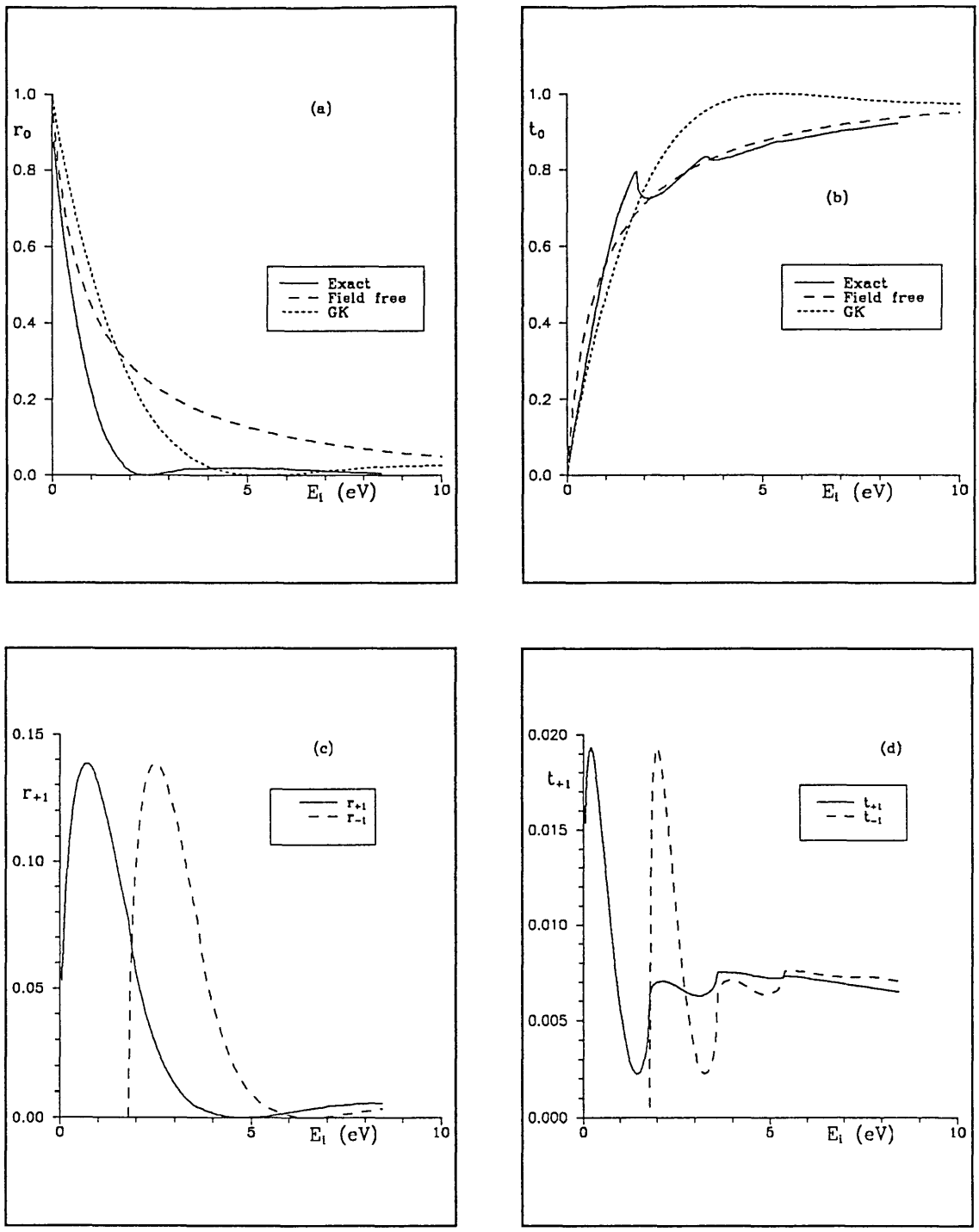

Figure 3.6 Reflection coefficient and transmission coefficients as functions of the incident energy E_i for case A. (a) and (b) elastic channel, (c) and (d) inelastic channels with exchange of one photon. ω = 1.8 eV, α_0 = 3 a.u., A = 1 a.u., β = 1 a.u.

energy for the emission of n photons. Naturally, the cusps are absent for the scattering from V(x) and $V_0(x)$ alone because they are single channel problems.

Another notable feature of these graphs is the difference between the exact solution and the approximate GK one represented by scattering from $V_0(x)$ alone in the case of the elastic channel. The discrepancy is to be expected because as we see from Table 1, the laser frequency is of the order of both the energy of the ground state of V_0 as well as the incident energy, thus violating the conditions (a) and (c). Having said that, we observe that both the exact and 'approximate' reflection coefficients have a feature in common: they exhibit minima at which they both go to zero on the scale of this graph. These minima are not present in r_0'.

To understand the origin of the minimum in r_0^{GK}, we go back to Fig (2.1) and note that as α_0 increases, $V_0(x)$ begins to look rather like a square well. This analogy with the square–well that we have already used in Chapter 2, will be useful in discussing many of the results in this Chapter. It is well known that the transmission coefficient for a square well peaks to unity whenever the condition

$$\kappa a = n\pi \tag{3.59}$$

is satisfied. Here, $\kappa = \sqrt{[2(E_i - v)]}$, v is the depth and a the width of the well and n = 1, 2, 3, ... If as in Chapter 2, we approximate $V_0(x)$ by a square well of width $2\alpha_0$ and depth $V_0(\alpha_0)$; for $\alpha_0 = 3$, we find a = 6 a.u. and $v \simeq 0.23$ a.u. With these values and n = 1, Eq (59) gives a negative value for E_i , but with n = 2, we get $E_i \simeq 9$ eV while for n = 3 we get $E_i \simeq 27$ eV for minima in r_0^{GK}. While these values are not very close to those seen in Fig 6, they are rather sensitive to the choice of a; for example, if we choose a = 7, we get $E_i = 5$ eV and 18 eV instead. Nevertheless, this analogy does qualitatively explain the reason for the minimum in r_0^{GK}. It appears

that although the full scattering solution is not well described by the the GK approximation in this regime, it is possible that the minimum in r_0 is due to the same reason, but modified by the strong influence of the higher order components $V_{\pm 1}$, $V_{\pm 2}$ etc.

We now turn our attention to inelastic transmission and reflection. In Figs 6c and 6d, we have plotted $r_{\pm 1}$ and $t_{\pm 1}$ as a function of E_i again for the case A. We see immediately that $t_{+1}(E_i) = t_{-1}(E_i + \omega)$. Further results, not shown here, prove that $t_{+n}(E_i) = t_{-n}(E_i + n\omega)$, with an analogous relation for the reflection coefficients. If the frequency of the laser were very small compared with the incident energy, then we would find that $t_{+1}(E_i) \simeq t_{-1}(E_i)$ *i.e.* absorption and emission would be symmetric with respect to the number of photons exchanged, exactly as seen in the experiment of Weingartshofer *et al.*[9] (see Figure 1.3).

We also observe narrow peaks at $E_i \simeq 0.2$ eV in t_{+1} and at $E_i \simeq 2.0$ eV in t_{-1} and wider peaks in $r_{\pm 1}$ at slightly higher energies. There is a new bound state of V_0 at $E = -1.6$ eV for this value of α_0 and the peaks, particularly in the transmission coefficients, occur at the right energies for the incident electron to have undergone multi–photon transitions via the bound state. We have plotted t_{+1} as a function of E_i in the vicinity of the peak for several values of α_0 in Fig 7. It is seen that the peak disappears when $\alpha_0 = 1$, when V_0 has only one bound state which is the low–lying ground state. This suggests that the peaks may be resonances due to the new bound state, but further calculations are required to ascertain this. Since it is hard to predict the best conditions for observing resonances, to establish firmly the existence of such laser induced resonances, one would need to scan a range of parameters (α_0, ω, A, β) and match the energies at which peaks occur with the bound state energy levels of V_0. This would be computationally expensive, and limited resources have prevented

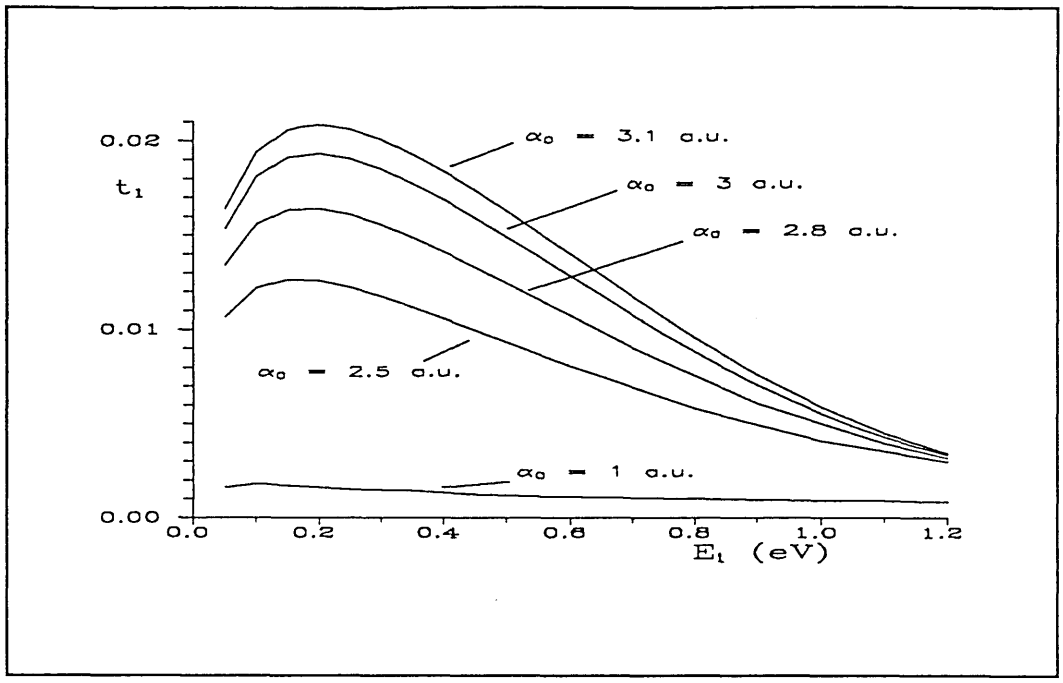

Figure 3.7 Transmission coefficient t_{+1} as a function of the incident energy for case A, but different values of α_0. ω = 1.8 eV, A = 1 a.u., β = 1 a.u.

us from examining this further. But it could be a promising path to follow, particularly in view of the results of Bardsley and Comella[19] who have also found new bound states, even when the time–dependent components have been included.

Peaks are also observed in the graphs of r_{+1} and t_{+1} for case B (Fig 8c, d). This time the new bound state is at –0.87 eV which is too high to be important at the photon and incident energies considered here. However, the ground state of V_0 is at –5.8 eV and again the peaks in r_{+1} and t_{+1} are at an energy approximately corresponding close to the absorption and re–emission of one photon. As before, these peaks do not appear in r_0 or t_0 (Fig 8a, b). There is a peak in t_0 at around

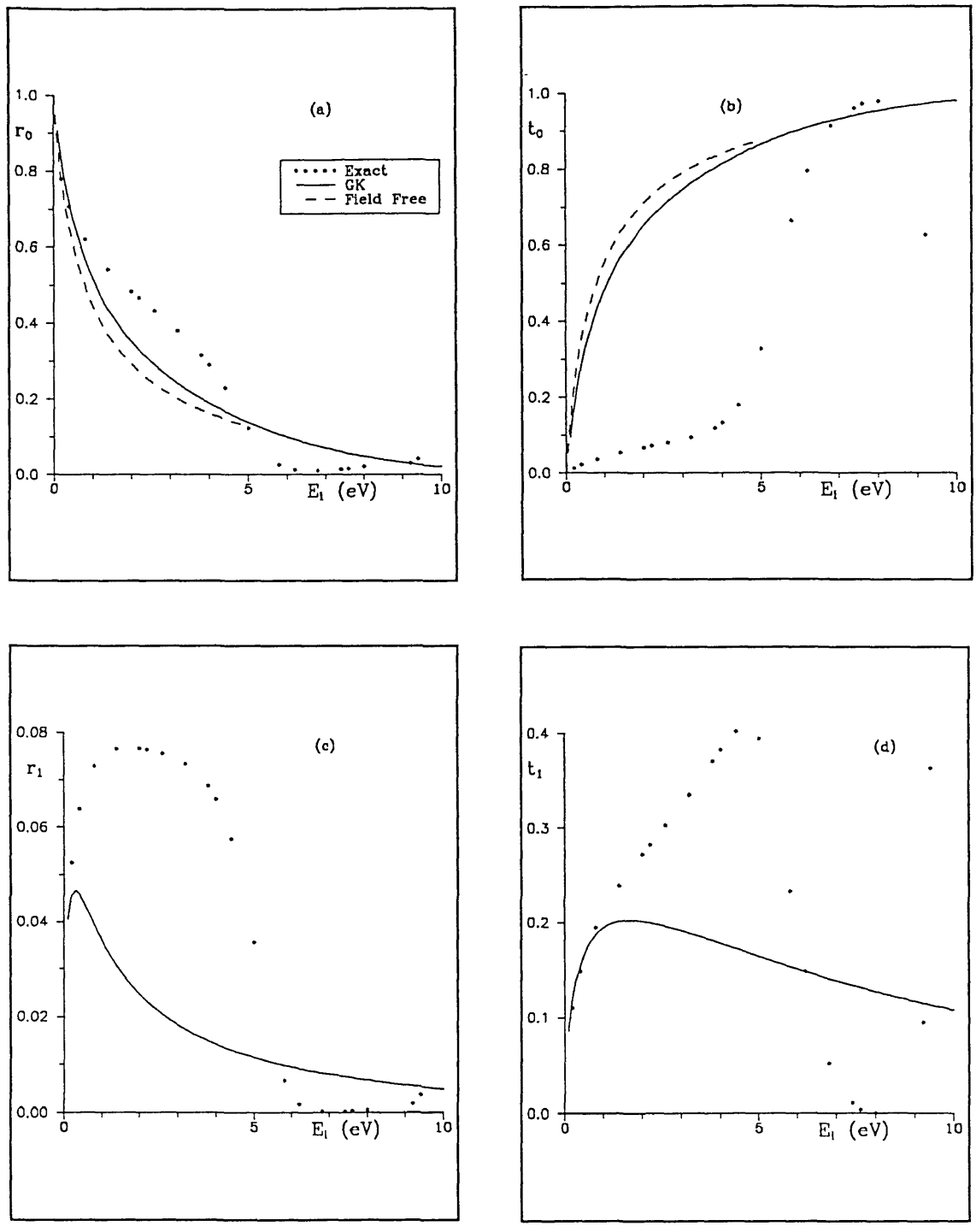

Figure 3.8 Reflection and transmission coefficients as functions of the incident energy E_i for case B. (a) and (b) elastic channel, (c) and (d) inelastic channel with absorption of one photon. ω = 10 eV, α_0 = 2 a.u., A = 1 a.u., β = 1 a.u.

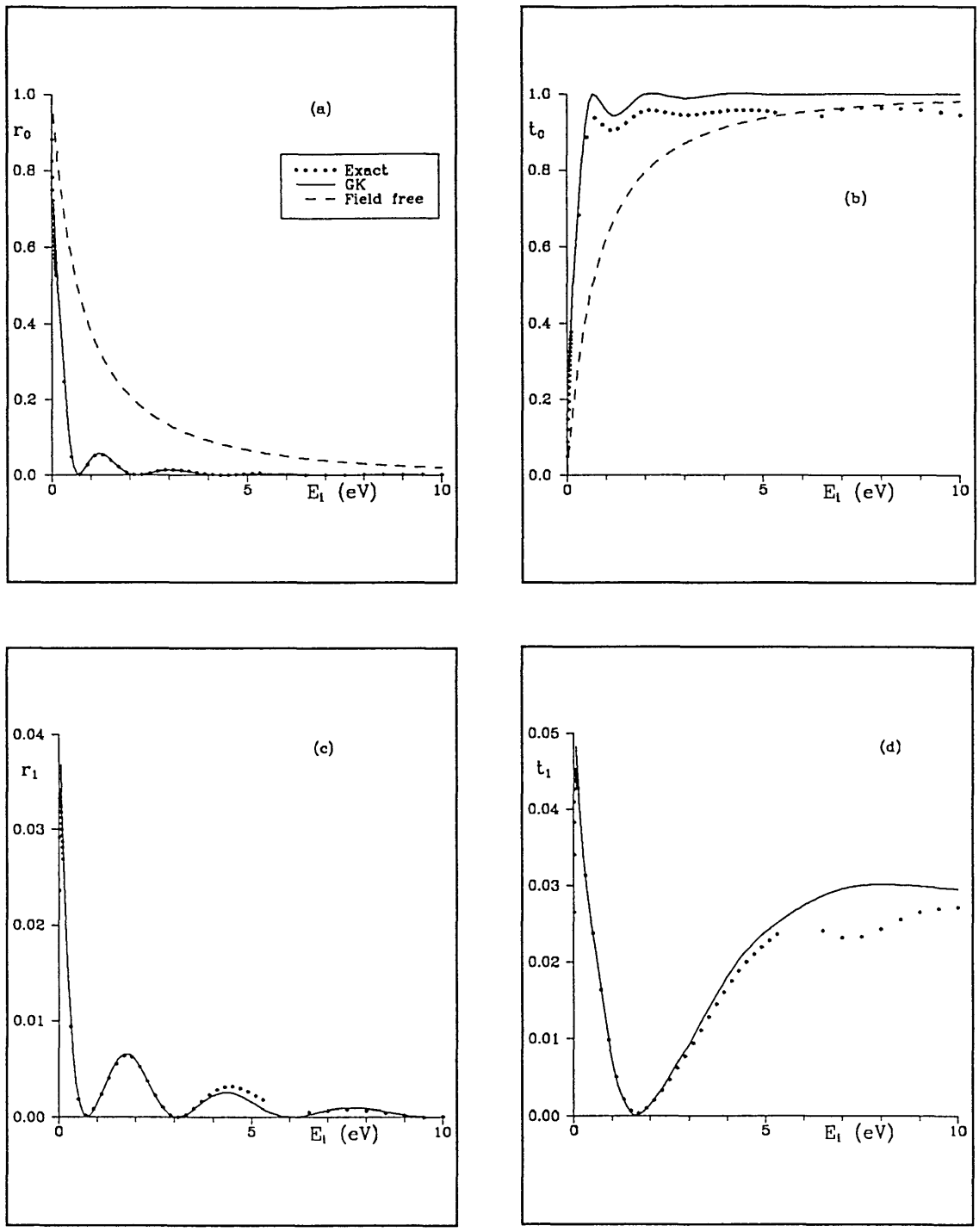

Figure 3.9 Reflection and transmission coefficients as functions of the incident energy E_i for case C. (a) and (b) elastic channel, (c) and (d) inelastic channel with absorption of one photon. $\omega = 6$ *eV,* $\alpha_0 = 10$ *a.u.,* $A = 0.2$ *a.u.,* $\beta = 1$ *a.u.*

$E_i \simeq 7.5$ eV which cannot be identified with either any bound state or a resonance of the square well type. We also note that the GK approximation is completely dissimilar to the exact solution, the laser frequency being of the same order as the energy of the ground state of V_0. Note that because α_0 is small enough that the distortion of V_0 compared to V is not too great, the field free scattering is close to that from V_0 only.

So far, we have concentrated on a potential that is deep compared to the photon energy: For A = 1, V(0) = 27.2 eV. In addition α_0 has been quite small so that even allowing for the fact that the ground state energy increases with α_0, the laser frequency still does not satisfy condition (39a). In case C, the ground state energy for V_0 is at –0.25 eV and hence for small enough incident energies, we expect the GK approximation to be in good agreement with the exact results. Fig 9 confirms that the approximation is a good one for small incident energies. In fact, it appears to give good results, at least for r_0, r_{+1} and t_{+1}, over a wider range of energies than might be implied by condition (39c). The positions of the minima in r_0 (and the corresponding peaks in t_0) can be predicted fairly well by our earlier prescription of approximating the potential V_0 by a square well of depth $V_0(\alpha_0)$ and width $2\alpha_0$. This gives the values $E_i \simeq 0.6$ eV, 2.4 eV, 4.7eV for the positions of the first three minima, which inspection of Fig (9a) shows to be quite close.

Up to this point, our exact results seem to confirm the claim of GK that provided the conditions (39 a,c) are met, the lowest non–vanishing terms of Eqs (36) and (37) will provide an adequate solution of the scattering problem. We shall now make a more detailed analysis of the conditions under which this is true. This will be done in two ways: first we shall calculate the transmission and reflection coefficients for fixed laser frequency and incident energy, but with varying intensity and then with fixed α_0 but varying frequency. This should help to put the limits of validity of

the GK approximation on a firm footing.

§3.5.3 *Dependence on* α_0

Fig 10 shows r_0, r_1, t_0 and t_1 as a function of α_0 when $\omega = 6$ eV, $E_i = 0.1$ eV, $A = 0.2$ a.u. and $\beta = 1$ a.u. The fact that α_0 is varying means that the shape of the potential V_0 is also changing: it becomes wider and more shallow (see Fig 2.1) and so for a fixed incident energy, we observe resonance peaks at different α_0. As is apparent from the figure, the GK approximation gives results that are quite close to the exact ones, except in the region 3 a.u. $< \alpha_0 <$ 8 a.u. where there is a peak in t_0. As before, the position of this peak may be roughly estimated by Eq (59).

In Fig 11, we have plotted the same quantities but for a deeper well ($A = 1.0$) and higher frequency ($\omega = 10$ eV). It is quite clear from this figure that in the regions where there is a resonance in the scattering of the incident electron by V_0, the GK approximation is not valid. In some cases, the approximation even gives coefficients that are greater than 1. Examination of Figs 1.4 and 1.5 shows that the condition (39a) is satisfied for all the values of α_0 in Fig 10 and for $\alpha_0 > 10$ a.u. in Fig 11.

The reason for the discrepancy is probably as follows: When there is a transmission resonance, the electron wave undergoes multiple reflections inside the well. In wavepacket terms, the particle spends a longer time in the potential well when the mean energy of the wavepacket corresponds to a resonance energy than it would otherwise. This means that it experiences the influence of the higher order components for a greater length of time and our assumption that the wavefunction is dominated by the elastic channel breaks down. Therefore, whenever the incident energy of the particle is such that it is close to a resonance, we may expect

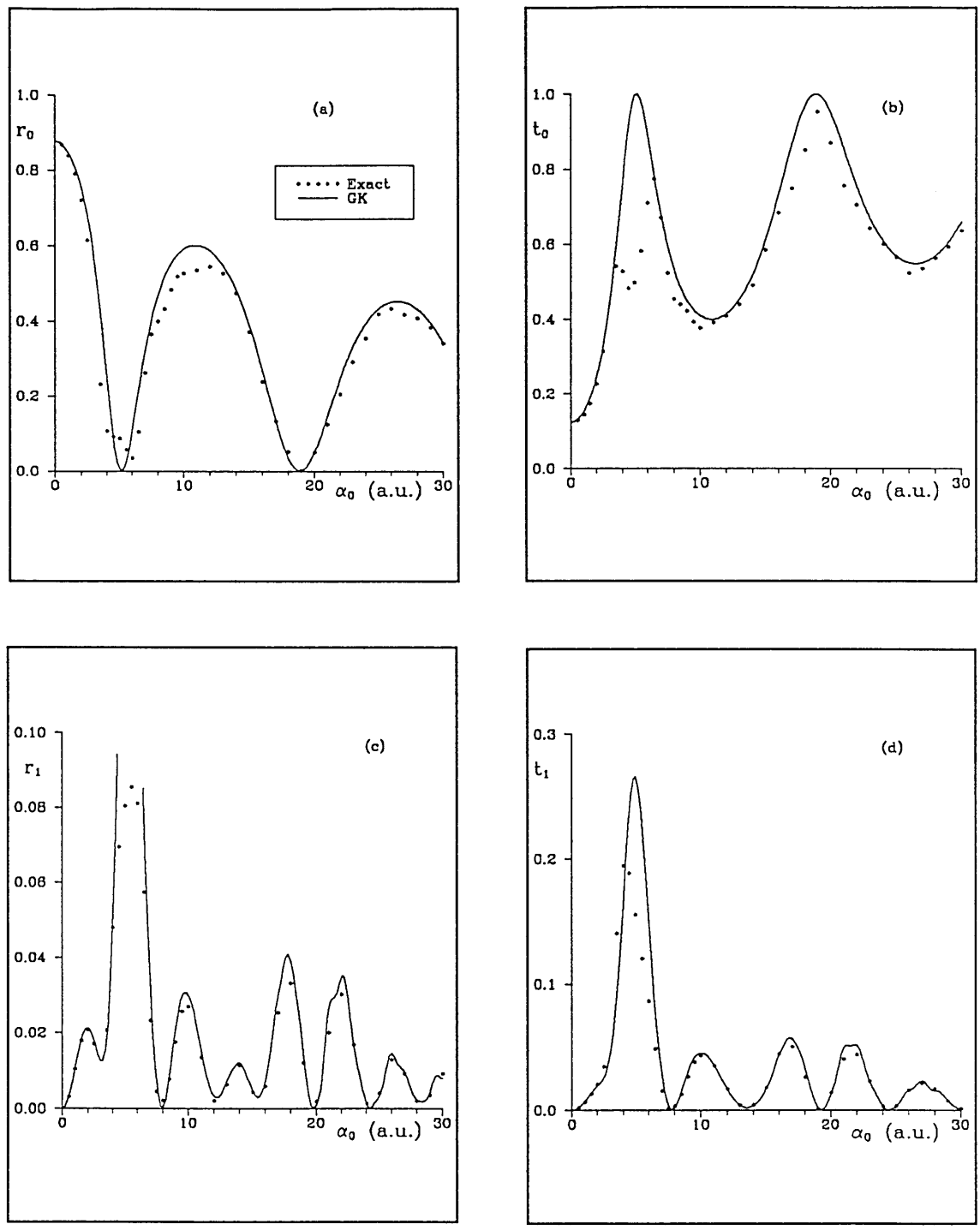

Figure 3.10 Reflection and transmission coefficients as functions of the laser parameter α_0. *(a) and (b) elastic channel, (c) and (d) inelastic channel with absorption of one photon.* $\omega = 6$ *eV,* $E_i = 0.1$ *eV,* $A = 0.2$ *a.u.,* $\beta = 1$ *a.u.*

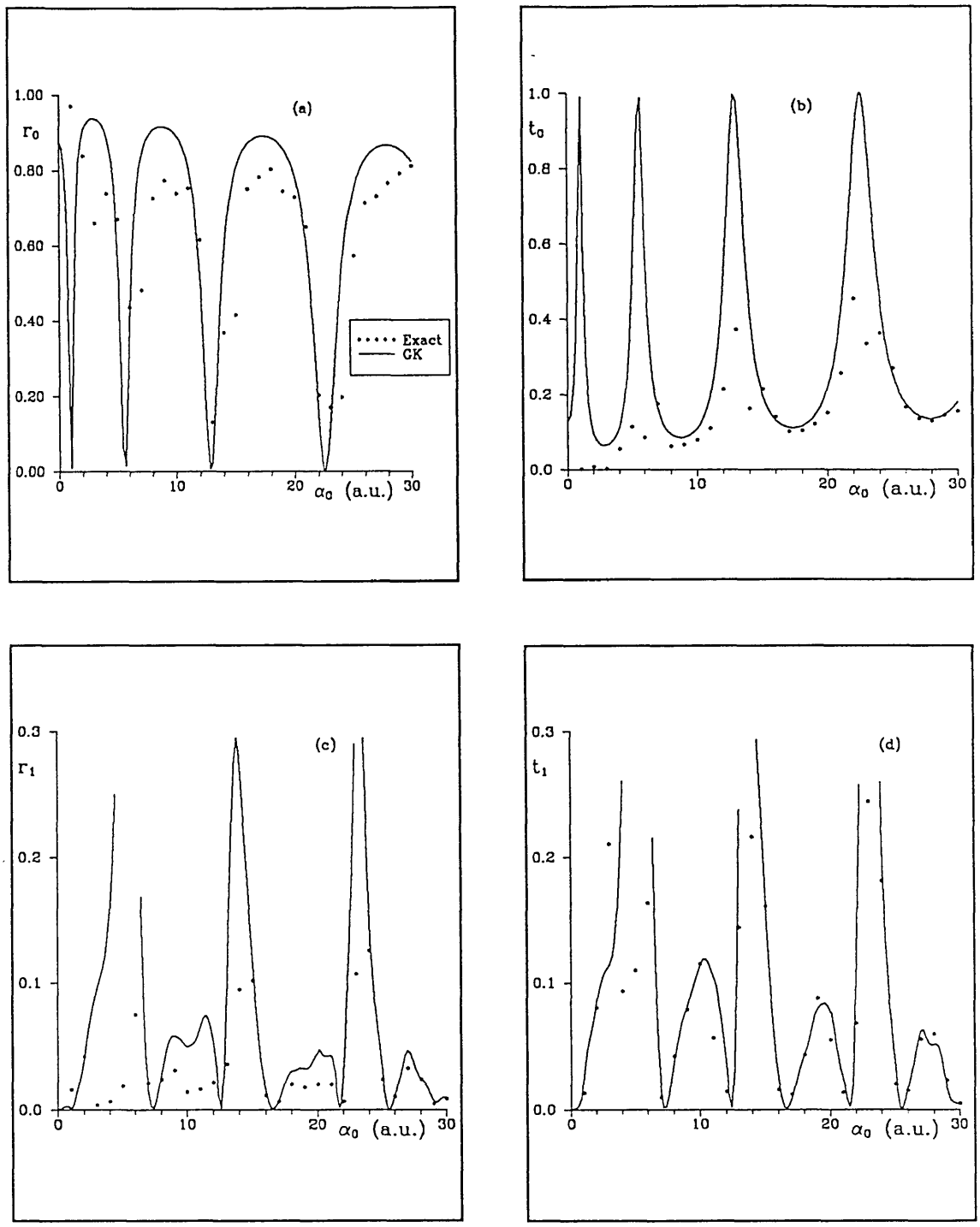

Figure 3.11 Reflection and transmission coefficients as functions of the laser parameter α_0. *(a) and (b) elastic channel, (c) and (d) inelastic channel with absorption of one photon.* ω = *10 eV,* E_i = *0.1 eV, A = 1 a.u.,* β = *1 a.u.*

disagreement with the GK approximation. When the well is deep (as in Fig 11), the resonances are narrow and closely spaced with respect to α_0, and the approximation hardly works at all, whereas if the well is shallow, the resonances are broad and further spaced apart, hence there is closer agreement with the GK result.

The above explanation is justified by the fact that the exact t_1 and r_1 also peak at the resonance positions, showing that more absorption of photons takes place compared to the background. However, in Fig 10 there appears to be a missing peak in both r_1 and t_1 at the position of the second resonance in t_0 near $\alpha_0 = 20$ a.u. Furthermore, there is a great deal of structure in r_1 and t_1 that is not present in the elastic coefficients, but is also reproduced fairly well by the GK result. The origin of this may lie in the fact that the electon wavefunction consists of a superposition of channel functions each associated with a different de Broglie wavelength. A shorter de Broglie wavelength would give rise to greater structure. In some cases, there may be destructive interference, for example near $\alpha_0 = 20$ a.u. in Fig 10, that attenuates the effect of the resonance in t_0 and allows the GK approximation to be valid.

Fig 12 illustrates the same quantities as Fig 10 with only one parameter changed, the laser frequency which is now 10 eV. The increase in frequency has two effects: The first is that the GK approximation is improved, at least for r_0 and t_0. Secondly, if our interpretation of the structure in t_1 and r_1 is correct, we would expect faster oscillation if the laser frequency is increased. This is also confirmed by the results in Fig 12. What is interesting is that in the region between $\alpha_0 = 10$ a.u. and $\alpha_0 = 15$ a.u. corresponding to a minimum in t_0 where by our previous arguments, we would expect the GK approximation to work, we find an appreciable difference between the two results.

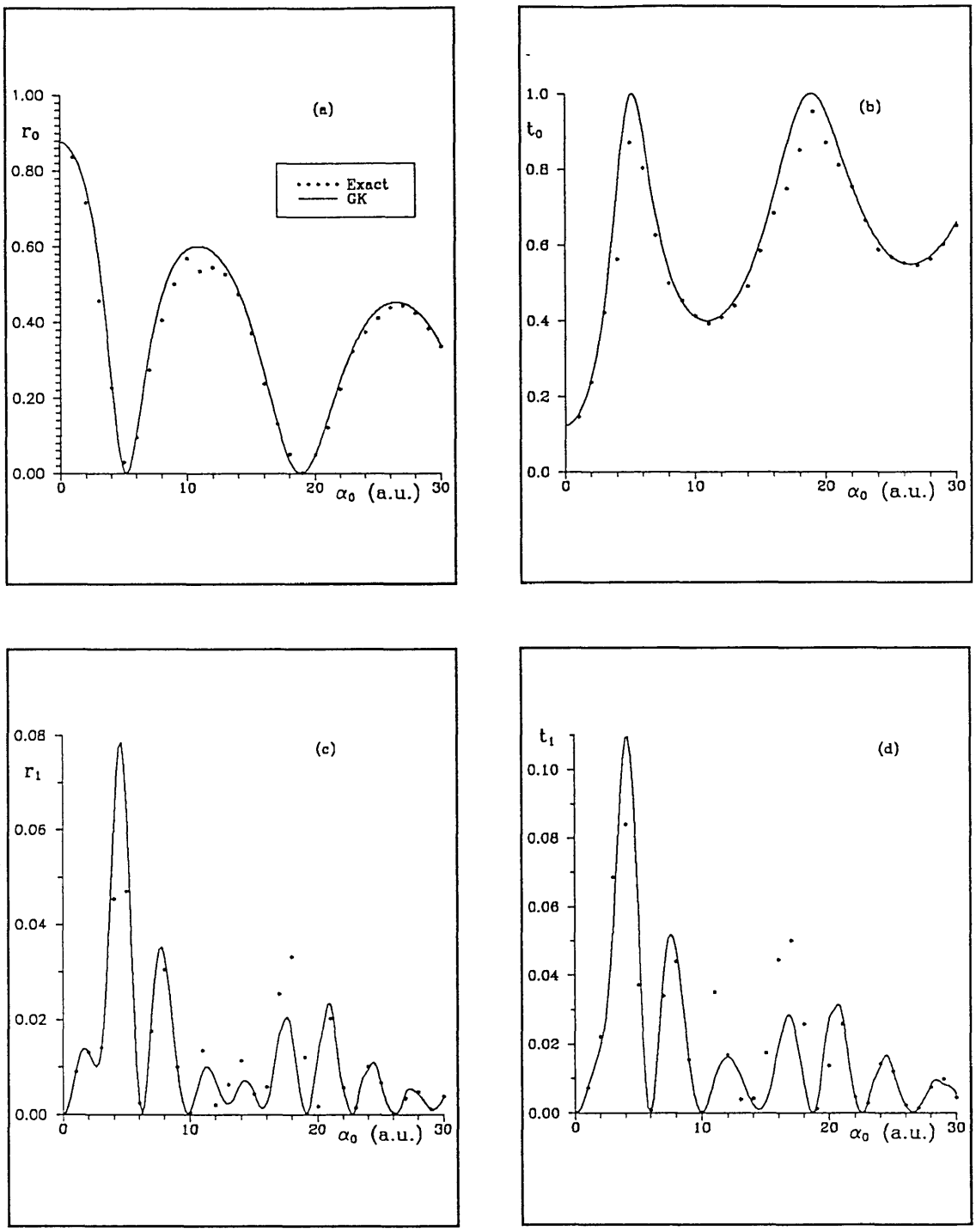

Figure 3.12 Reflection and transmission coefficients as functions of the laser parameter α_0 *(a) and (b) elastic channel, (c) and (d) inelastic channel with absorption of one photon.* ω = *10 eV,* E_i = *0.1 eV, A = 0.2 a.u.,* β = *1 a.u.*

§3.5.4 Dependence on frequency

To show the high frequency character of the approximation, we have plotted the reflection and transmission coefficients as a function of the frequency for fixed α_0 in Figs 13 and 14. Fixing α_0 means that as the frequency increases, the intensity of the laser increases correspondingly. Had the intensity been kept fixed, we would expect somewhat different results, because then α_0 would decrease with frequency, with an accompanying decrease in the energy of the ground state of $V_0(\alpha_0;x)$. In the GK approximation, r_0 and t_0 are independent of the frequency as long as α_0 is kept constant because they only depend on $V_0(x)$ which in turn is a function of the laser parameters only through α_0. In both figures α_0 = 10 a.u., the incident energy E_i = 0.1 eV, and A = 0.2 a.u. in Fig 13 while A = 1.0 a.u. in Fig 14. When A = 0.2 a.u., $|E_0|$ 0.25 eV, while for A = 1.0 a.u., $|E_0|$ = 1.7 eV. From Figs 10b and 11b, it is seen that in both cases α_0 = 10 a.u. is at a transmission minimum *i.e.* it is in a region where the GK approximation should work for high enough frequency. Figs 13 and 14 show that as the laser frequency is increased, the exact solution approaches the GK result. It appears that this occurs when ω is greater than $|E_0|$ by around an order of magnitude. Thus at very high frequencies, the scattering may be described well by V_0 only and the magnitude of r_1 and t_1 falls to zero, *i.e.* the probability of multiphoton absorption is reduced. It must be remembered that this is true when we are away from a transmission resonance in the elastic channel. At, or close to, a resonance, the picture would be considerably different, and extremely high frequencies would be required to get convergence.

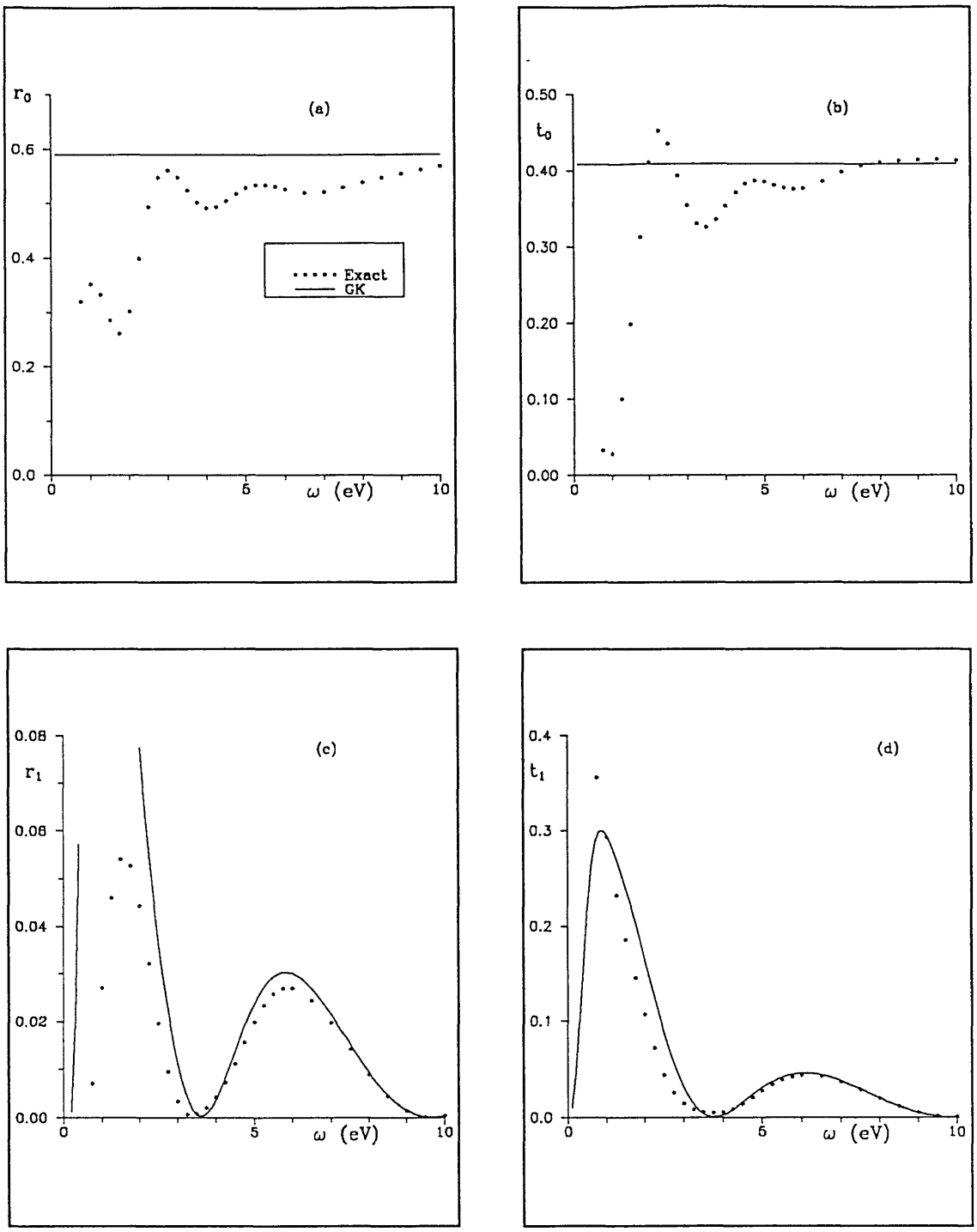

Figure 3.13 Reflection and transmission coefficients as functions of the laser frequency ω (a) and (b) elastic channel, (c) and (d) inelastic channel with absorption of one photon. $\alpha_0 = 10$ *a.u.,* $E_i = 0.1$ *eV,* $A = 0.2$ *a.u.,* $\beta = 1$ *a.u.*

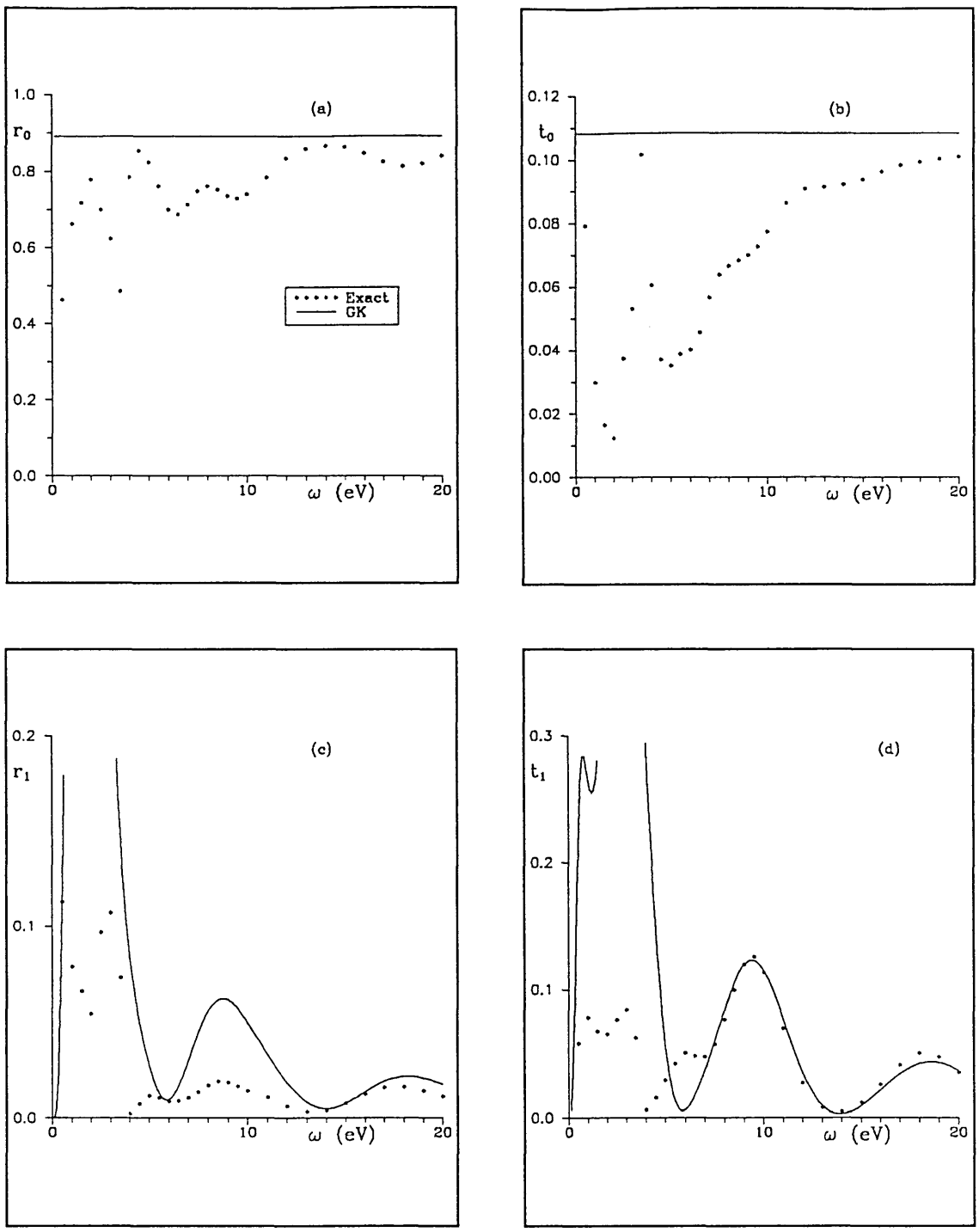

Figure 3.14 Reflection and transmission coefficients as functions of the laser frequency ω (a) and (b) elastic channel, (c) and (d) inelastic channel with absorption of one photon. $\alpha_0 = 10$ *a.u.,* $E_i = 0.1$ *eV,* $A = 1$ *a.u.,* $\beta = 1$ *a.u.*

§3.6 *Conclusions*

We have calculated numerically the reflection and transmission coefficients for potential scattering in the presence of laser fields in one dimension. We have computed them exactly by solving the full Schrodinger equation with only the dipole approximation, and used these results to test the non–perturbative approximation scheme of Gavrila and Kaminski. The exact results show evidence of laser–induced resonances, which are due to the bound states of the time–averaged potential $V_0(\alpha_0;x)$. It has been found that in regions which do not satisfy the conditions set out by Gavrila and Kaminski, the number of channels required for the computation can be very large. For a full three–dimensional calculation, this could prove to be a very serious limitation. In the GK regime, the scattering is generally dominated by a single channel, consequently the size of the problem is reduced. This statement requires qualification, because it has been found that the shape of V_0 can cause resonances, in the same way that a square well has transmission resonances whenever an integer number of half wavelengths fits in the well. The resonances mean that the particle has more time to feel the influence of the higher order components of the interaction, and consequently the probability of multiphoton absorption is increased. The assumption made by GK in deriving their expressions, that the probability of free–free transitions is small is therefore contradicted and we see poor agreement between the exact and GK results even when the high frequency condition is satisfied. In spite of the disagreement, the notion of the time–averaged potential is still of value in interpreting the results, but the message of this work is that caution must be exercised in viewing the results of any calculation that uses this approximation.

Appendix A

We derive the expression for the reflection and transmission coefficients, Eqs (36) and (37) following the method due to Gavrila and Kaminski[14], adapted here to one dimension. In Eq (34), we substitute for ϕ_m on the RHS for $n \neq 0$:

$$|\phi_n\rangle = -G^{(+)}(E_n)\left[V_n\,|\psi^{(+)}_{k0}\rangle - \sum_{\substack{l \\ l\neq n}}\sum_{\substack{m \\ m\neq l}} V_{n-l}\,G^{(+)}(E_l)\,V_{l-m}\,|\phi_m\rangle\right] \tag{A1}$$

$$= -G^{(+)}(E_n)\,|\zeta_n\rangle$$

where the function ζ_n has been introduced as a shorthand for the expression in parenthesis. We now define the free Green's function $G_0^{(+)}(E,x,x')$ as the solution of

$$\frac{d^2}{dx^2}\,G_0^{(+)}(E,x,x') + 2k^2\,G_0^{(+)}(E,x,x') = -\delta(x-x') \tag{A2}$$

with $k = \sqrt{(2E)}$. It can be shown that the function given by[20]

$$G_0^{(+)}(E,x,x') = \frac{-1}{ik}\exp\,(ik|x-x'|) \tag{A3}$$

is a solution of (A2) behaving asymptotically as

$$G_0^{(+)}(E,x,x') \xrightarrow[x\to\infty]{} \frac{-1}{ik}\exp\,[ik(x-x')] \tag{A4a}$$

$$G_0^{(+)}(E,x,x') \xrightarrow[x\to-\infty]{} \frac{-1}{ik}\exp\,[-ik(x-x')] \tag{A4b}$$

The scattering solutions $|\psi^{(\pm)}_{k_0}\rangle$ may be written in terms of the free electron

wavefunctions $u_{k_0}(x) = \exp(ik_0x)$ and the Green's function (A3) as

$$|\psi^{(\pm)}_{k_0}\rangle = (1 + G^{(\pm)} V_0)|u_{k0}\rangle \tag{A5}$$

Since $(G^{(\pm)})^{\dagger} = G^{(\mp)}$, we may rewrite (A5) as

$$\langle\psi^{(\pm)}_{k_0}| = \langle u_{k_0}|(1 + V_0 G^{(\mp)}) \tag{A6}$$

Using the following relation between the Green's functions G(E,x,x′) and G_0(E,x,x′)[6d]:

$$G^{(\pm)} = G_0^{(\pm)} (1 + V_0 G^{(\pm)}) \tag{A7}$$

the channel function $\phi_n(x)$ may be written as

$$\langle x|\phi_n\rangle = \langle x|G^{(\pm)}|\zeta_n\rangle = \langle x|G_0^{(\pm)} (1 + V_0 G^{(\pm)})|\zeta_n\rangle . \tag{A8}$$

As $x \to \infty$, this becomes, using (A4a)

$$\phi_n(x) \xrightarrow[x\to\infty]{} \frac{-1}{ik_n} e^{ik_n x} \int_{-\infty}^{\infty} e^{-ik_n x'} \langle x'|G_0^{(\pm)} (1 + V_0 G^{(\pm)})|\zeta_n\rangle dx' \tag{A9}$$

and, since $\langle u_{k_n}|x'\rangle = e^{-ik_n x'}$,

$$\phi_n(x) \xrightarrow[x\to\infty]{} \frac{-1}{ik_n} e^{ik_n x} \langle u_{k_n}| 1 + V_0 G^{(+)} |\zeta_n\rangle \tag{A10}$$

$$\xrightarrow[x\to\infty]{} \frac{-1}{ik_n} e^{ik_n x} \langle \psi^{(-)}_{k_n} | \zeta_n \rangle \tag{A11}$$

where the last step involved substituting (A6) into (A10). Finally, substituting for $|\zeta_n\rangle$ from (A1) yields

$$\phi_n(x) \xrightarrow[x\to\infty]{} \frac{1}{ik_n} e^{ik_n x} \left\{ \langle \psi^{(-)}_{k_n} | V_n | \psi^{(+)}_{k0} \rangle - \right.$$

$$\left. \sum_{\substack{l \\ l\neq n}} \sum_{\substack{m \\ m\neq l}} \langle \psi^{(-)}_{k_n} | V_{n-l} G^{(+)}(E_l) V_{l-m} | \phi_m \rangle \right\} \tag{A12}$$

The reflection coefficients R_n may be extracted from (A12) by comparing with the asymptotic conditions (32) to give Eq (36). The transmission coefficients T_n may be obtained in a similar way by taking the limit $x \to -\infty$ in (A8) and using (A4b).

Appendix B

We describe here the procedures carried out in order to test the program for the calculation of the reflection and transmission matrices using the de Vogelaere method[18]. Since the procedure outlined in §3.4.3 does not automatically ensure that probability is conserved according to the law given by Eq (52), this equation is a good test of the computational method. In all the cases presented, the number of channels and step size were chosen so as to give a total probability that was different from 1 by less than 10^{-5}.

Secondly, we tested the numerical results obtained when V_0 and the coupling terms V_n are replaced by constants against the exact analytical solution. In this case, with

$$V_0(x,\alpha_0) = \begin{Bmatrix} V, \forall x \in I_2 \\ 0, \forall x \notin I_2 \end{Bmatrix} \tag{B1}$$

$$V_n(x,\alpha_0) = \begin{Bmatrix} \nu, \forall x \in I_2, n \neq 0 \\ 0, \forall x \notin I_2, n \neq 0 \end{Bmatrix}, \tag{B2}$$

Eq (44) can be solved by diagonalising the matrix $\underline{E}$. Since $\underline{E}$ is hermitian, it is always possible to find a unitary matrix $\underline{\mathcal{J}}$ such that

$$\underline{E}' = \underline{\mathcal{J}}^{-1}\,\underline{E}\,\underline{\mathcal{J}} = \text{diag}\,(\lambda_1, \lambda_2, \ldots\ldots \lambda_N) \tag{B3}$$

where λ_i (i = 1 to N) are the eigenvalues of the matrix $\underline{E}$ and may be negative. We now set $\underline{D} = \underline{I}\, d^2/dx^2$ so that Eq (44) is written as

$$\underline{D}\,\underline{\Phi} = \underline{E}\,\underline{\Phi}. \tag{B4}$$

If we now multiply both sides of (B4) by $\mathcal{J}^{-1}$ on the left and $\mathcal{J}$ on the right, we get

$$\begin{aligned}\underline{D}\,\mathcal{J}^{-1}\,\underline{\Phi}\,\mathcal{J} &= \mathcal{J}^{-1}\,\underline{E}\,\underline{\Phi}\,\mathcal{J} \\ &= \mathcal{J}^{-1}\,\underline{E}\,\mathcal{J}\mathcal{J}^{-1}\,\underline{\Phi}\,\mathcal{J} \\ &= \underline{E}'\,\mathcal{J}^{-1}\,\underline{\Phi}\,\mathcal{J}\end{aligned} \tag{B5}$$

By writing

$$\underline{\Psi} = \mathcal{J}^{-1}\,\underline{\Phi}\,\mathcal{J} \tag{B6}$$

we get the following set of differential equations

$$\underline{D}\,\underline{\Psi} = \underline{E}'\,\underline{\Psi} \tag{B7}$$

whose solution in the interval I_2 is given by

$$\underline{\Psi} = \begin{bmatrix} e^{-i\sqrt{\lambda_1}x} & & 0 \\ & e^{-i\sqrt{\lambda_2}x} & \\ & & \ddots \\ 0 & & e^{-i\sqrt{\lambda_N}} \end{bmatrix} \times \underline{A} + \begin{bmatrix} e^{i\sqrt{\lambda_1}x} & & 0 \\ & e^{i\sqrt{\lambda_2}x} & \\ & & \ddots \\ 0 & & e^{i\sqrt{\lambda_N}} \end{bmatrix} \times \underline{B} \tag{B8}$$

where $\underline{A}$ and $\underline{B}$ are constant matrices. The wavefunction Φ is easily obtained by reversing the transformation in (B6):

$$\underline{\Phi} = \mathcal{J}\,\underline{\Psi}\,\mathcal{J}^{-1}. \tag{B9}$$

The derivative $\underline{\Phi}'$ is derived in a similar way. The eigenvalues and eigenvectors of $\underline{E}$ are calculated numerically, and the transformation matrix, $\mathcal{T}$ is formed from the eigenvectors. The solution (B9) and its derivative are then matched with the boundary conditions at $x = \pm x_t$ as described in §3.4.3 to obtain the reflection and transmission coefficients. These are then compared with the coefficients obtained using the de Vogelaere method. Since the derivatives of the coupling matrix at the boundaries of I_2 are infinite, it is necessary to use the solution (B9) at $x = x_t + \eta$ where η is the step size for the integration as the starting solution for the numerical propagation. The reflection and transmission coefficients were calculated as in §3.4.3 and were found to agree with those obtained from the diagonalisation procedure to at least 6 significant figures. This guaranteed that the integration procedure and the calculation of the reflection and transmission matrices were working correctly.

As a final check, we set some of the elements of the original coupling matrix to zero so that any channel m ($m \neq 0$, in the notation where the label runs from $-n_e$ to n_a) is coupled only to the elastic channel i.e. $V_{n-m} = 0$ if $n \neq 0$. This corresponds to solving the following set of equations:

$$[d^2/dx^2 - 2V_0 + 2(E_i + n\omega)]\varphi_n - 2V_n\phi_0 = 0 \quad -n_e \leq n \leq n_a,\ n \neq 0 \tag{B10}$$

$$[d^2/dx^2 - 2V_0 + 2E_i]\ \phi_0 = 0. \tag{B11}$$

Using the Green's operator defined in Eq (33), to solve Eqs (B10) and (B11) gives an approximation for the channel functions:

$$|\phi_0\rangle = |\psi_{k_0}^{(+)}\rangle \tag{B12}$$

$$|\phi_n\rangle = -G^{(+)}(E_n)\, V_n\, |\phi_0\rangle = -G^{(+)}(E_n)\, V_n\, |\psi_{k_0}^{(+)}\rangle . \qquad \text{(B13)}$$

Comparing Eqs (B12) and (B13) to Eq (A1) and following the analysis of Appendix A shows that this approximation is exactly equivalent to the lowest order high frequency approximation of §3.4.2. We thus have two independent means of calculating the reflection and transmission coefficients in this approximation. These methods have shown very good agreement in our calculations.

Appendix C

We detail the de Vogelaere method[18] for integrating numerical second order equations. The method is described here for a single differential equation:

$$\frac{d^2y}{dx^2} = f(x,y). \tag{C1}$$

The generalisation to a set of equations as in Eq (30) is straightforward. We divide each integration step into two intervals of step h. If y_0, y_1 and y_2 are the solutions at the three points x_0, x_1 and x_2 separated by h, and y_0 is known, then

$$y_1 = y_0 + hz_0 + h^2(f_{-1} + 4f_0)/6 \tag{C2}$$

where z_0 is $z = dy/dx$ at $x = x_0$ and f_{-1} and f_0 are $f(x_{-1}, y_{-1})$ and $f(x_0,y_0)$ respectively. Then, for $x = x_2$, y is given by

$$y_2 = y_0 + 2hz_0 + h^2(2f_0 + 4f_1)/3 \tag{C3}$$

and z is given by

$$z_2 = z_0 + h(f_0 + 4f_1 f_2)/3. \tag{C4}$$

These values may then be used for the next step. The process is of fourth order for both the function y and the first derivative z, *i.e.* the error is of order h^4.

References

1 F. W. Byron Jr, P. Francken and C. J. Joachain, J. Phys. B 20 (1987) 5487.

2 R. Shakeshaft, Phys. Rev. A 34 (1986) 4567.

3 F. H. M. Faisal, Phys. Lett. A 119 (1987) 375.

4 N. M. Kroll and K. M. Watson, Phys. Rev. A 8 (1973) 804.

5 B. Piraux, Annexe Thesis, Universite Catholique de Louvain (1983) unpublished.

6 L. I. Schiff, *Quantum Mechanics*, (McGraw–Hill Kogakusha Ltd., Tokyo, 1968) a) p138, b) p298, c) p315, d) p306.

7 T. W. B. Kibble, Phys. Rev. 150 (1966) 1060.

8 P. Agostini and G. Petite, Contemp. Phys. 29 (1988) 57, and references therein.

9 A. Weingartshofer, J. K. Holmes, J. Sabbagh and S. L. Chin, J. Phys. B 16 (1983) 1805.

10 H. Kruger and C. Jung, Phys. Rev. A 17 (1978) 1706.

11 M. H. Mittleman, Phys. Rev. A 38 (1988) 82.

12 C. Jung and H. S. Taylor, Phys. Rev. A 23 (1981) 1115.

13 H. Kruger and C. Jung, Phys. Rev. A 17 (1978) 1706.

14 M. Gavrila and J. Z. Kaminski, Phys. Rev. Lett. 52 (1984) 613.

15 M. Pont and M Gavrila, Phys. Lett. A 123 (1987) 469.

16 M. Pont, N. R. Walet, M. Gavrila and C.W. McCurdy, Phys. Rev. Lett. 61 (1988) 939.

17 J.Van de Ree, J. Z. Kaminski and M. Gavrila, Phys. Rev. A 37 (1988) 4536.

18 R. de Vogelaere, J. Res. Nat. Bur. Stand. 54, (1955) 119.

19 J. N. Bardsley and M. J. Comella, Phys. Rev. A 39 (1989) 2252.

20 Morse and Feshbach, *Methods of Theoretical Physics*, (McGraw–Hill, New York, 1953).

CHAPTER 4

MODEL STUDY OF THRESHOLDS IN PHOTO–IONISATION

§4.1 *Introduction*

In this chapter, we make a departure from multiphoton processes in charged particle scattering and instead consider multiphoton ionisation of atoms. We shall be concerned with threshold effects in multiphoton ionisation, with emphasis on the modifications caused by the presence of an autoionising state near the threshold.

Several recent works have been devoted to the problem of near–threshold photoionisation (or photodetachment in the case of a negative ion). The traditional Weisskopf–Wigner description[1] of the coupling of a discrete state to a continuum of states makes the assumption that the coupling is only weakly dependent upon the energy, thereby neglecting the lower bound of the continuum. This enables the "pole" approximation to be made with the result that the discrete state is shifted in energy and decays exponentially with a rate given by Fermi's Golden Rule. This approximation is accurate provided that the energy of the discrete state is well above the threshold. An alternative method is the exact diagonalisation procedure of Fano[2], which in its original form makes the same assumptions and predicts the same results as the Weisskopf–Wigner theory. A modification to Fano's method is required for the correct treatment of the near–threshold case. This is described later in this chapter.

One of the main consequences of the presence of the threshold in discrete state continuum coupling is non–exponential decay. This was demonstrated by

Khalfin[3] and has been studied theoretically in the context of spontaneous emission[4 5] where non–exponential decay has been shown to occur for very short and very long times such that it would be difficult to observe experimentally. Cohen–Tannoudji and Avan[6] have systematically examined a model in which a discrete state is coupled by a laser to a structured continuum with a low energy cutoff. They obtained corrections to the Weisskopf–Wigner result in the weak–field limit, indicating the onset of non–exponential decay. As the intensity is increased, damped Rabi oscillations are seen to occur and above a critical coupling, a stable bound state appears which leads to incomplete decay even for very long times. Subsequent workers have treated the problem in greater detail by employing specific models, often those mimicking photodetachment of negative ions close to threshold[7–12]. Motivation for this work has partly been stimulated by the possibility of observing non–exponential decay, because, as pointed out by Rzazewski *et al.*[11], the coupling between the discrete state and the continuum can be controlled in an experiment through the power and the frequency of the laser field.

Photoionisation in the vicinity of an autoionisation resonance is another problem of much current interest, and one in which the lower bound of the continuum is neglected in most papers[13]. The rest of this section is devoted to a description of this process using the method of Fano. The atomic energy level scheme for the problem is shown in Fig 1a. The state $|\phi_1\rangle$ is the autoionising state embedded in the continuum labelled $|\phi_{E'}\rangle$ by a time independent interaction V_c and the ground state $|\phi_0\rangle$ is coupled to both $|\phi_1\rangle$ and $|\phi_{E'}\rangle$ by a laser interaction V_L. The $|\phi_1\rangle - |\phi_{E'}\rangle$ system may be prediagonalised to give the Fano wavefunction $|\phi_E\rangle$:

$$|\phi_E\rangle = a(E)\ |\phi_1\rangle + \int_0^\infty dE'\ b(E,E')\ |\phi_{E'}\rangle \qquad (4.1)$$

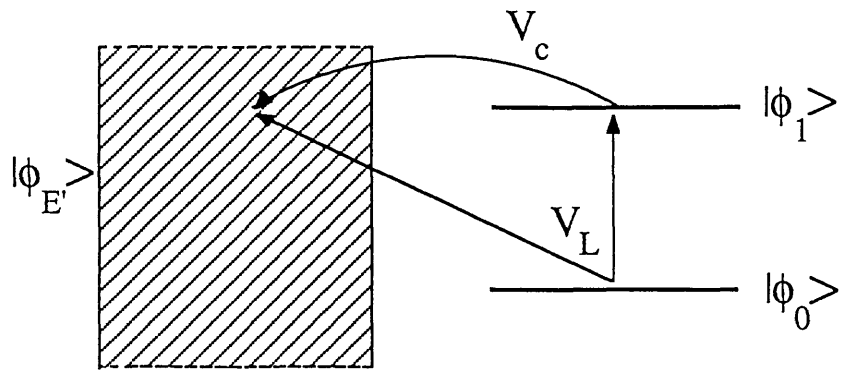

(a)

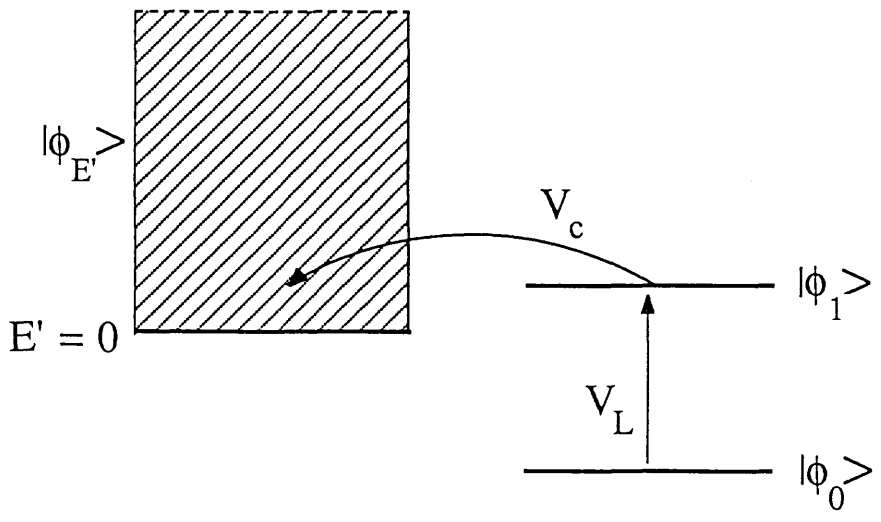

(b)

Figure 4.1 Schematic energy level diagrams.

where E is a continuous eigenvalue of the Hamiltonian $H = H_0 + V_c$, H_0 being the atomic Hamiltonian:

$$H\,|\phi_E\rangle = E\,|\phi_E\rangle. \tag{4.2}$$

Using Eq (1) and the expressions for the amplitudes a(E) and b(E,E') which are derived in Appendix A, the matrix element of the interaction between the ground state and the Fano continuum may be written as

$$V_{E_0} = \langle\phi_E|V_L|\phi_0\rangle =$$

$$\frac{1}{[(E_1 - E + \Delta)^2 + \pi^2|V_1|^4]^{1/2}}\left[V_1\langle\Phi|V_L|\phi_0\rangle - (E_1 - E - \Delta)\langle\phi_{E'}(E)|V_L|\phi_0\rangle\right]. \tag{4.3}$$

Here, the notation $\phi_{E'}(E)$ means the wavefunction $\phi_{E'}$ evaluated at E' = E, V_1 is the matrix element $\langle\phi_{E'}|V_c|\phi_1\rangle = V_{E'_1}$, also evaluated at E' = E and Δ is given by $\mathbb{P}\int |V_1|^2/(E - E')\,dE'$, where $\mathbb{P}$ denotes the Cauchy principal part. $|\Phi\rangle$ is the state $|\phi_1\rangle$ modified by the interaction V_c to

$$|\Phi\rangle = |\phi_1\rangle + \mathbb{P}\int_0^\infty dE\,\frac{V_1|\phi_{E'}\rangle}{E - E'}. \tag{4.4}$$

Eq (3) may be rearranged to give

$$V_{E_0} = \frac{\langle\phi_{E'}(E)|V_L|\phi_0\rangle}{[(E_1 - E + \Delta)^2 + \pi^2|V_1|^4]^{1/2}}\left[q\,\pi|V_1|^2 - (E_1 - E - \Delta)\right] \tag{4.5}$$

where q is the Fano asymmetry parameter defined as

$$q = \frac{\langle \Phi | V_L | \phi_0 \rangle}{\pi V_1 \langle \phi_{E'}(E) | V_L | \phi_0 \rangle}. \tag{4.6}$$

Note that if the direct transition from $|\phi_0\rangle$ to the continuum states $|\phi_{E'}\rangle$ is weak compared with the coupling between the two bound states, q becomes very large.

It has been shown that the above model is equivalent to the case where $|\phi_1\rangle$ is coupled to the continuum by a laser field instead of a static Coulombic interaction[14]. Selection rules allow the states $|\phi_0\rangle$ and $|\phi_{E'}\rangle$ to be of equal parity, different from $|\phi_1\rangle$, and hence the matrix element $\langle \phi_{E'} | V_L | \phi_0 \rangle = 0$. In this case the matrix element V_{E_0} simplifies to

$$V_{E_0} = \frac{V_1 \langle \phi_1 | V_L | \phi_0 \rangle}{[(E_1 - E + \Delta)^2 + \pi^2 |V_1|^4]^{1/2}} \tag{4.7}$$

and q is infinite. Hence if the atomic continuum $|\phi_{E'}\rangle$ is flat, *i.e.* V_1 is constant, then the coupling between the ground state and the Fano continuum is Lorentzian with width $\gamma = \pi |V_1|^2$. In this particular case, the long–time photoelectron spectrum, defined as the population in the atomic continuum, is symmetrical if the laser is tuned to resonance with the auto–ionising state. For a high enough field, Autler–Townes splitting occurs in the spectrum[15] and the population of the ground state undergoes Rabi oscillations. For finite q–values, $|V_{E_0}|^2$ becomes highly asymmetric with a zero at E = –q (on an energy scale where $E_1 = 0$) and a maximum at a position approaching E = 0 with increasing q. The photoelectron exhibits Autler–Townes splitting as before, but one of the peaks becomes extremely narrow as it approaches the position of the zero with increasing laser intensity. This

phenomenon, which is due to the interference between the two ionisation channels has been named a "confluence of coherences"[16].

In the analysis discussed above, the presence of the threshold has been neglected. Voitkiv and Pazdzersky[17] have studied a model similar to that of Fig 1a, but one in which the continuum has an edge. The interactions of the ground and autoionising states with the continuum are chosen to vary as some power of the energy. In addition, the autoionising level has an irreversible decay channel into another continuum. The complexity of their model has meant that the authors were only able to derive analytical results in some limiting cases and only qualitative time–evolutions and photoelectron spectra were presented. It is clear, however, from their work that the threshold causes marked differences to the decay process.

In this Chapter, we study a model similar to that depicted in Fig 1a, the main differences being that our model (Fig 1b) includes a threshold in the continuum, but no direct ionisation from the ground state. In contrast to Voitkiv and Pazdzersky's model our autoionising level does not have an extra decay channel. The advantage of our model is that it easily affords exact solutions (within the rotating wave approximation), either numerical or analytical. Thus, we are able to discuss the threshold effects in greater detail than the previous authors.

The plan of this chapter is as follows. We first study, in Sections 2 and 3, a simple model of a single discrete state interacting with a continuum. The coupling to the continuum is chosen so that its variation with energy is of a Lorentzian form, but bounded from below. This form is interesting in itself to study, but also it might be expected that diagonalising the excited state–continuum part of the system shown in Fig 1b, would result in a continuum with a Lorentzian dependence on the energy above the threshold. In Section 2, we solve the equations of motion, following

Piraux[18], for this model using the method of Laplace Transforms, and obtain the time–evolution for the ground state population. We then study the population in the Fano continuum. In Section 3, we take a different approach, using Fano's method to obtain the stationary states of the complete Hamiltonian for the system. By imposing suitable initial conditions, we re–derive the results of Section 2 and interpret them in terms of the stationary states.

We begin Section 4 by discussing the conditions under which the single discrete state–continuum model represents the model of Fig 1b. We then go on to study the latter model, again using the Laplace Transform technique but using a basis which includes the dressed states of the discrete state system which allows a clear interpretation of the long–time populations.

§4.2 Discrete State Coupled to Fano Continuum

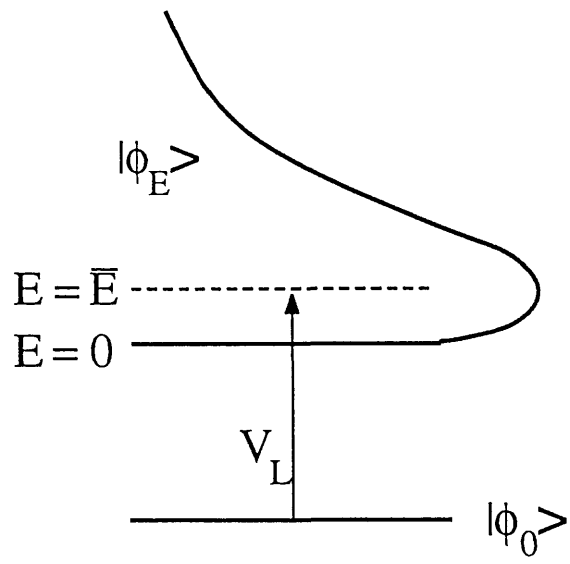

Figure 4.2 Schematic energy level diagram for discrete state coupled to a structured continuum. The coupling strength $|V_{0E}|^2$ *is given as a function of the energy E.*

The model (Fig 2) that we consider in this section consists of a single discrete atomic state of energy E_0, coupled by a laser field to a continuum of states. The continuum is characterised by the energy E, whose range is taken to be from E = 0 (the threshold) to E = $+\infty$. The wavefunctions are assumed to be normalised so that

$$\langle \phi_0 | \phi_0 \rangle = 1 \tag{4.8}$$

$$\langle \phi_E | \phi_{E''} \rangle = \delta(E-E'') \, . \tag{4.9}$$

The classical laser field is described by

$$\underline{\mathcal{E}} = \underline{\mathcal{E}}_0 \cos \omega t \tag{4.10}$$

where $\underline{\mathcal{E}}_0$ is the amplitude, and ω the frequency of the electric field which is assumed to be turned on suddenly at t = 0. The Schrodinger Equation for the system is then given by (we work in units such that $\hbar = c = 1$ from now on)

$$i \frac{d}{dt} |\Psi(t)\rangle = (H_0 + \underline{\mathcal{E}}_0 . \underline{r} \cos \omega t) \; |\Psi(t)\rangle \, . \tag{4.11}$$

The electronic wavefunction after the field has been switched on may be expanded in terms of the states $|\phi_0\rangle$ and $|\phi_E\rangle$

$$|\Psi(t)\rangle = d_0(t) \, |\phi_0\rangle \exp -iE_0 t + \int_0^\infty dE \; d_E(t) \, |\phi_E\rangle \exp -iEt \, . \tag{4.12}$$

In making this expansion, it has been assumed that we may neglect other atomic states, either because they are far off resonance or because the coupling to $|\phi_0\rangle$ and $|\phi_E\rangle$ is very small. In the case of an negative ionic system, this assumption is not

generally necessary since there is usually only a small number of bound states present.

Equations of motion for $d_0(t)$ and $d_E(t)$ may be derived by substituting Eq(12) into Eq(11). The following infinite set of differential equations is obtained

$$i\dot{d}_0(t) = 2\int_0^\infty dE\, d_E(t)V_{E_0} \cos \omega t \exp i(E_0 - E)t \tag{4.13}$$

$$i\dot{d}_E(t) = 2d_0(t)V_{0E} \cos \omega t \exp i(E - E_0)t \tag{4.14}$$

where for later convenience we have absorbed a factor of 1/2 into V_{0E}:

$$V_{0E} = \frac{1}{2}\langle \phi_0 | \underline{\mathscr{E}}_0 \cdot \underline{r} | \phi_E \rangle = V^*_{E_0} . \tag{4.15}$$

If we write cos ωt as (exp iωt + exp –iωt)/2, then Eqs (13) and (14) will consist of two terms, one oscillating with frequency $E_0 - E + \omega$ and the other at $E_0 - E - \omega$. Since we are interested in the region of the continuum which is nearly at resonance with the bound state at frequency ω, the first term will oscillate much more slowly than the second. We therefore make the Rotating Wave Approximation (RWA) and neglect terms oscillating at around twice the laser frequency. At the lowest order in the electric field, this approximation consists of neglecting a shift in the energy of the bound state (the Bloch–Siegert shift[19]). At higher orders, the rapidly varying terms, also called the counter–rotating terms, induce transitions to the continuum via non–energy conserving intermediate stages. These transitions involve absorption of 3, 5, 7 *etc.* photons and are particularly important when other discrete states are present[20]. As this is not so for the present case, we may consider the RWA to be justified.

Making the transformation

$$C_0 = d_0 \exp[-i(E_0+\omega)t] \tag{4.16}$$

$$C_E = d_E \exp[-iEt] \tag{4.17}$$

eliminates the remaining oscillation and with the definition $\tilde{E} = E_0 + \omega$, we get the following set of equations:

$$i\dot{C}_0 = \tilde{E}C_0 + \int_0^\infty dE\, C_E\, V_{E_0} \tag{4.18}$$

$$i\dot{C}_E = EC_E + C_0\, V_{0E} \tag{4.19}$$

where the explicit time–dependences have been dropped.

§4.2.1 Method of Solution

In order to solve the differential equations (18) and (19), for the complex amplitudes C_0 and C_E we use the Laplace Transform defined by

$$\tilde{g}(s) = \int_0^\infty dt\, g(t)e^{-st}. \tag{4.20}$$

Here, g(t) is an arbitrary function of t, the tilde denotes the transformed function and s is the Laplace Transform variable. We shall take the initial conditions to be: $C_0(t=0) = 1$ and $C_E(t=0) = 0$. In Laplace space, Eqs (18) and (19) become

$$s\tilde{C}_0 - 1 = -i\tilde{E}C_0 - i\int_0^\infty dE\, \tilde{C}_E\, V_{E_0} \tag{4.21}$$

$$s\tilde{C}_E = -iE\tilde{C}_E + -i\tilde{C}_0 V_{0E} . \tag{4.22}$$

Solving these algebraic equations yields

$$\tilde{C}_0(s) = [s + i\tilde{E} + f(s)]^{-1} \tag{4.23}$$

$$\tilde{C}_E(s) = \frac{-iV_{0E}}{(s + iE)\,[s\ + iE + f(s)]} \tag{4.24}$$

where

$$f(s) = \int_0^\infty dE\ \frac{|V_{0E}|^2}{s\ + iE} . \tag{4.25}$$

As discussed in Section 1, the form of the matrix element $|V_{0E}|^2$ is assumed to be the truncated Lorentzian given by

$$|V_{0E}|^2 = \frac{V^2A}{(E - \bar{E})^2 + \gamma^2}\,\Theta(E) \tag{4.26}$$

where $\bar{E}$ is the centre of the Lorentzian and γ is the width. $\Theta(E)$ is the Heaviside step function which causes the matrix element to fall off to zero sharply when E becomes negative. The factor V^2 is proportional to the intensity of the laser field. This particular form has the advantage that it can be solved analytically and results in relatively simple forms for the probability amplitudes. In Eq (26), A is a normalisation constant which would be γ/π in the absence of the step function. Because of the truncation, the normalisation is given by

$$A = \left[\int_0^{\infty} \frac{dE}{(E-\bar{E})^2 + \gamma^2} \right]^{-1} = \gamma \left[\frac{\pi}{2} + \tan^{-1}\left[\frac{\bar{E}}{\gamma}\right] \right]^{-1}. \tag{4.26}$$

The integral in the above equation is evaluated easily by means of partial fractions. When $\bar{E} \gg \gamma$, we recover the threshold–less normalisation: $A \simeq \gamma/\pi$. It might be expected that this condition defines the region where threshold effects are unimportant, but as we shall see later, this is not necessarily true.

§4.2.2 Analytical Properties of $\tilde{C}_0(s)$

Having specified the form of $|V_{0E}|^2$, we can proceed to evaluate $C_0(t)$ by inserting (26) and (25) into Eq (23). The integral in Eq (25) may be carried out by using contour integration in the complex s–plane (Appendix B) to give

$$f(s) = ic_1 \left(\frac{c_2}{is - \bar{E} + i\gamma} + \frac{\gamma}{(is-\bar{E})^2 + \gamma^2} \ln\left[\frac{is}{\bar{E} + i\gamma}\right] \right) \tag{4.28}$$

where

$$\frac{-\pi}{2} < \arg(s) < \frac{3\pi}{2} \tag{4.29}$$

$$c_1 = \frac{|V|^2}{\frac{\pi}{2} + \tan^{-1}(\bar{E}/\gamma)} \tag{4.30}$$

$$c_2 = \pi - \tan^{-1}(\gamma/\bar{E}) \, . \tag{4.31}$$

The presence of the factor $[s + iE]^{-1}$ in (25) gives rise to a branch cut along the negative imaginary s–axis and $\tilde{C}_0(s)$ has a pole on the positive imaginary axis with

the imaginary part, $y = \xi$, given by the solution of

$$y + \bar{E} = \frac{c_1}{(\bar{E} + y)^2 + \gamma^2}\left[c_2(\bar{E} + y) + \gamma \ln \frac{|\bar{E} + i\gamma|}{y}\right], \qquad y > 0 . \tag{4.32}$$

In Fig 3, we have plotted both sides (divided by V^2) of Eq (32) separately as functions of y for several values of γ and V^2. The solution of this equation is given by the points at which the straight line, representing the LHS, intersects the curve, representing the RHS. It is clear from the figure that there is only one solution which tends to zero either as $V^2 \rightarrow 0$ or $\gamma \rightarrow \infty$.

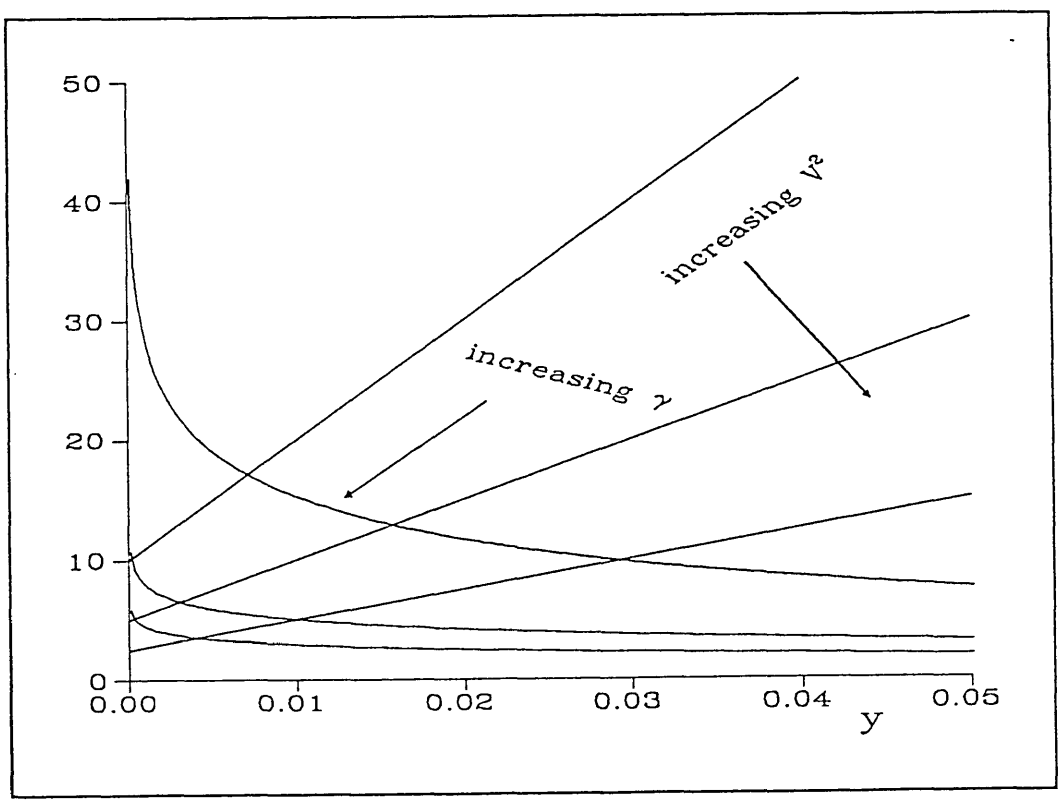

Figure 4.3 LHS (straight line) and RHS (curves) of Eq (32) as functions of y. The solution of Eq (32) is given by the intersection of the straight lines and the curves.

Knowing the position of the pole, $C_0(t)$ may be obtained by means of the inverse Laplace Transform:

$$g(t) = \frac{1}{2\pi i} \int_{\beta - i\infty}^{\beta + i\infty} ds\, e^{st}\, \tilde{g}(s) \tag{4.33}$$

where β is an arbitrary constant such that all poles of $\tilde{g}(s)$ are to the left of the line along which the integral is taken. If the contour is closed as shown in Fig 4, the

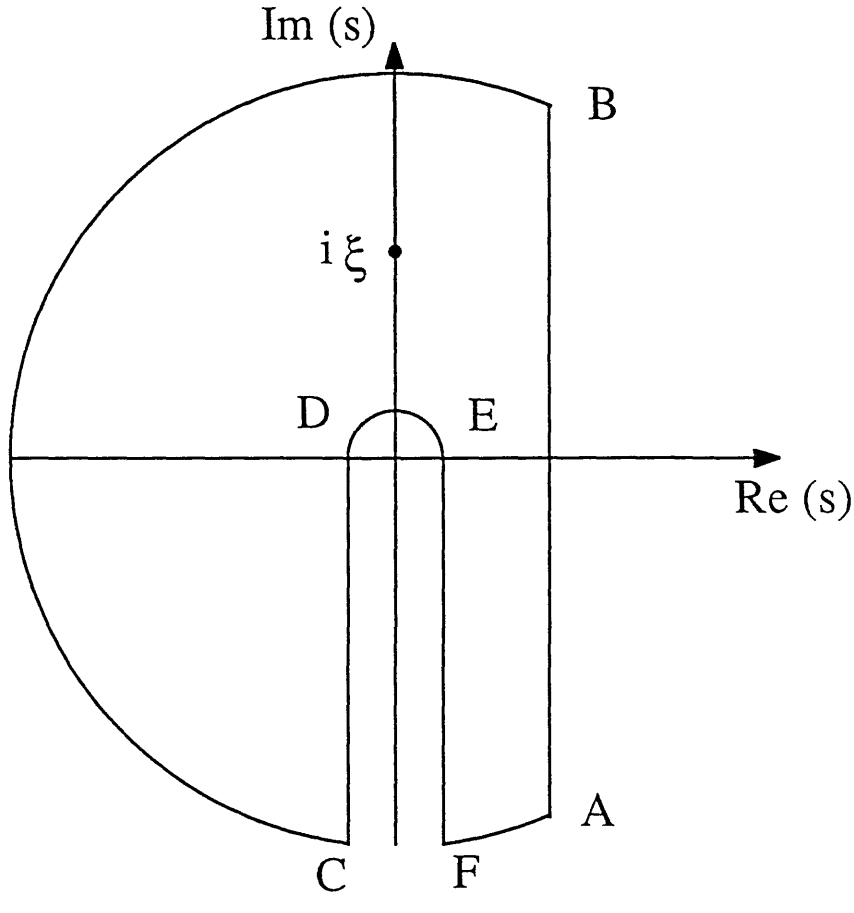

Figure 4.4 Contour of integration for calculating the inverse Laplace Transform of $\tilde{C}_0(s)$.

Residue theorem may be used to yield the following expression for $C_0(t)$

$$C_0(t) = \frac{e^{i\xi t}\,[\gamma^2 + (\xi + \bar{E})^2]}{\gamma^2 + (\xi + \bar{E})^2 + c_1\gamma/\xi - c_1c_2 + 2(\xi + \bar{E})(\xi + \tilde{E})}$$

$$+ \gamma c_1 \int_0^\infty dx \frac{e^{-ix\,t}[(x - \bar{E})^2 + \gamma^2]}{[(x - \bar{E})^2 + \gamma^2]^2\,[h(x)]^2 + \gamma^2\pi^2 c_1^2}. \qquad (4.34)$$

Here, h(x) is defined as

$$h(x) = (x - \tilde{E}) - \frac{c_1}{[(x - \bar{E})^2 + \gamma^2]}\left[c_2(x - \bar{E}) + \gamma \ln\left|\frac{x}{\bar{E} + i\gamma}\right|\right]. \qquad (4.35)$$

The steps required to arrive at this expression are analogous to those used in Section 4. In order to be able to concentrate on the results in this Section, we relegate the details of the calculation to the latter section. It is sufficient at this stage to point out that the first term on the RHS of Eq (34) represents the residue at the pole while the second term is the contribution from the branch cut. All other contributions to the contour integral vanish. The integral over x must be carried out numerically. However, because at $t = 0$, it must be finite and the integrand without the phase factor is positive, the contribution of the integral becomes zero as $t \to \infty$ by the Riemann–Lebesgue Lemma[21]. Hence, we also have that the probability, $P_0(t \to \infty)$, that the ground state has not decayed at very long times is

$$P_0(t \to \infty) = |C_0(t \to \infty)|^2 =$$

$$\left[\frac{\gamma^2 + (\xi + \bar{E})^2}{\gamma^2 + (\xi + \bar{E})^2 + c_1\gamma/\xi - c_1c_2 + 2(\xi + \bar{E})(\xi + \tilde{E})}\right]^2 . \tag{4.36}$$

This means that the ground state never decays completely, in contrast to the situation where the Lorentzian is not truncated (see Appendix C). One could also attempt to define the spectrum of the ionised electron's kinetic energy as $t \to \infty$ by making use of the final value theorem for Laplace Transforms which states that

$$\lim_{t\to\infty} g(t) \exp(iEt) = \lim_{s\to -iE} \tilde{g}(s) . \tag{4.37}$$

We then obtain using Eqs (24) and (28)

$$P_E(t\to\infty) = |C_E(t\to\infty)|^2 = \frac{\gamma c_1[(E - \bar{E})^2 + \gamma^2]}{[(E - \bar{E})^2 + \gamma^2]^2\,[h(x)]^2 + \gamma^2\pi^2 c_1^2} . \tag{4.38}$$

Putting $t = 0$ in Eq (34), and using Eqs (36) and (38), we see that:

$$C_0(t = 0) = 1 = |C_0(t \to \infty)| + \int_0^\infty dE\, P_E(t \to \infty). \tag{4.39}$$

Note that the first term on the RHS of Eq (39) is <u>not</u> the probability of the electron being in the ground state, but its square root. This implies that the total probability, P_T, defined as

$$P_T = |C_0(t = \infty)|^2 + \int_0^\infty dE\, P_E(t = \infty) \tag{4.40}$$

cannot be equal to 1 unless the ground state population vanishes at long times. The reason for the apparent violation of probability conservation is that the Final Value Theorem is valid only if there is a single pole contributing to the long–time behaviour. In the present case, there are two, at $s = -iE$ and $s = i\xi$, and Eq (38) may be used to obtain the long–time photoelectron spectrum only if the contribution of the pole at $s = i\xi$ is negligible. The numerical results to be presented below will show the conditions under which Eq (38) is valid.

Figs 5 to 8 illustrate some of the observations made in the discussion above. We have chosen, in all these figures, the resonant case, so that $\bar{E} = \tilde{E}$. Fig 5 shows the population of the ground state as a function of time elapsed after the field has been turned on. The result obtained by ignoring the threshold is also shown for comparison. Two different values of V are shown, one less than $\bar{E}$ and γ (Fig 5a) and the other greater (Fig 5b). In the former case, the population appears to decay irreversibly to zero with a rate larger than in the no–threshold case.. When V is increased, as in Fig 5b, the population exhibits damped oscillations at the effective Rabi frequency 2V. The oscillations die out completely after about 10 cycles, and the population stabilises at a value of around 0.25. In both Figs 5a and 5b, for very short times ($t \ll 1/\gamma$ and $t \ll 1/V$), the presence of the threshold appears to make no difference to the time–evolution and differences between the two cases only become apparent at longer times.

Fig 6 shows $P_0(t = \infty)$ as a function of log V^2 for (a) $\bar{E} = 0.01$ and various values of γ and (b) $\gamma = 0.01$ but different values of $\bar{E}$. It is seen that as long as γ is less than $\bar{E}$, the final value of P_0 increases from 0 to some peak value (determined by γ) when V becomes greater than $\bar{E}$. The increase gets sharper as γ gets smaller. For γ larger than $\bar{E}$, the change starts to occur when V exceeds γ. As $V \rightarrow \infty$, the value of $P_0(t = \infty)$ tends to the same constant value of 0.25 independent of $\bar{E}$ and γ.

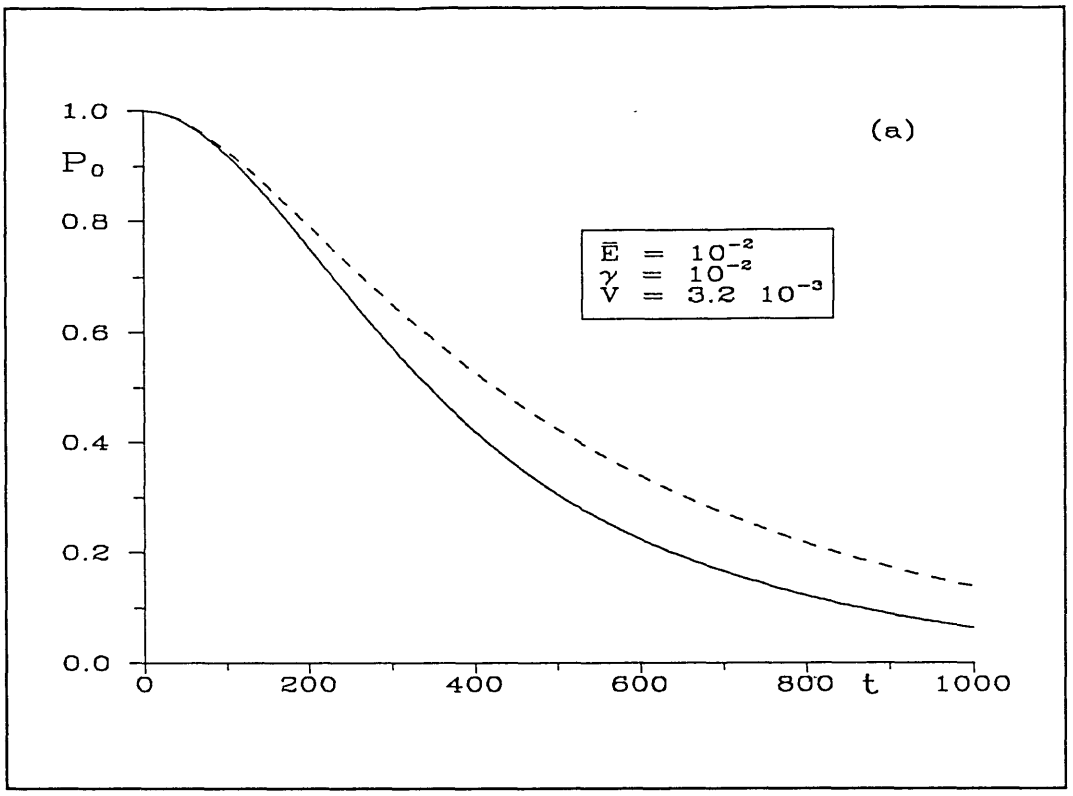

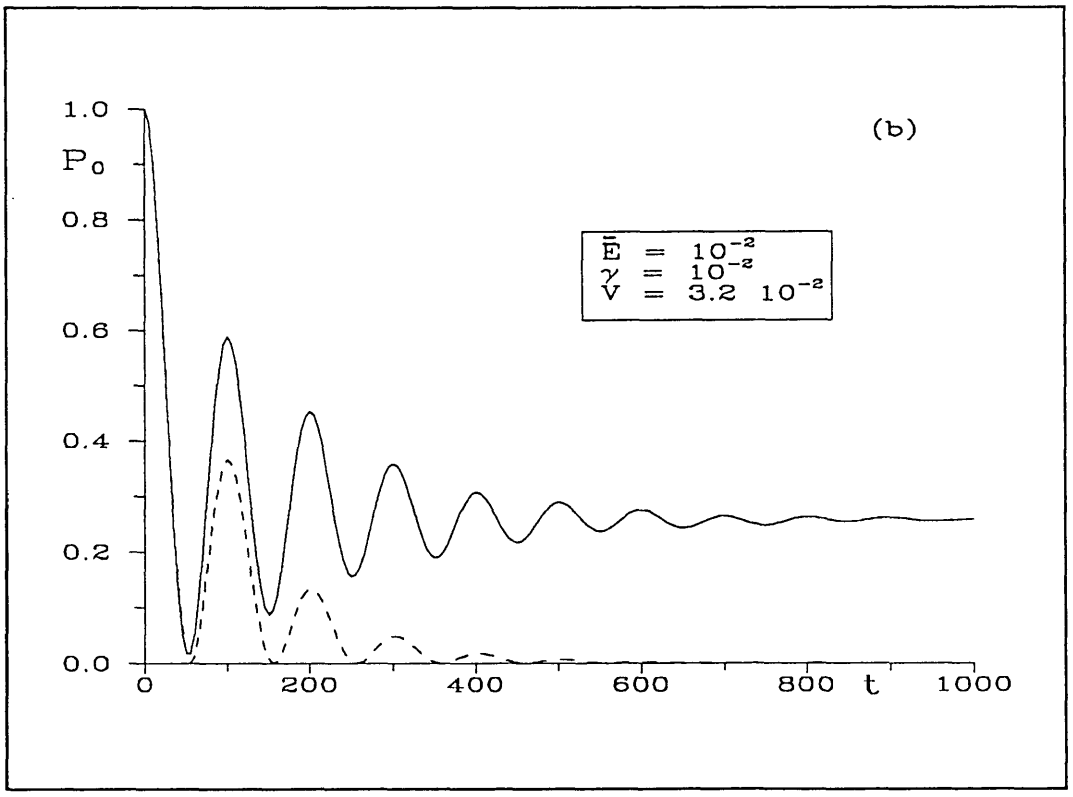

Figure 4.5 Time evolution of the ground state probabilty —— Threshold - - - No threshold.

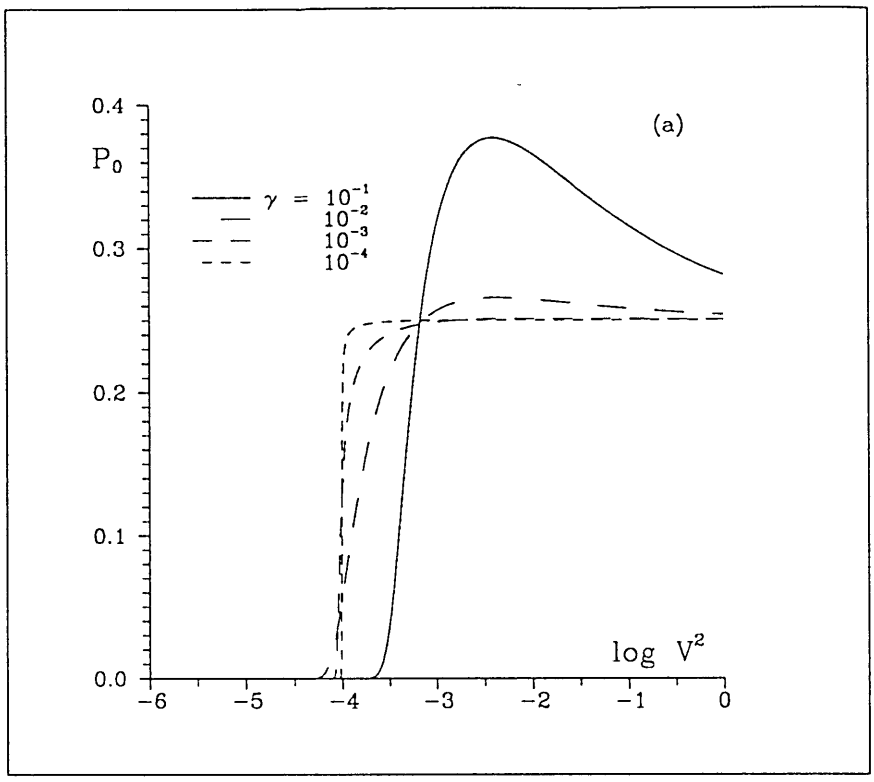

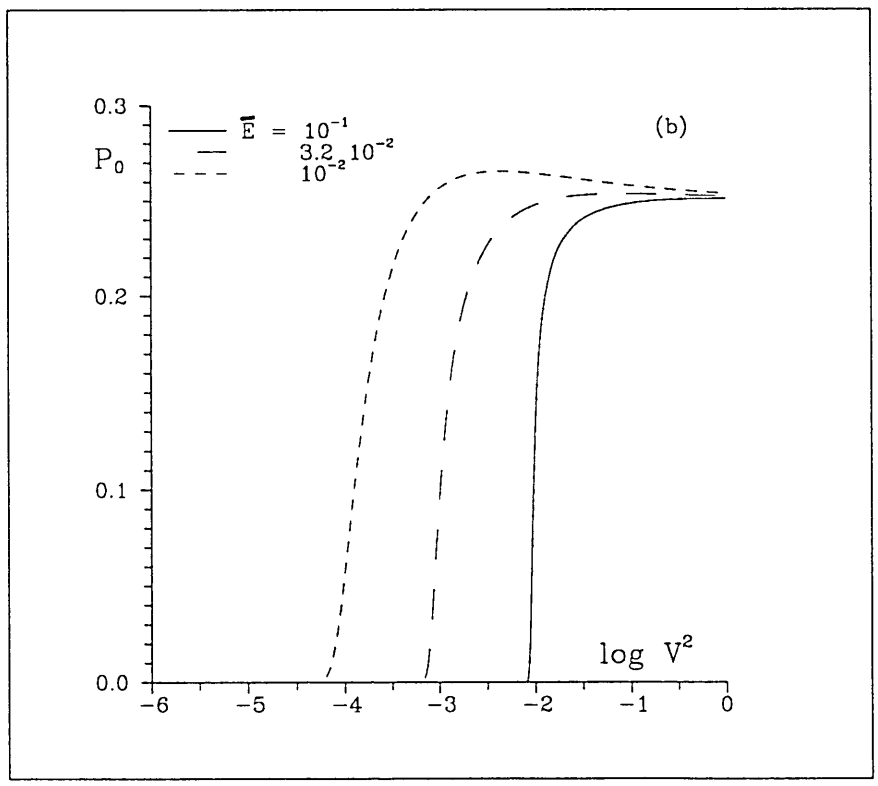

Figure 4.6 Ground state probability as $t \to \infty$ (a) $\bar{E} = 0.01$, various values of γ (b) $\gamma = 0.01$, various values of $\bar{E}$.

The variation of the long–time total probability as defined by Eqs (38) and (40) is shown in Fig 7. Its value exhibits a drop from 1 to 0.75 at the same value of V as the increase in $P_0(t = \infty)$. Therefore, for large values of V, there are two effects: firstly, a quarter of the population gets trapped in the ground state and, secondly, the total population in the Fano continuum, as given by the Final Value Theorem, is only one half – a quarter of the population remains unaccounted for. From these results, we deduce that the Final Value Theorem gives an accurate result for the long–time spectrum when either of the following conditions is satisfied:

$$V \ll \bar{E}, \qquad \gamma < \bar{E} \tag{4.41}$$

$$V \ll \gamma, \qquad \gamma > \bar{E} \tag{4.42}$$

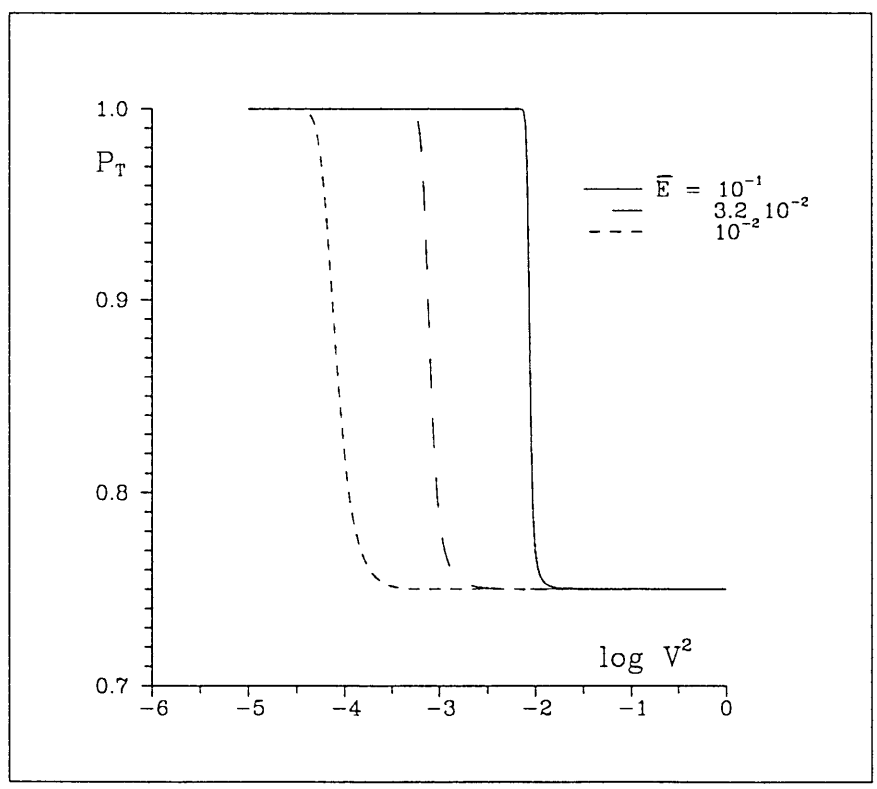

Figure 4.7 Total probabilty as $t \to \infty$ derived using the Final Value Theorem. $\gamma = 0.01$.

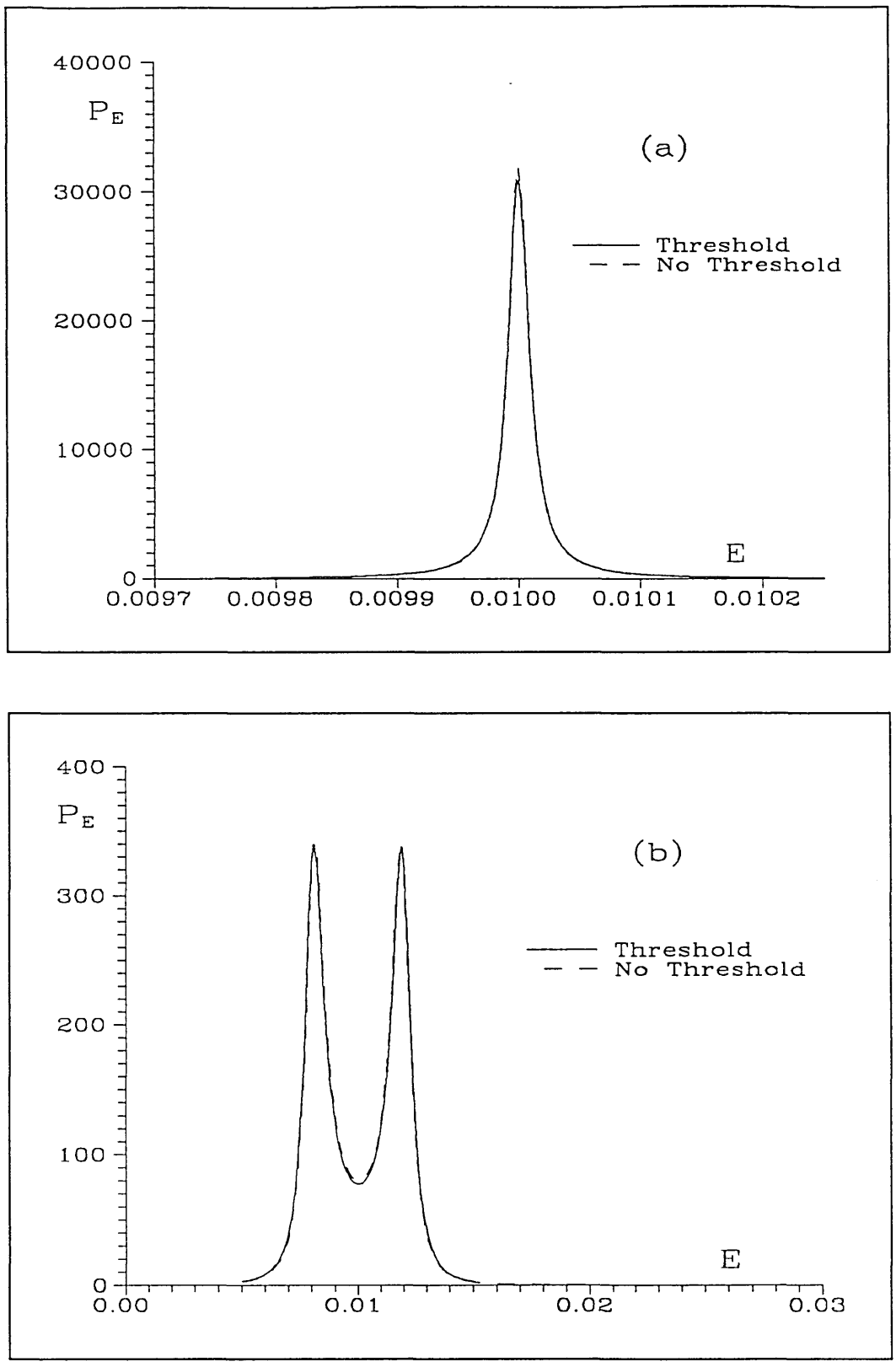

Figure 4.8 Photoelectron spectra in the $|\phi_E\rangle$ *continuum derived using the Final Value Theorem.* $\gamma = 0.001$, *(a)* $V = 10^{-4}$ *(b)* $V = 0.002$.

In Fig 8, we present spectra for $\gamma = 0.001$, $\bar{E} = 0.01$ and two different values of V such that one of the conditions above is met. We see that for small V, Fig 8a, the spectrum shows a single peak, centred at $E = \bar{E}$, while for larger V, Autler–Townes splitting is observed. In each case, the spectrum when the threshold is neglected is also plotted in the same figure, and is seen to be barely distinguishable from the case with the threshold. The threshold does cause a slight asymmetry, but this cannot be discerned in Fig 8. Clearly therefore, in the weak–field case defined by the conditions in Eqs (41) and (42), the threshold may be neglected without significant error. In order to see threshold effects in the spectrum, we must go to higher V, but in that case, we cannot simply use the Final Value Theorem to obtain the spectrum because of the pole at $s = i\xi$. In the next section, we shall probe more deeply into the role of the pole at $s = i\xi$ and solve the above problem in terms of the eigenstates of the complete Hamiltonian governing the dynamics. The physical meaning of the final values of P_0 and P_T and the conditions in Eqs (41) and (42) will be discussed in Section 4 together with the long–time photoelectron spectrum for large V.

§4.3 *Complete Fano Diagonalisation*

It is instructive to solve the problem of Section 2 using the method of Fano to diagonalise the complete Hamiltonian for the system. In doing this, we are going one stage further than the first diagonalisation which was assumed to yield the truncated Lorentzian. The new Fano continuum states will be denoted by $|\psi_\varepsilon\rangle$, which may be expanded in terms of the states $|\phi_0\rangle$ and $|\phi_E\rangle$ as follows:

$$|\psi_\varepsilon\rangle = a(\varepsilon)\ |\phi_0\rangle + \int dE\ b(\varepsilon, E)\ |\phi_E\rangle . \tag{4.43}$$

The procedure is similar to that outlined in Section 1, but the expansion coefficients

in the above equation must not be confused with those in Eq (1) because they refer to different sets of states. In contrast to the usual Fano theory, the continuous energy values ε and E are restricted to the range 0 to ∞. In the resonant case, the coefficients a(E) and b(ε, E) are given by (see Appendix A for details):

$$|a(\varepsilon)|^2 = \frac{|V_\varepsilon|^2}{[\varepsilon - \bar{E} - F(\varepsilon)]^2 + \pi^2 |V_\varepsilon|^4} \tag{4.44}$$

$$b(\varepsilon, E) = \frac{1}{\{[\varepsilon - \bar{E} - F(\varepsilon)]^2 + \pi^2 |V_\varepsilon|^4\}^{1/2}} \frac{V_\varepsilon V_E}{(\varepsilon - E)} - \cos\alpha\, \delta(\varepsilon - E)\,. \tag{4.45}$$

F(ε) is given by

$$F(\varepsilon) = \mathbb{P} \int_0^\infty dE \frac{|V_E|^2}{\varepsilon - E} \tag{4.46}$$

and

$$\alpha = -\tan^{-1} \frac{\pi |V_\varepsilon|^2}{\varepsilon - \bar{E} - F(\varepsilon)}\,. \tag{4.47}$$

We have simplified the notation somewhat by writing $V_E = V_{0E}$ and $V_\varepsilon = V_{0E}(E = \varepsilon)$. It is clear that both a(ε) and b(ε,E) vanish if $\varepsilon < 0$, unless the denominator of the RHS of Eqs (44) and (45) also vanishes. This latter case occurs when for $\varepsilon < 0$

$$\varepsilon - \bar{E} - F(\varepsilon) = 0 \tag{4.48}$$

since V_ε also vanishes. This possibility, which corresponds to a bound eigenstate of

the total Hamiltonian, does not arise in the case when the continuum extends to infinity in both directions because then V_ε is never zero. In the following, we generalise the Fano theory to take into account the appearance of a new bound state and relate this to the results of Section 2.

We begin by introducing a new eigenstate of the Hamiltonian, $|\psi_\xi\rangle$, where $-\xi$ satisfies Eq (48). The eigenfunctions $|\psi_\varepsilon\rangle$ and $|\psi_\xi\rangle$ must satisfy the orthonormality conditions:

$$\langle\psi_\varepsilon|\psi_{\varepsilon'}\rangle = \delta(\varepsilon - \varepsilon'), \tag{4.49}$$

$$\langle\psi_\xi|\psi_\varepsilon\rangle = 0 \tag{4.50}$$

$$\langle\psi_\xi|\psi_\xi\rangle = 1\ . \tag{4.51}$$

The eigenfunctions with continuous energy eigenvalues may still be expanded as in Eq (43) with coefficients $a(\varepsilon)$ and $b(\varepsilon, E)$ given by Eqs (44) and (45). We expand $|\psi_\xi\rangle$ in a like manner:

$$|\psi_\xi\rangle = a(\xi)\ |\phi_0\rangle + \int dE\ b(\xi, E)\ |\phi_E\rangle \tag{4.52}$$

where the coefficients $a(\xi)$ and $b(\xi, E)$ satisfy

$$\bar{E}\ a(\xi) + \int_0^\infty dE\ V_E^*\ b(\xi, E) = -\xi\ a(\xi) \tag{4.53}$$

$$b(\xi, E) = V_E\ a(\xi)/(-\xi - E)\ . \tag{4.54}$$

Note that because $\xi > 0$, the denominator in Eq (54) can never be zero, hence the δ–function required for the positive–energy eigenfunctions is omitted (cf. Eq (45)). Substituting (54) into (53), we get the following equation to solve for ξ

$$\xi + \bar{E} + F(-\xi) = 0 . \qquad (4.55)$$

This corresponds precisely to the solution of Eq (32) because, for the particular case of a truncated Lorentzian continuum,

$$F(-\xi) = \lim_{s \to i\xi} -i \times f(s) = \frac{-c_1}{(\xi + \bar{E})^2 + \gamma^2} \left[c_2 (\xi + \bar{E}) + \gamma \ln \frac{|\bar{E} + i\gamma|}{\xi} \right] . \qquad (4.56)$$

By using condition (51) and Eqs (53) and (54), we find that

$$|a(\xi)|^2 = \left[1 + \int_0^\infty dE \, \frac{|V_E|^2}{(\xi + E)^2} \right]^{-1} . \qquad (4.57)$$

The coefficients $b(\xi, E)$ may be obtained easily from Eqs (54) and (57) if one ignores a phase factor. With the above expression for $a(\xi)$, it may be shown that all three orthonormality conditions, Eqs (49–51) are satisfied.

By inserting Eq (26) into (57), we may obtain explicit expressions for the expansion coefficients for the case in hand. The integral in Eq (57) is evaluated by means of partial fractions to yield

$$|a(\xi)|^2 = \left[\frac{\gamma^2 + (\xi + \bar{E})^2}{\gamma^2 + (\xi + \bar{E})^2 + c_1\gamma/\xi - c_1c_2 + 2(\xi + \bar{E})(\xi + \tilde{E})} \right]^2 . \qquad (4.58)$$

In order to obtain $a(\varepsilon)$, we note that $F(\varepsilon) = -i \times \text{Im}\,[f(s \rightarrow -i\varepsilon)]$ where $f(s)$ is given by Eq (28). Although there is a branch cut along the negative part of the imaginary axis in the s–plane, the limit can be taken in either direction as this does not affect the imaginary part of $f(s \rightarrow -i\varepsilon)$. Substituting for V_ε and $F(\varepsilon)$ in Eq (44) gives

$$|a(\varepsilon)|^2 = \frac{\gamma c_1 \,[(\varepsilon - \bar{E})^2 + \gamma^2]}{[(\varepsilon - \bar{E})^2 + \gamma^2]\;\;[h(\varepsilon)]^2 + \pi^2\gamma^2 c_1{}^2} . \tag{4.59}$$

As an illustration of the use of these expressions, we now calculate the time development of this system with the initial condition that all the population is in the ground bound state $|\phi_0\rangle$ at t=0. We expand the wavefunction in the two bases, "unperturbed" and complete Fano, as follows:

$$|\Psi(t)\rangle = C_0(t)\,|\phi_0\rangle + \int_0^\infty dE\; C_E(t)\,|\phi_E\rangle \tag{4.60}$$

$$= C_\xi\,|\psi_\xi\rangle \exp i\xi t + \int_0^\infty d\varepsilon\; C_\varepsilon\,|\psi_\varepsilon\rangle \exp -i\varepsilon t\,. \tag{4.61}$$

Note that because $|\psi_\xi\rangle$ and $|\psi_\varepsilon\rangle$ are eigenstates of the total Hamiltonian, C_ξ and C_ε are not time–dependent. All the time–dependence in $|\psi(t)\rangle$ is due to the beating of the phases of the states. At t=0, $|\Psi(0)\rangle = |\phi_0\rangle$, therefore from Eq (61),

$$C_\xi\,|\psi_\xi\rangle + \int_0^\infty d\varepsilon\; C_\varepsilon\,|\psi_\varepsilon\rangle = |\phi_0\rangle \tag{4.62}$$

and thus,

$$C_\xi = \langle\psi_\xi\,|\phi_0\rangle = a(\xi) \tag{4.63}$$

$$C_\varepsilon = \langle \psi_\varepsilon | \phi_0 \rangle = a(\varepsilon) \tag{4.64}$$

where the second equality is arrived at from the definition of the amplitudes $a(\xi)$ and $a(\varepsilon)$. Substituting into (61), we get

$$|\Psi(t)\rangle = a(\xi)\,|\psi_\xi\rangle \exp i\xi t + \int_0^\infty d\varepsilon\, a(\varepsilon)\,|\psi_\varepsilon\rangle \exp -i\varepsilon t \tag{4.65}$$

and by projecting out the state $|\phi_0\rangle$ from (60) and (65), we obtain

$$C_0(t) = |a(\xi)|^2 \exp i\xi t + \int_0^\infty d\varepsilon\, |a(\varepsilon)|^2 \exp -i\varepsilon t \tag{4.66}$$

which, using Eqs (58) and (59) is seen to be identical to Eq (34). Clearly, the incomplete decay of the ground state, represented by the residual amplitude $|a(\xi)|^2$, is due to the fact that some of the population is trapped in the stable bound state $|\psi_\xi\rangle$. We can derive an expression for $C_E(t)$ in a similar way:

$$C_E(t) = a(\xi)\, b(\xi, E) \exp i\xi t + \int_0^\infty d\varepsilon\, a(\varepsilon)\, b(\varepsilon, E) \exp -i\varepsilon t\,. \tag{4.67}$$

The integral on the RHS must be carried out numerically in order to obtain the time–evolution of $C_E(t)$, but it is possible to derive the long–time behaviour analytically. Consider

$$J(E,t) = \int_0^\infty d\varepsilon\, a(\varepsilon)\, b(\varepsilon, E) \exp -i\varepsilon t$$

$$= \int_0^\infty d\varepsilon \left[\frac{|a(\varepsilon)|^2\ V_\varepsilon}{\varepsilon - E} - a(\varepsilon) \cos\alpha\, \delta(\varepsilon - E) \right] \exp -i\varepsilon t\,. \tag{4.68}$$

The first term of J(E,t) may be re–expressed by closing the contour in the complex ε–plane as shown in Fig (9), and using the Residue Theorem. There is a branch cut along the positive real axis in this plane, and a pole for each value of E on the branch cut itself. To simplify the integration, we rotate the branch cut into the upper half–plane, keeping the branch point at the origin fixed. The pole on the axis is now fully exposed and the Residue Theorem may be used without any problem.

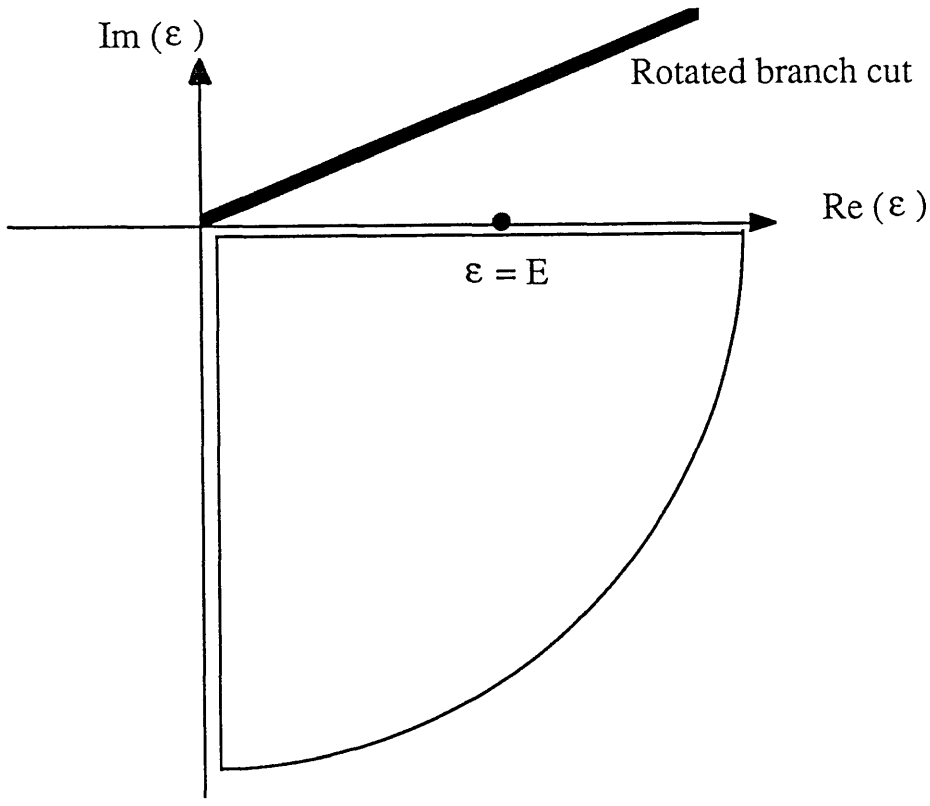

Figure 4.9 Complex ε-plane showing rotation of branch cut to reveal pole at $\varepsilon = E$.

As $t \rightarrow \infty$, the contributions from the integral along the imaginary axis, as well as the poles inside the contour vanish, because of the factor exp –iεt, and hence, in this limit, the integral is equal to $1/2 \times (2\pi i$ residue at $\varepsilon = E)$:

$$\lim_{t\to\infty} \int_0^\infty d\varepsilon \frac{|a(\varepsilon)|^2 \; V_\varepsilon}{\varepsilon - E} \exp -i\varepsilon t \; = \; i\pi \; |a(E)|^2 \, V_E \exp -iEt. \tag{4.69}$$

and from this we have

$$\lim_{t\to\infty} J(E,t) = [i\pi \; |a(E)|^2 \, V_E - a(E) \cos \alpha] \exp -iEt \tag{4.70}$$

which becomes, on using Eqs (48) and (59)

$$\lim_{t\to\infty} J(E,t) = \frac{-V_E}{[E - \bar{E} - F(E) - i\pi V_E^2]} \exp -iEt. \tag{4.71}$$

Finally, we may write

$$\lim_{t\to\infty} C_E(t) \exp iEt = -V_E \left[\frac{a^2(\xi)}{\xi + E} \exp i\xi t - \frac{\exp -iEt}{[\bar{E} - E - F(E) - i\pi V_E^2]} \right]. \tag{4.72}$$

Comparing Eqs (66) and (47), we see that $a^2(\xi)$ is $2\pi i \times$ residue of $\tilde{C}_0(s)$ at $s = i\xi$ and so, from Eq (24), the above expression is just $2\pi i \times$ the sum of the residues of $\tilde{C}_E(s)$ at $s = i\xi$ and $s = iE$. These two contributions beat with each other at all times, and so there is no true steady state for $C_E(t)$. If, however, the overlap with the bound state $|\psi_\xi\rangle$ is small enough to be neglected, then we may define the photoelectron spectrum at long times by the square of the absolute value of the second term in Eq (72), which is exactly the result obtained using the Final Value Theorem, Eq (38).

§4.4 The Dressed States Picture

We have seen in the previous two sections that the appearance of the new bound state makes the definition of a photoelectron spectrum problematic except in the low–field case when the effect of the threshold is not very important. For this reason, we 'undo' the two diagonalisations and reconsider the problem in terms of the atomic continuum $|\phi_{E'}\rangle$, which is physically more relevant than the continuum $|\phi_E\rangle$ because in an experiment, only electrons in the atomic continuum will be detected outside the laser field. Any population in the bound states $|\phi_0\rangle$ and $|\phi_1\rangle$ must be excluded from the photoelectron spectrum.

Before we proceed, we justify the claim made in the introduction that the system discussed in Section 2 represents a part diagonalisation of that illustrated in Fig 1b. To do this, we recall the expression (7) for the matrix element of the interaction between the ground state and the Fano continuum $|\phi_E\rangle$ (with no direct ionisation from the ground state):

$$V_{E_0} = \frac{V_1 \langle\phi_1|V_L|\phi_0\rangle}{[(E_1 - E + \Delta)^2 + \pi^2|V_1|^4]^{1/2}}. \qquad (4.7)$$

It is clear that provided V_1 (defined as the matrix element $\langle\phi_{E'}|V|\phi_1\rangle$ at E' = E) is constant in the region of interest near the threshold, Eq (7) represents a truncated Lorentzian since $V_1 = 0$ if $E' < 0$. The quantity Δ (given by $\mathbb{P}\int |V_1|^2/(E - E')\, dE'$) can be regarded as an energy shift of the autoionising state when E is replaced by E_1. This causes the centre of the Lorentzian to be shifted away from E_1, but if V_1 is small enough the shift may be ignored. However, we must not forget that because of the threshold, the diagonalisation of the $|\phi_1\rangle - |\phi_{E'}\rangle$ also results in a bound state that we denote $|\phi_{\xi'}\rangle$. The matrix element of the interaction between this and the

state $|\phi_0\rangle$ is

$$\langle\phi_{\xi'}|V_L|\phi_0\rangle = a(\xi')\, V_{10} \tag{4.73}$$

where $a(\xi')$ is given by analogy with Eq (58). From our previous results, we know that $a(\xi')$ is small when the discrete state–continuum interaction is small compared with the width of the continuum [condition (42)]. Therefore, if the width of the atomic continuum is large enough, we may neglect the coupling between $|\phi_0\rangle$ and $|\phi_{\xi'}\rangle$. We have thus shown that the systems of Figs 1b and 2 are very similar under the condition stated above. The results to be presented later in this section will confirm this statement.

§4.4.1 Method of solution

Having split up the truncated Lorentzian continuum into a flat one and an embedded discrete state we pre–diagonalise the sub–system formed by the discrete states, the aim being to interpret the results of the previous section in terms of the dressed states of the discrete sub–system. We shall work with a fully quantised Hamiltonian and atom–plus–field states, *i.e.* products of atomic states and photon number states. These will be denoted by

$$|0\rangle = |\phi_0\rangle|n+1\rangle \tag{4.74}$$

$$|1\rangle = |\phi_1\rangle|n\rangle \tag{4.75}$$

$$|E\rangle = |\phi_E\rangle|n\rangle \tag{4.76}$$

where n and n+1 label the number of photons in that state. For convenience, the primes have been dropped in the labelling of the atomic continuum. We have taken the embedding interaction to be of the configuration interaction type, but a laser interaction could just as easily have been considered. The full electronic wavefunction may be expanded in these states as follows:

$$|\Psi(t)\rangle = d_0(t)e^{-i[E_0 + (n+1)\omega]t}|0\rangle + d_1(t)e^{-i(E_1 + n\omega)t}|1\rangle$$

$$+ \int_0^\infty dE\, d_E(t)e^{-i(E + n\omega)t}|E\rangle. \tag{4.77}$$

If the interaction with the continuum is ignored, the above wavefunction is restricted to a superposition of the states $|0\rangle$ and $|1\rangle$ only, with the initial condition that $C_0(t=0) = 1$. The equations of motion for the amplitudes $C_0(t) = d_0(t)e^{-i[E_0 + (n+1)\omega]t}$ and $C_1(t) = d_1(t)e^{-i(E_1 + n\omega)t}$ may be written in matrix form as

$$i\begin{bmatrix}\dot{C}_0\\ \dot{C}_1\end{bmatrix} = \begin{bmatrix}E_0 + (n+1)\omega & V_{01}\\ V_{10} & E_1 + n\omega\end{bmatrix}\begin{bmatrix}C_0\\ C_1\end{bmatrix} \tag{4.78}$$

where,

$$V_{01} = \tfrac{1}{2}\langle 0|\underline{\mathcal{E}}.\underline{r}|1\rangle = V_{10}^* \tag{4.79}$$

with $\underline{\mathcal{E}}$ now the electric field operator, and the RWA has been made. The eigenvalues of the matrix on the RHS of Eq (78) are

$$E_\pm = \frac{1}{2}\left[E_1 + E_0 + (2n+1)\omega \pm \Omega\right]. \tag{4.80}$$

The detuning $D = E_1 - E - \omega$ and Ω is the generalised Rabi frequency given by

$$\Omega = \sqrt{D^2 + 4|V_{01}|^2}\,. \tag{4.81}$$

The eigenstates, which we call the dressed states[22], are

$$|+\rangle = \cos\theta\ |0\rangle + \sin\theta\ |1\rangle \tag{4.82}$$

$$|-\rangle = -\sin\theta\ |0\rangle + \cos\theta\ |1\rangle\,. \tag{4.83}$$

Here, $\cos^2\theta = (\Omega - \Delta)/2\Omega$ and $\sin^2\theta = (\Omega + \Delta)/2\Omega$. The wavefunction $|\Psi(t)\rangle$ may also be expanded using $|+\rangle$ and $|-\rangle$ so that instead of Eq (77), we have

$$|\Psi(t)\rangle = d_+(t)e^{-iE_+t}|+\rangle + d_-(t)e^{-iE_-t}|-\rangle + \int_0^\infty dE\ d_E(t)e^{-i(E + n\omega)t}|E\rangle\,. \tag{4.84}$$

We now allow $|1\rangle$ to interact with the continuum and write the quantised total Hamiltonian as

$$H = H_0 + H_F + \underline{\sigma}.\underline{r} + V_c \tag{4.85}$$

where V_c represents the embedding interaction and H_F the field Hamiltonian. Redefining the complex amplitudes in the dressed state picture by $C_+(t) = d_+(t)e^{-iE_+t}$, $C_-(t) = d_-(t)e^{-iE_-t}|-\rangle$ and $C_E(t) = d_E(t)e^{-i(E + n\omega)t}|E\rangle$, we get, from Schrodinger's Equation, the following equations of motion

$$i\dot{C}_+ = E_+C_+ + \sin\theta \int_0^\infty dE\ C_E\ V_{1E} \tag{4.86}$$

$$i\dot{C}_- = E_-C_- + \cos\theta \int_0^\infty dE\ C_E\ V_{1E} \tag{4.87}$$

$$i\dot{C}_E = EC_E + [\sin\theta\, C_+ + \cos\theta\, C_-]V_{E_1} \tag{4.88}$$

where we have used Eqs (82) and (83) to express the coupling of the dressed states with the continuum in terms of V_{E_1}. Note that by comparing Eqs (77) and (84), the following relation between the complex amplitudes in the two pictures may be obtained:

$$C_0(t) = \cos\theta\, C_+(t) - \sin\theta\, C_-(t) \tag{4.89}$$

$$C_1(t) = \sin\theta\, C_+(t) + \cos\theta\, C_-(t)\,. \tag{4.90}$$

The complex amplitudes for the continuum states are, of course, unchanged. Eqs (86–88) may be solved as before using the Laplace Transform. The initial conditions $C_0(0) = 1$ and $C_1(t) = 0$ become $C_+(0) = \cos\theta$ and $C_-(0) = -\sin\theta$. The Laplace space equations are

$$(s + iE_+)\tilde{C}_+(s) = \cos\theta \;\; i\sin\theta\int_0^\infty dE\, \tilde{C}_E\, V_{1E} \tag{4.91}$$

$$(s + iE_-)\tilde{C}_-(s) = -\sin\theta - i\cos\theta\int_0^\infty dE\, \tilde{C}_E\, V_{1E} \tag{4.92}$$

$$(s + iE)\tilde{C}_E(s) = -i[\sin\theta\, \tilde{C}_+ + \cos\theta\, \tilde{C}_-]V_{E_1} \tag{4.93}$$

where, as before, the tilde denotes the transformed function. Substitution of $\tilde{C}_E(s)$ from (93) into (91) and (92) yields

$$[s + iE_+ + \sin^2\theta\, f(s)]\tilde{C}_+ = \cos\theta\,[1 - \sin\theta\, f(s)\, \tilde{C}_-] \tag{4.94}$$

$$[s + iE_- + \cos^2\theta\, f(s)]\tilde{C}_- = \sin\theta\,[-1 - \cos\theta\, f(s)\,\tilde{C}_+] \tag{4.95}$$

with $f(s) = \int_0^\infty dE\ |V_{1E}|^2/(s + iE)$. Note that the dressed states $|+\rangle$ and $|-\rangle$ are now coupled to each other through the interaction of each with the continuum. Solving Eqs (94) and (95) gives

$$\tilde{C}_\pm = \frac{\begin{matrix}\cos\theta \\ -\sin\theta\end{matrix}\ [s + iE_\mp + f(s)]}{(s + iE_+)(s + iE_-) + f(s)[s + i(E_- \sin^2\theta + E_+ \cos^2\theta)]}\,. \tag{4.96}$$

This expression is simplified if we consider the case when the laser is resonant with the energy difference between $|\phi_0\rangle$ and $|\phi_1\rangle$ so that D = 0 and $\cos\theta = \sin\theta = 1/\sqrt{2}$:

$$\tilde{C}_\pm = \pm\frac{1}{\sqrt{2}}\ \frac{s + iE_\mp + f(s)}{s^2 + s[iE_1' + f(s)] + if(s)E_1' - E_1'^2 + |V_{01}|^2} \tag{4.97}$$

where we have made use of Eqs (80) and (81) and defined $E_1' = E_1 + n\omega = (n+)\omega$. We may now proceed to invert Eq (97) to obtain $C_\pm(t)$ from which we can deduce the amplitudes as $t\to\infty$. We do this by using Eq (33), closing the contour as shown in Fig (4) and using the Residue Theorem. We may therefore write

$$C_\pm(t) = \int_{BCDEFA} e^{st}\,\tilde{C}_\pm(s)\,ds - \sum \mathrm{Res}[e^{st}\,\tilde{C}_\pm(s)]\,. \tag{4.98}$$

We now assume that $|V_{1E}|^2$ is of the form (26), with a width Γ, centre $\bar{E}$ and strength V_s. For an exact correspondence with the system of Fig 2, the coupling would need to be a constant, however this makes the imaginary part of the integral

f(s) divergent. Several methods have been employed to overcome this problem, for example, the use of a high energy cutoff which leads to rather complicated expressions involving exponential integrals[4]. Our choice of coupling function is satisfactory provided that Γ is large enough as discussed earlier in this Section, and has the advantage that the results of Section 2 can also be used here. The choice of $\bar{E}$ is not very important because of the large width, but for convenience we shall take it to be equal to the energy of $|1\rangle$, *i.e.* $\bar{E} = E_1'$. If in Eq (7), we replace V_1 by its peak value, V_p, given by

$$|V_p|^2 = \frac{|V_s|^2}{\Gamma\,[\pi/2 + \tan^{-1}\bar{E}/\Gamma]} \tag{4.99}$$

then the width of the Fano continuum (the result of the $|\phi_1\rangle - |\phi_{E'}\rangle$ diagonalisation) is approximately $2|V_s|^2/\Gamma$ if $\bar{E} \ll \Gamma$. The centre of the Fano continuum will be shifted from $\bar{E}$ but the shift will be small if $|V_s|^2$ is small compared to Γ.

With this choice of matrix element, the integrals along BC, DE and AF in Eq (98) are negligible as $R\to\infty$ and $\varepsilon\to 0$ and so we are left with the integral around the branch cut and the residues at the poles to evaluate. The argument of s along CD is $3\pi/2$, while that along EF is $-\pi/2$. Let

$$I_1 = \lim_{s \to x e^{3i\pi/2}} \int_{CD} e^{st}\,\tilde{C}_{\pm}(s)\,ds \tag{4.100}$$

$$I_2 = \lim_{s \to x e^{-i\pi/2}} \int_{EF} e^{st}\,\tilde{C}_{\pm}(s)\,ds\,. \tag{4.101}$$

Adapting the results of Section 2 to the present case, we find that

$$f(xe^{i3\pi/2}) = \frac{ic_1}{[(x-\bar{E})^2+\Gamma^2]}\left(c_2(x-\bar{E}) + \Gamma \ln\left|\frac{x}{\bar{E}+i\Gamma}\right| + i\Gamma\pi\right) \tag{4.102}$$

$$f(xe^{-i\pi/2}) = \frac{ic_1}{[(x-\bar{E})^2+\Gamma^2]}\left(c_2(x-\bar{E}) + \Gamma \ln\left|\frac{x}{\bar{E}+i\Gamma}\right| - i\Gamma\pi\right). \tag{4.103}$$

Using Eqs (102) and (103), Eqs (100) and (101) become

$$I_1 = -i\int_{-\infty}^{0} dx \frac{e^{-ixt}\left[h(x) - i\Gamma\pi c_1[(x-\bar{E})^2+\Gamma^2]^{-1} \pm V_{10}\right]}{(x-\bar{E})\left[h(x) - i\Gamma\pi c_1[(x-\bar{E})^2+\Gamma^2]^{-1}\right] - |V_{10}|^2} \tag{4.104}$$

$$I_2 = -i\int_{0}^{\infty} dx \frac{e^{-ixt}\left[h(x) + i\Gamma\pi c_1[(x-\bar{E})^2+\Gamma^2]^{-1} \pm V_{10}\right]}{(x-\bar{E})\left[h(x) + i\Gamma\pi c_1[(x-\bar{E})^2+\Gamma^2]^{-1}\right] - |V_{10}|^2} \tag{4.105}$$

After some algebra, we find that the integral round the branch cut is

$$I_1 + I_2 = \int_{0}^{\infty} dx \frac{e^{-ixt}\ 2V_{10}\Gamma\pi c_1[(x-\bar{E})^2+\Gamma^2]^{-1}[\mp(x-\bar{E}) - V_{10}]}{\left[(x-\bar{E})h(x) - |V_{10}|^2\right]^2 + \left[\Gamma\pi c_1[(x-\bar{E})^2+\Gamma^2]^{-1}\right]^2} \tag{4.106}$$

At t=0, this quantity must be finite, therefore, by the Riemann–Lebesgue Lemma[21], as $t\to\infty$, it tends to zero. Hence, the only remaining contribution to the integral in

Eq (98) is that from the poles. Since the function whose poles we require contains the factor e^{st}, any pole at $s = \zeta$ such that $\mathrm{Re}(\zeta) \neq 0$ has a residue that either grows or dies away exponentially as $t \to \infty$. Obviously, the first possibility cannot arise, $C_{\pm}(t)$ always being finite quantities, and so there cannot be any poles in the right hand half–plane. The poles in the left–hand half–plane will not contribute at long times; only a pole on the positive imaginary axis will have a non–vanishing contribution. To locate any such pole, we set the real and imaginary parts of the denominator of $\tilde{C}_{\pm}(s)$ to zero separately. Writing $s = x + iy$ and $f(s) = j(s) + ik(s)$, we get

$$x^2 + xj(s) - (y + \bar{E})k(s) - (y + \bar{E})^2 + |V_{10}|^2 = 0 \tag{4.107}$$

$$(2x + j(s))(y + \bar{E}) + xk(s) = 0 \, . \tag{4.108}$$

Now,

$$j(s) = \mathrm{Re}[f(s)] = x \int_0^{\infty} dE \, \frac{|V_{1E}|^2}{x^2 + (E + y)^2} \, . \tag{4.109}$$

Therefore, putting $x = 0$ ensures that the imaginary part of the denominator is zero, while Eq (107) reduces to

$$y^2 + y[k(iy) + 2\bar{E}] + k(iy)\bar{E} + \bar{E}^2 - |V_{10}|^2 = 0 \, . \tag{4.110}$$

This equation must be solved numerically. In Fig 10a, we have plotted the function Q(y) defined by the LHS of Eq (110), with $|V_{10}|^2 = 0$. It can be seen that for $V_s \gg \Gamma$, the function has two turning points, but as V_s decreases relative to Γ, the turning points disappear. This is seen more clearly in in Fig 10b, where we have plotted the derivative Q'(y) of Q(y) with respect to y – for large V_s, Q'(y) crosses the

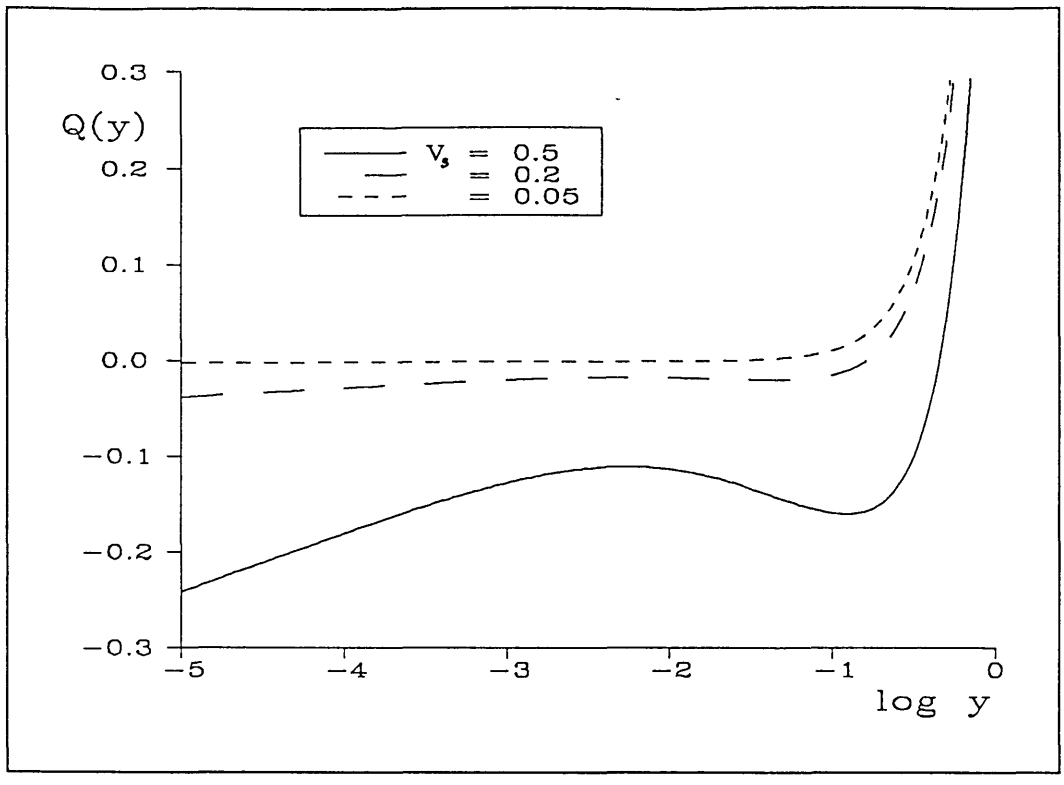

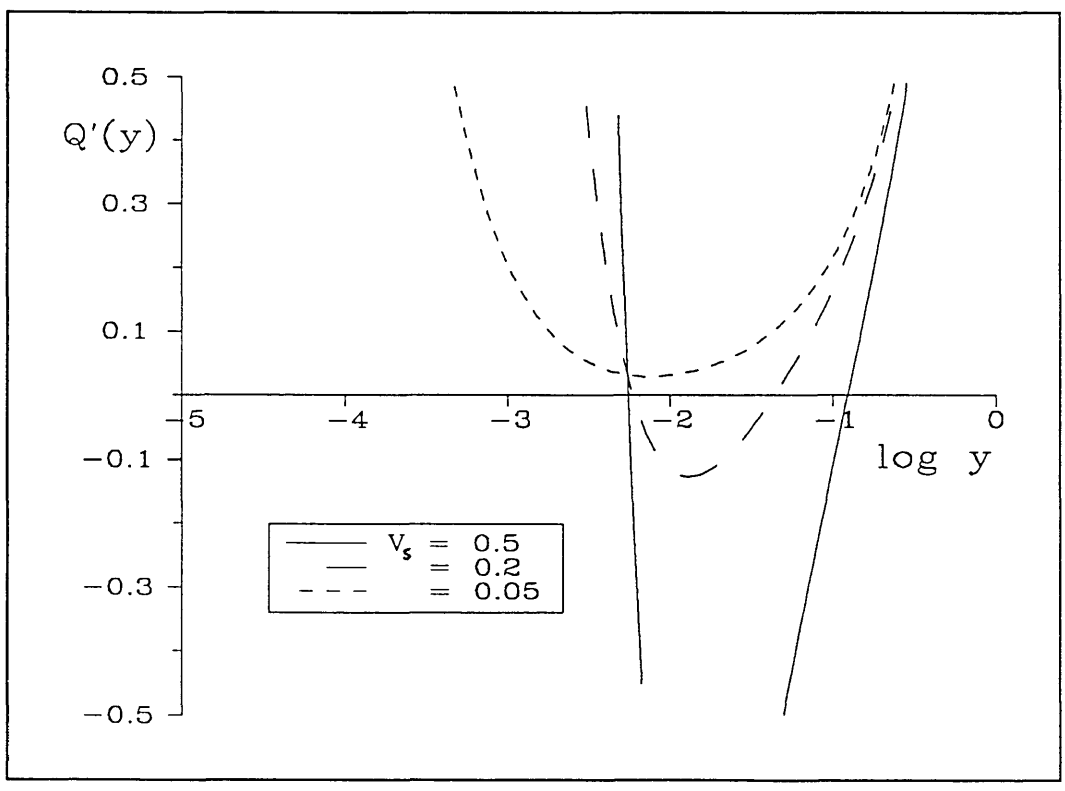

Figure 4.10 Graph of LHS [Q(y)] of Eq (110) and its derivative [Q'(y)] as functions of y with $|V_{10}|^2 = 0$, $\Gamma = 0.05$, $\bar{E} = 0.01$.

abscissa at two points, while for small V, it does not cross the axis at all. The solution of Eq (110) is given by the point at which Q(y) crosses the abscissa for non–zero values of $|V_{10}|^2$. As $|V_{10}|^2$ is increased, Q(y) moves downward with respect to the the axes, hence the equation has only one solution , and $\tilde{C}_{\pm}(s)$ have only one pole at, say, $s = i\zeta$, for $\zeta < 0$. We now have that

$$|C_{\pm}(t\rightarrow\infty)|^2 = |\mathrm{res}[e^{st}\tilde{C}_{\pm}(s)]_{s=i\zeta}|^2$$

$$= |\mathrm{res}[\tilde{C}_{\pm}(s)]_{s=i\zeta}|^2 \qquad (4.111)$$

which we calculate using L'Hôpital's rule. This gives

$$\mathrm{res}[\tilde{C}_{\pm}(s)]_{s=i\zeta} = \frac{[\zeta + E_{\mp} + k(i\zeta)]}{2[\zeta + \bar{E} + k(i\zeta)/2] + (\zeta + \bar{E})\left.\frac{\partial k(iy)}{\partial y}\right|_{y=\zeta}}. \qquad (4.112)$$

with

$$\left.\frac{\partial k(iy)}{\partial y}\right|_{y=\zeta} = c_1 \frac{c_2\,[(\zeta + \bar{E})^2 - \Gamma^2] - 2\Gamma(\zeta + \bar{E})\ \ln\ \zeta/|\bar{E} + i\Gamma| + \Gamma/\zeta\,[(\zeta + \bar{E})^2 + \Gamma^2]}{[(\zeta + \bar{E})^2 + \Gamma^2]^2} \qquad (4.113)$$

§4.4.2 Results and discussion

In Fig 11, we plot the probability that the electron is in one of the two dressed states as $t\rightarrow\infty$ as functions of log $|V_{10}|^2$. For this picture, and all the others in this Section, we have chosen values of V_s and Γ such that the diagonalisation of the

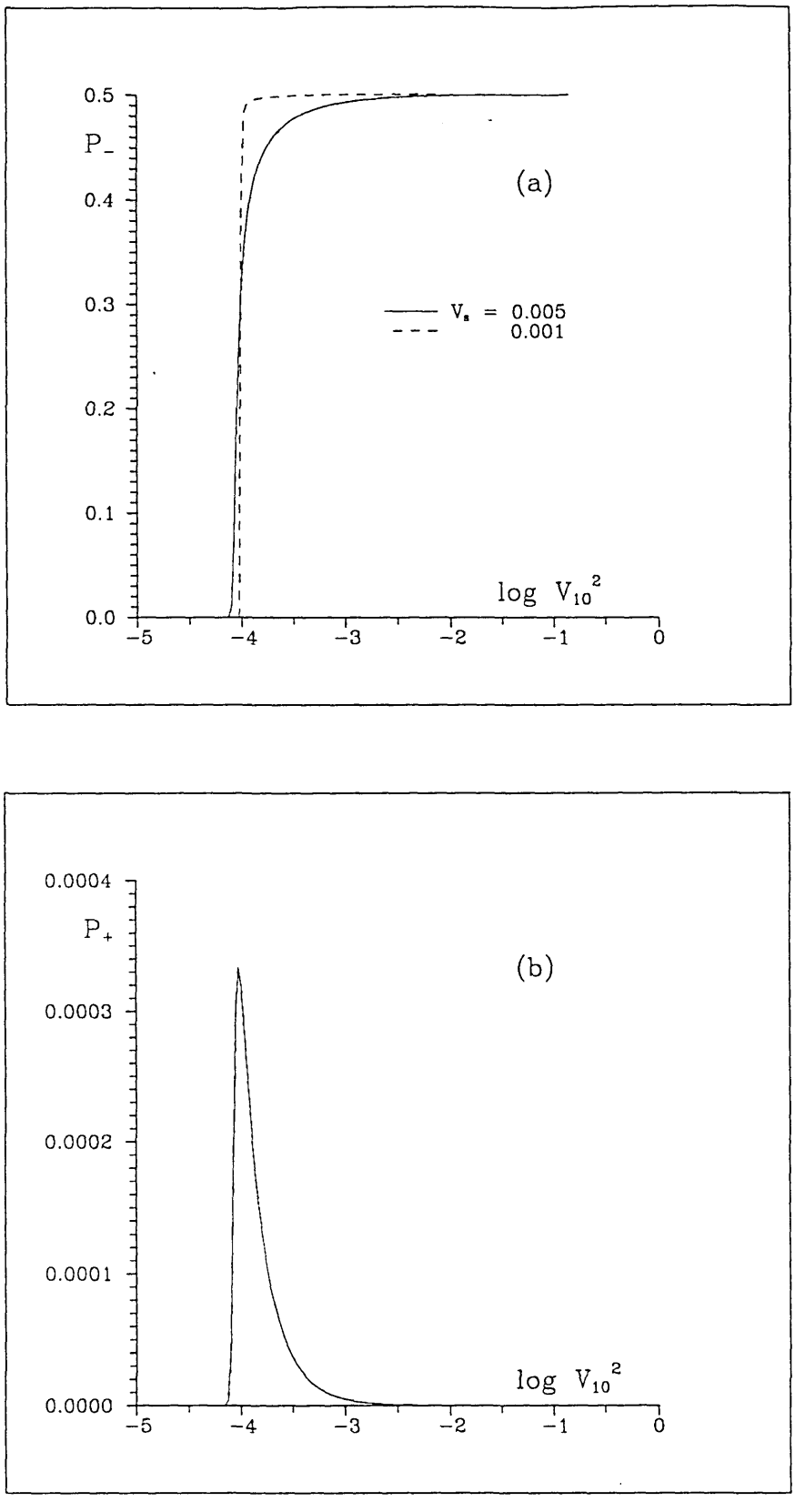

Figure 4.11 Dressed state probabilities P_+ and P_- as $t \to \infty$. —— $V_s = 0.005$, $\Gamma = 20$, - - - $V_s = 0.001$, $\Gamma = 0.05$, $\bar{E} = 0.01$. P_+ in the latter case is not visible on this scale.

excited state–continuum states system leads to a truncated Lorentzian coupling to the ground state as discussed previously. The widths of the *Fano* continuum for the two values of V_s shown in Fig 11 are approximately 10^{-3} and 0.4×10^{-4}. We see that for small values of $|V_{10}|^2$ both populations have decayed almost to zero, but that as the coupling increases, P_- stays at approximately 0.5 which was its starting value. In other words, the decay of the dressed state $|-\rangle$ has been been almost suppressed, while the state $|+\rangle$ continues to decay completely. The change in P_- occurs rather abruptly when the value of V_{10} is approximately that of $\tilde{E}$, while in this region, P_+ has a small peak, orders of magnitude lower than P_-. Since we are considering the resonant case, the probabilities for the electron being in the ground and excited states are simply

$$P_0(t) = |C_+(t) - C_-(t)|^2/2 \tag{4.114}$$

$$P_1(t) = |C_+(t) + C_-(t)|^2/2 \,. \tag{4.115}$$

Fig 12 shows P_0 and P_1 as functions of log $|V_{10}|^2$, for the same values of V_s and Γ as Fig 11. It is seen that the graph of P_0 looks very similar to the corresponding one, Fig 6a, in Section 2, including the increasing abruptness of the change in P_0 with a reduction in γ, or the effective width. This confirms that the present model does indeed correspond very closely to the one in Section 2. Fig 11 suggests the following interpretation of the decay process in the dressed states picture. As the field strength is increased, the energy separation of the dressed states also increases, pushing the lower dressed state below the continuum threshold. Because there are no energy–conserving continuum levels that are accessible this state is unable to decay. Moreover, as it is a superposition of the states $|0\rangle$ and $|1\rangle$, this means that at long times, both atomic states have some population trapped in them. The exact amount depends on the initial population of the lower dressed state. In this case it was 0.5

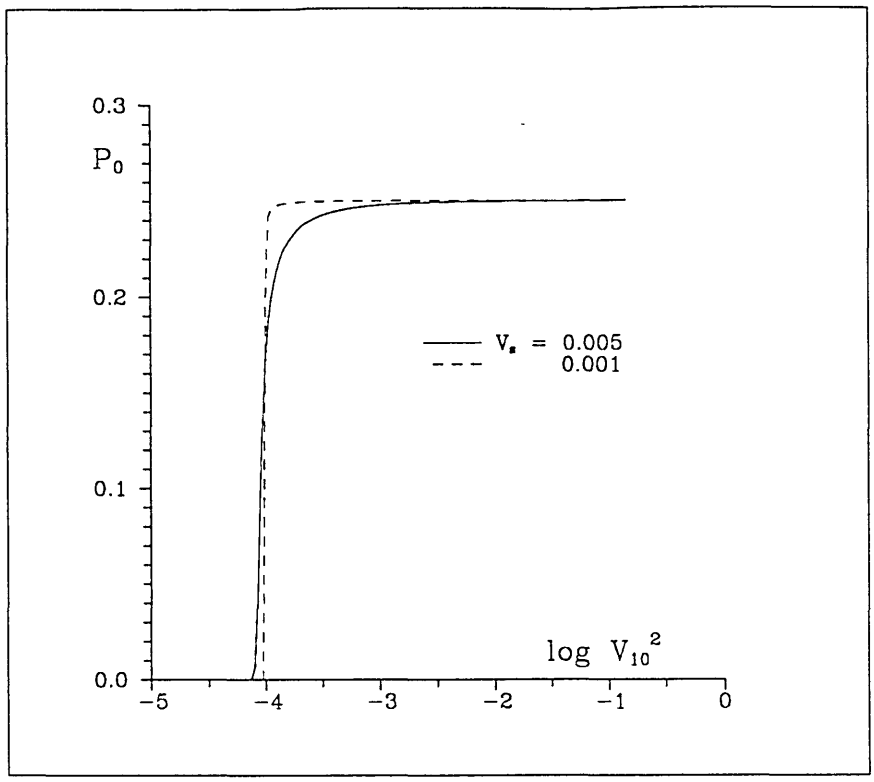

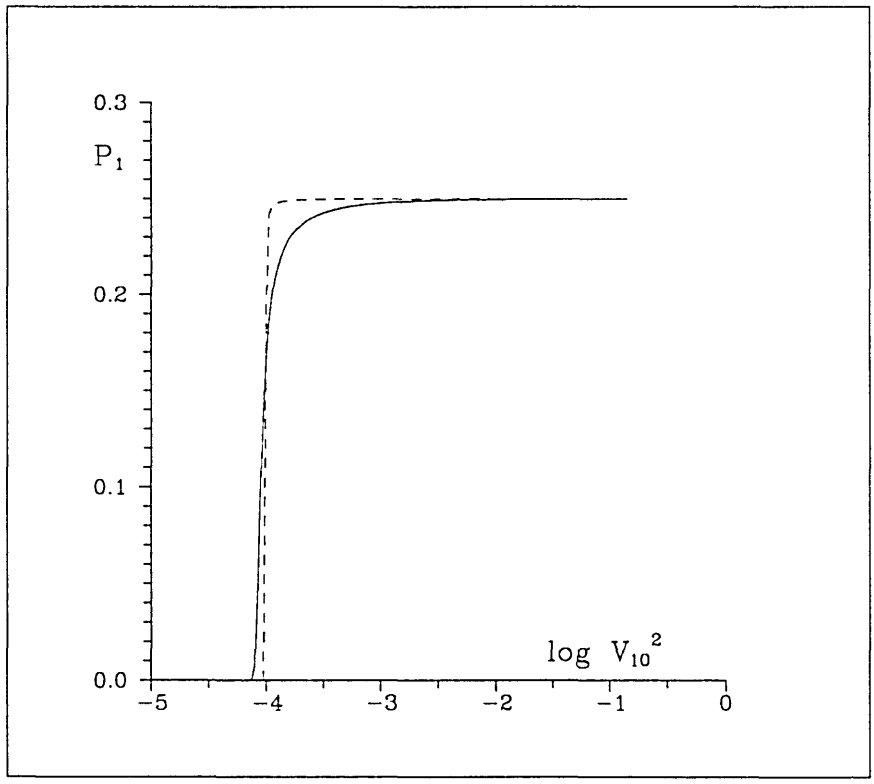

Figure 4.12 Ground and excited state probabilities P_0 and P_1 as $t \to \infty$. ____ $V_s = 0.005, \Gamma = 0.05$, - - - $V_s = 0.001, \Gamma = 0.05, \bar{E} = 0.01$.

giving an equal probability for the electron to be in each of the unperturbed states, as confirmed by Fig 12. This explains why in Section 2, $P_0(t\rightarrow\infty) \rightarrow 0.25$ for large values of $|V_{10}|^2$. It is also the reason for the total probability defined in Eq (40) not being equal to unity, for the population in the state $|1\rangle$ is not accounted for in the single discrete state–Fano continuum model.

Having established that the ground state population behaves in a similar way in both models, we now ask whether it is possible to define a long–time photoelectron spectrum with the present model. The problem is that there is still a pole on the positive imaginary axis in the complex s–plane and we need to know how large its contribution to $C_{E'}(t\rightarrow\infty)$ is compared with the pole at $s = -iE'$ which is, as we saw in Section 3, the pole that gives the result of the Final Value Theorem. We first write down the expression for $\tilde{C}_{E'}(s)$ from Eqs (93) and (96):

$$\tilde{C}_{E'}(s) = \frac{-V_{E_1}V_{10}}{s^2 + s[i\bar{E} + f(s)] + if(s)\bar{E} - \bar{E} + |V_{10}|^2](s + iE')} . \tag{4.116}$$

By the Residue Theorem, we have, since all other pole and branch cut contributions vanish in the limit $t\rightarrow\infty$,

$$\lim_{t\rightarrow\infty} C_{E'}(t) = \sum_{s=i\zeta,\, iE'} \text{Res}\,[\tilde{C}_{E'}(s)\, e^{st}]$$

$$= -V_{E_1} V_{10} \left\{ \left[2[\zeta + \bar{E} + k(i\zeta)/2] + (\zeta + \bar{E}) \frac{\partial k(iy)}{\partial y}\Big|_{y=\zeta} \right]^{-1} (\bar{E} + \zeta)^{-1} \right.$$

$$\left. - [(E' - \bar{E})^2 + i\,((E' - \bar{E}) f(-iE') - |V_{10}|^2]^{-1} \right\} . \tag{4.117}$$

An easy way to check the effect of the contribution of the pole ζ is to calculate the total probability P_T', as $t \to \infty$ in the states $|+\rangle$, $|-\rangle$ and the continuum, using only the second term of Eq (117) to calculate $P_{E'}(t \to \infty)$. This is illustrated in Fig (13) as a

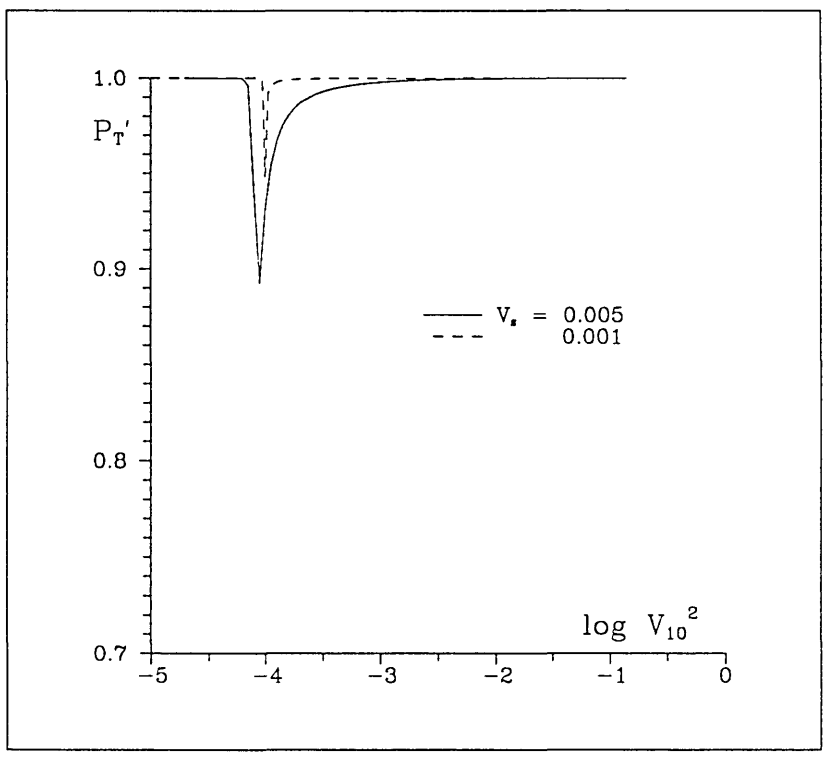

Figure 4.13 Total probability P_T', defined as the sum of the dressed state probabilities and the population in the continuum labelled by E' as $t \to \infty$. ——— *$V_s = 0.005$, $\Gamma = 0.05$,* - - - *$V_s = 0.001$, $\Gamma = 0.05$, $\bar{E} = 0.01$.*

function of log $|V_{10}|^2$, and is seen to be very nearly unity except in a small window between $|V_{10}|^2 = 10^{-4}$ and $|V_{10}|^2 = 10^{-3}$, for $V_s = 0.005$, and in a much smaller window for $V_s = 0.001$. In this region, the absolute values of the residues at the two poles are comparable for all values of E' except where the second pole contribution peaks strongly, while outside this region the pole at $s = iE'$ dominates the one at $s = i\zeta$, so the Final Value Theorem can be used accurately only outside the window.

In Fig (14), we illustrate the long–time photoelectron spectra using the Final Value Theorem at different points outside this window. When the coupling between the ground and excited states is weak, a single sharp peak centred on the energy $\bar{E}$ is observed. The area under the peak is unity, showing that all the population has decayed into this continuum. As the coupling is increased, the spectrum splits into two peaks as expected. However, what is surprising is that although we have chosen resonance conditions *i.e.* the energies E_0' and E_1' are the same and equal to $\bar{E}$, the Autler–Townes doublet shows a marked asymmetry. The reason for the asymmetry is that the excited state experiences a shift, Δ [see Eq (3)] which, from Appendix A, is equal to $F(\bar{E})$. The shift causes the excited state to be pulled out of resonance with the ground state and the distribution of the initial population between the dressed states becomes unequal as can be seen from Eqs (81–83), with the result that each peak in the doublet has a different height. The shift can be seen in Fig (15) which is a plot of the coupling, $|V_{E_0}|^2$, between the ground state and the Fano continuum, calculated using Eq (7). The peak of the curve is not at $\bar{E}$, the unperturbed energy of the excited state, but at $E = 0.0095$. Another consequence of the shift is that the structure in the spectrum is itself shifted, the minimum between the two peaks occurs at $E' = 0.00975$ and not at $E' = 0.01$, as would be expected from the threshold–less case. That the shift in the spectrum should be only half the shift of the energy state can be seen from the expression for the energy eigenvalues $E_{\pm}$ which determine the positions of the peaks and minimum in the spectrum. One might wonder why a

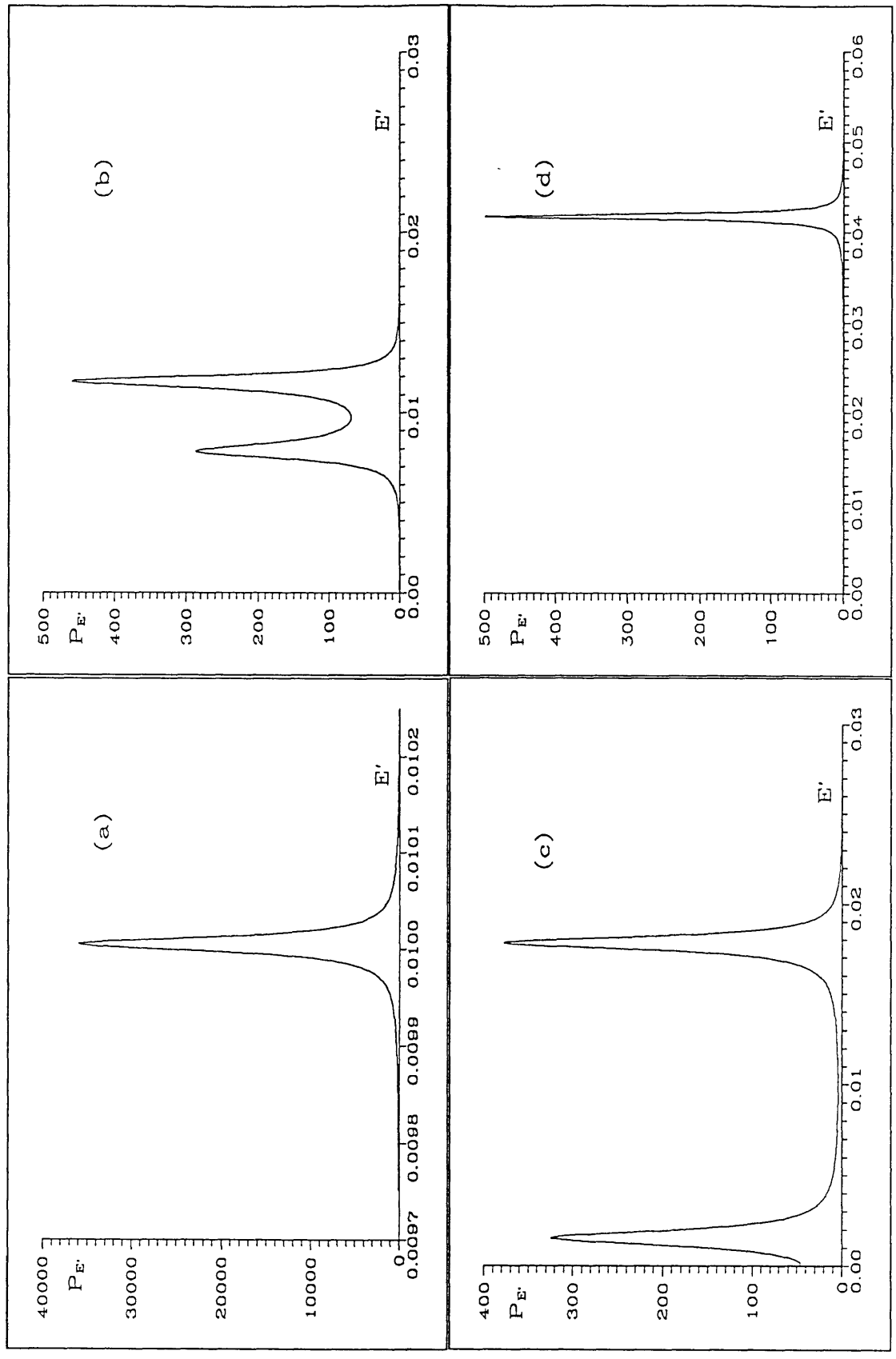

Figure 4.14 Photoelectron spectra in the continuum labelled by E′ as $t \to \infty$. $V_s = 0.005$, $\Gamma = 0.05$, $\bar{E} = 0.01$, *(a)* $\log |V_{10}|^2 = -8$ *(b)* $\log |V_{10}|^2 = -5.4$ $(V_{10} = 0.02)$ *(c)* $\log |V_{10}|^2 = -4.2$ $(V_{10} = 0.02)$ *(d)* $\log |V_{10}|^2 = -3$.

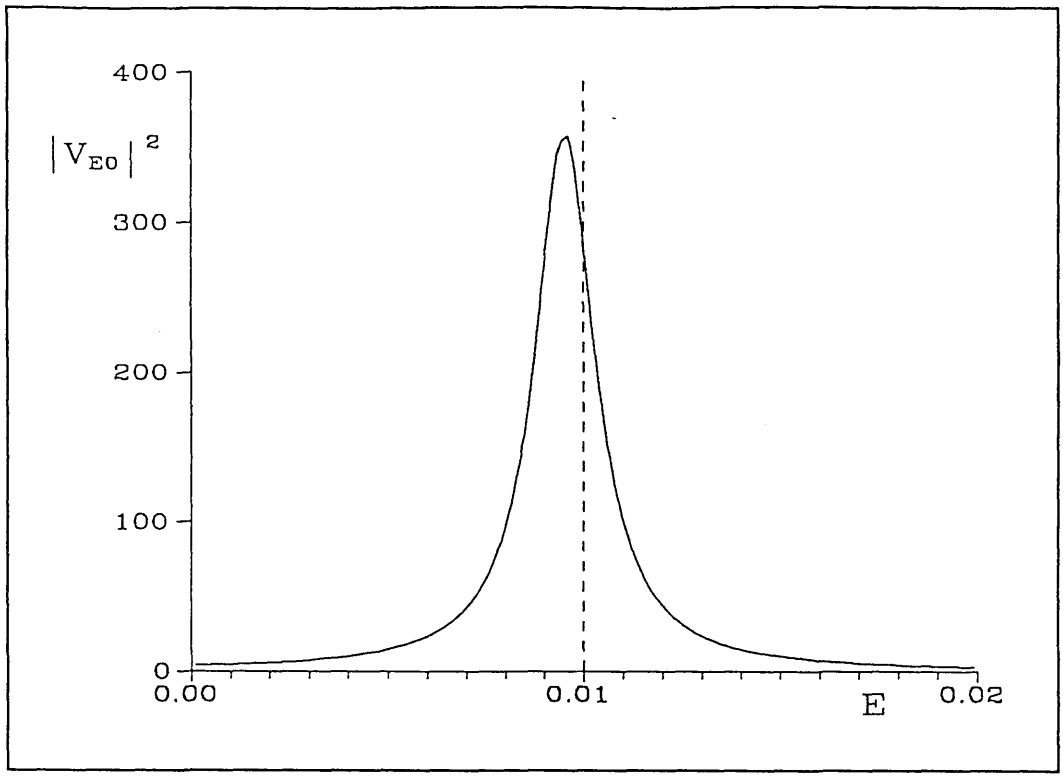

Figure 4.15 Matrix element for interaction of ground state with Fano continuum $V_s = 0.005$, $\Gamma = 0.05$, $\bar{E} = 0.01$.

similar shift is not observed in Fig (14a), for a low value of V_{10}. This can be explained in terms of the Fano continuum whose width is large compared to the coupling with the ground state. Since its centre is also large compared with the other parameters, the Wigner–Weisskopf result is applicable. This predicts a photoelectron peak at the ground state energy with a shift determined by V_{10} which in this case is so small that no shift can be seen in the photoelectron spectrum. When V_{10} is large, the Wigner–Weisskopf theory cannot be used to predict the photoelectron spectrum.

As V_{10} increases further, the relative importance of the shift and hence the difference in height of the two peaks is reduced (Fig 14c). When V_{10} becomes greater than $\bar{E}$, as in Fig 14d, the doublet structure disappears and only one peak is seen, the area under this peak being one half reflecting the decay of only one of the dressed states, $|+\rangle$, while the peak due to the decay of the lower dressed state, $|-\rangle$, has disappeared since its energy, E_-, is below the threshold.

Appendix A

In this appendix, we derive the expansion coefficients for the continuous energy Fano eigenstates[2] for a system of one discrete state interacting with one continuum. Each Fano state is expanded in terms of the unperturbed states as in Eq (1). Premultiplying Eq (1) by $\langle\phi_1|H$ and integrating over all space gives

$$E_1\, a(E) + \int dE'\, b(E,E')\, V_{1E'} = E\, a(E)\,. \tag{A1}$$

Repeating the same operation but with $\langle\phi_E|H$ gives

$$V_{E'_1}\, a(E) + E'\, b(E,E') = E\, b(E,E') \tag{A3}$$

where the matrix element $V_{E'_1}$ is defined after Eq (3). Eqs (A3) and (A4) may be solved by first expressing b(E,E') in terms of a(E), but if E = E', this involves a division by zero. We therefore split $(E - E')^{-1}$ into principal and δ–function parts:

$$b(E,E') = V_{E'_1}\, a(E) \left[\mathbb{P}\, \frac{1}{E - E'} + z(E)\, \delta(E - E') \right] \tag{A5}$$

where z(E) is to be determined. By substituting (A5) into (A3), we get

$$E_1 + F(E) + z(E)\, |V_1|^2 = E \tag{A6}$$

where

$$F(E) = \mathbb{P} \int dE'\, \frac{|V_1|^2}{E - E'} \tag{A7}$$

and $V_1 = V_{E'_1}(E' = E)$ so that z(E) is given by

$$z(E) = \frac{E - E_1 - F(E)}{|V_1|^2}. \qquad \text{(A8)}$$

The coefficient a(E) may be determined from the normalisation condition on the Fano states

$$\langle \phi_E | \phi_{E''} \rangle = \delta(E - E'')$$

$$= a^*(E'')\, a(E) + \int dE'\, b^*(E'',E')\, b(E,E')$$

$$= a^*(E'')\, a(E) \left\{ 1 + \int dE'\, V_{E'_1} \left[\mathbb{P} \frac{1}{E'' - E'} + z(E'')\, \delta(E'' - E') \right] \times \right.$$

$$\left. V_{1E'} \left[\mathbb{P} \frac{1}{E - E'} + z(E)\, \delta(E - E') \right] \right\}. \qquad \text{(A9)}$$

In the last step, Eq (A5) was used. Note that in Eq (A9) there is a double singularity at E'' = E because of the product of principle parts. It has been shown by Fano that the factor $1/(E'' - E')(E - E')$ can be expressed as

$$\frac{1}{(E'' - E')(E - E')} = \frac{1}{E'' - E} \left[\frac{1}{E - E'} - \frac{1}{E'' - E'} \right] + \pi^2\, \delta(E'' - E')\, \delta(E - E') \qquad \text{(A10)}$$

so that (A9) becomes

$$\delta(E'' - E) = |a(E)|^2\, |V_1|^2\, [\pi^2 + z^2(E)]\, \delta(E'' - E) + a^*(E'')\, a(E) \times$$

$$\left[1 + \frac{1}{E'' - E} [F(E) - F(E'') + z(E)\, |V_1|^2 - z(E'')\, |V_1''|^2] \right] \qquad \text{(A11)}$$

But using Eq (A8), the expression in the large square brackets vanishes, and Eq (A11) becomes

$$|a(E)|^2 = \frac{|V_1|^2}{[E - E_1 - F(E)]^2 + \pi^2|V_1|^4}. \tag{A12}$$

Using Eqs (A5), (A8) and (A12), the coefficient b(E,E') is easily seen to be

$$b(E,E') = V_{E'1} \frac{|V_1|}{\{[E - E_1 - F(E)]^2 + \pi^2|V_1|^4\}^{1/2}} \times$$

$$\left[\mathbb{P} \frac{1}{E - E'} + \frac{E - E_1 - F(E)}{|V_1|^2} \delta(E - E') \right]. \tag{A13}$$

Equations A(12) and (A13) may be expressed more compactly by defining the angle α such that

$$\tan \alpha = \frac{-\pi|V_1|}{E - E_1 - F(E)}. \tag{A14}.$$

We then have

$$a(E) = \sin \alpha/\pi_1 \tag{A15}$$

$$b(E,E') = \frac{V_{E'1}}{\pi V_1} \left[\mathbb{P} \frac{\sin \alpha}{E - E'} - \cos \alpha \, \delta(E - E') \right]. \tag{A16}$$

Appendix B

Following Piraux[18], we evaluate the integral f(s) in Eq (25) for a truncated Lorentzian. Let

$$I = \int_0^{\beta} dE \, \frac{1}{[(E - \bar{E})^2 + \gamma^2]\,(s + iE)} \tag{B1}$$

The required integral will be obtained by taking the limit $\beta \to \infty$. The integrand in Eq (B1) can be decomposed into partial fractions to yield

$$I = \frac{1}{2\gamma} \int_0^{\beta} dE \left\{ \frac{1}{is - \bar{E} - i\gamma} \left[\frac{1}{E - \bar{E} - i\gamma} - \frac{1}{E - is} \right] - \right.$$

$$\left. \frac{1}{is - \bar{E} + i\gamma} \left[\frac{1}{E - \bar{E} + i\gamma} - \frac{1}{E - is} \right] \right\} \tag{B2}$$

But

$$\int_0^{\beta} dE \left[\frac{1}{E - \bar{E} \pm i\gamma} - \frac{1}{E - is} \right] = \ln \left[\frac{\bar{E} \mp i\gamma - \beta}{is - \beta} \right] + \ln \left[\frac{is}{\bar{E} \mp i\gamma} \right] \tag{B3}$$

In the limit that $\beta \to \infty$, the first term on the RHS of (B3) goes to zero, and so

$$\lim_{\beta \to \infty} I = \frac{1}{2\gamma} \left\{ \frac{1}{is - \bar{E} - i\gamma} \ln \left[\frac{is}{\bar{E} + i\gamma} \right] - \frac{1}{is - \bar{E} + i\gamma} \left[\frac{is}{\bar{E} - i\gamma} \right] \right\} \tag{B4}$$

In the E–plane, the branch cut is along the positive real axis, and so the argument of the logarithm is between 0 and 2π. Therefore, we have

$$\ln (\bar{E} + i\gamma) = \ln |\bar{E} + i\gamma| + i \tan^{-1}(\gamma/\bar{E}) \tag{B5}$$

$$\ln (\bar{E} - i\gamma) = \ln |\bar{E} + i\gamma| - i \tan^{-1}(\gamma/\bar{E}) + 2\pi i \tag{B6}$$

so that (B4) becomes

$$\lim_{\beta\to\infty} I = \frac{i\pi - \tan^{-1}(\gamma/\bar{E})}{\gamma} - \frac{i}{is - \bar{E} + i\gamma} + \frac{i}{(is - \bar{E})^2 + \gamma^2} \ln \left[\frac{is}{\bar{E} + i\gamma} \right] \tag{B7}$$

Substituting (B7) into Eq (25) and using Eqs (26), (30) and (31) yields Eq (28).

Appendix C

In this appendix, we obtain the time evolution and photoelectron spectrum for a model which is a simplified version of the one shown in Fig 2. The simplification consists of neglecting the threshold and extending the lower limit of the integral in Eq (25) to $-\infty$. The integral is then carried out by contour integration and closing the contour in the lower half–plane, giving

$$f(s) = \frac{|V|^2}{s + i\tilde{E} + \gamma} \tag{C1}$$

Substituting this expression for f(s) instead of (28) into Eq (23), we get, for $\bar{E} = \tilde{E}$

$$\tilde{C}_0(s) = \frac{s + i\bar{E} + \gamma}{(is - E_+)(is - E_-)} \tag{C2}$$

where

$$E_{\pm} = \bar{E} - \frac{i\gamma}{2} \pm \frac{1}{2}\Omega' \qquad \Omega' = \sqrt{4|V|^2 - \gamma^2} \tag{C3}$$

Eq (C2) is inverted using, for example, Eq (33) to give

$$C_0(t) = \exp -i(E - i\gamma/2)t \, [\cos \Omega' t/2 + \gamma/\Omega' \sin \Omega' t/2] \tag{C4}$$

The presence of the exponential factor as well as the complex Rabi frequency ensure that the ground state population always decays to zero as $t \to \infty$. In this case there are no poles on the positive imaginary axis, as both E_+ and E_- are complex. This means that we can obtain the long–time photoelectron spectrum using the Final Value

Theorem which using Eqs (37), (24) and (C2) gives

$$P_E(t\to\infty) = \frac{\gamma|V|^2}{\pi\,|(E-E_+)(E-E_-)|^2} \tag{C5}$$

By substituting for $E_\pm$, it can be seen that $P_E(t\to\infty)$ is an even function in $E-\bar{E}$, hence the spectrum is always symmetric around $\bar{E}$. Note that the spectrum must extend to negative values of E in order to satisfy probability conservation.

The two limiting cases $V \ll \gamma$ and $V \gg \gamma$ are interesting to consider:

a) $V \ll \gamma$

In this case, the Rabi frequency Ω' can be expanded to give

$$\Omega' = -i\gamma(1-4V^2/\gamma^2)^{1/2} \simeq -i\gamma(1-2V^2/\gamma^2) \tag{C6}$$

Substituting into (C4) gives

$$C_0(t) \simeq \exp(-V^2t/\gamma - i\bar{E}t), \qquad P_0(t) = \exp(-2V^2t/\gamma) \tag{C7}$$

The dressed energies are approximately

$$E_+ = \bar{E} - i\gamma + O(V^2/\gamma) \qquad\qquad E_- = E - iV^2/\gamma \tag{C8}$$

so that

$$P_E(t=\infty) = \frac{\gamma|V|^2/\pi}{[(E-\bar{E})^2+\gamma^2]\;\;[(E-\bar{E})^2+V^4/\gamma^2]} \tag{C9}$$

Therefore, in this regime, the decay of the ground state probability is purely exponential and the photoelectron spectrum consists of a product of two Lorentzians, one of width γ, and the other with a much smaller width V^2/γ which is the usual Golden Rule rate. The spectrum exhibits a sharp peak at $E = \bar{E}$.

b) $V \gg \gamma$

In this case, the Rabi frequency is

$$\Omega' = 2V(1 - \gamma^2/4V^2)^{1/2} \simeq 2V - \gamma^2/4V \tag{C10}$$

and the dressed energies are

$$E_{\pm} = \bar{E} - \frac{i\gamma}{2} \pm V + O(\gamma^2/V) \tag{C11}$$

so that

$$C_0(t) \simeq \cos Vt \exp(-\gamma t/2 - i\bar{E}t) \qquad P_0(t) \simeq e^{-\gamma t} \cos^2 Vt \tag{C12}$$

which exhibits oscillations of frequency 2V damped with at rate γ. The photoelectron spectrum can be expressed as

$$P_E(t = \infty) \simeq \frac{\gamma |V|^2/\pi}{|(E - \bar{E} - V - i\gamma/2)(E - \bar{E} + V - i\gamma/2)|^2} \tag{C13}$$

which is also a product of two Lorentzians, this time of the same width but centred at $E = \bar{E} \pm V$. By decomposing into partial fractions, Eq (C13) can be rewritten as

$$P_E(t=\infty) \simeq \frac{\gamma}{4\pi}\left[\frac{1}{(E-\bar{E}-V)^2+\gamma^2/4)}+\frac{1}{(E-\bar{E}+V)^2+\gamma^2/4)}\right]+$$

$$\frac{\gamma\,[(E-\bar{E})^2-V^2+\gamma^2/4]}{4\pi\,[(E-\bar{E}-V)^2+\gamma^2/4]\,[(E-\bar{E}+V)^2+\gamma^2/4]}$$

(C14)

Because there is no threshold in this problem, and we are considering resonance conditions, $\bar{E}$ can be arbitrarily set equal to zero. At $E = \pm V$, the last term in (C14) is then of order γ/V^2 and so may be neglected. Consequently, the spectrum consists of two Lorentzians centred at $E = \bar{E} \pm V$ each of width $\gamma/2$. If the original Lorentzian continuum is regarded as the combination of a discrete state and a flat infinite continuum, then each peak in (C14) represents the decay of one dressed state of the two discrete state sub–system. In the high V limit, the coupling between the dressed states through the continuum becomes negligible, and so each dressed state decays indepenently, but at half (because of the resonance condition) the rate of the ground state, giving rise to its own Lorentzian in the spectrum.

References

1 W. H. Louisell, *Quantum Statistical Properties of Radiation*, (Wiley, New York, 1973) p285.

2 U. Fano, Phys. Rev. 124, (1961) 1866.

3 L. A. Khalfin, Sov. Phys. JETP, 6 (1958) 1053.

4 P. L. Knight and P. W. Miloni, Phys. Lett. 56A (1976) 275.

5 J. Seke and W. N. Herfort, Phys. Lett. A 7 (1988) 422.

6 C. Cohen–Tannoudji and P. Avan, Colloques Internationaux du C.N.R.S. No. 273 (Paris: CNRS, 1977) 93–106.

7 S. E. Kumekov and V. I. Perel, Sov. Phys. JETP 54 (1981) 899.

8 M. V. Fedorov and A. E. Kazakov, J. Phys. B 16 (1983) 3641.

9 M. V. Fedorov and A. E. Kazakov, J. Phys. B 16 (1983) 3653.

10 A. E. Kazakov and M. V. Fedorov, Sov. Phys. JETP 56 (1982) 1179.

11 K. Rzazewski, M. Lewenstein and J. H. Eberly, J. Phys. B 15 (1982) L661.

12 S. L. Haan and J. Cooper, J. Phys B 17 (1984) 3481.

13 P. L. Knight, Comments At. Mol. Phys. 15 (1984) 193 and references therein.

14 L. Armstrong Jr., B. L. Beers and S. Feneuille, Phys. Rev. A 12 (1975) 1903.

15 S. H. Autler and C. H. Townes, Phys. Rev. 100 (1955) 703.

16 K. Rzazewski and J. H. Eberly, Phys. Rev. Lett. 47 (1981) 408.

17 A. B. Voitkiv and V. A.Pazdzersky, J. Phys. B 19 (1986) 1633.

18 B. Piraux, Private Communication.

19 F. Bloch and A. J. F. Siegert, Phys. Rev. 57 (1940) 522.

20 B. Piraux and P. L. Knight, Phys. Rev. A (in press).

21 C. M. Bender and S. A. Orszag, *Advanced Mathematical Methods for Scientists and Engineers* (McGraw–Hill, 1978) p277.

22 C. Cohen–Tannoudji, B. Diu and F. Laloe, *Quantum Mechanics*, (Wiley–Interscience, 1977) p395.

CHAPTER 5

CONCLUSIONS

In the first part of this thesis, we studied the potential scattering of electrons in the presence of a laser field. Chapter 2 focused on the Kramers–Henneberger transformation and its application to a model consisting of an electron interacting with polarisation potential in the presence of a classical radiation field. In view of computational difficulties, we restricted our analysis to one dimension. In the Kramers–Henneberger reference frame, the simultaneous effect of the potential and laser field on the electron is described by a static potential 'dressed' by time–dependent components. We found that for the model potential chosen, the number of bound states supported by the static potential increases with the laser parameter α_0 which is proportional to the square root of the intensity and inversely proportional to the square of the frequency.

Chapter 3 set out exact results for this scattering problem in one dimension, valid for all intensities and frequencies. The reflection and transmission coefficients show evidence of resonances caused by the new bound states which are entirely laser induced. We compared the results of these exact calculations with those we obtained using an approximation scheme suggested by Gavrila and Kaminski and discussed the validity of this approximation. It was found that in the regions which do not satisfy the high frequency requirement of the Gavrila–Kaminski approximation, the exact solution of the problem requires a very large number of channels to be taken into account. The size of the problem is considerably reduced within the high frequency limit, and good agreement was found between the exact results and those obtained using the approximation, except close to a resonance caused by the shape of

the static potential. In the resonance region large deviations were found between the exact and approximate results. Away from this region, for a fixed value of α_0 the agreement improves with increasing frequency and hence increasing intensity.

In Chapter 4, we analysed the photodecay of a discrete state via an intermediate discrete state to a structured continuum with a threshold. This was done using three different approaches. First we assumed that the continuum and intermediate bound state could be diagonalised using the method of Fano to give a Lorentzian continuum with a threshold. We then went on to study the decay of the ground state to such a continuum and showed that for strong fields the decay of the ground state was incomplete. By diagonalising the whole system, it was found that the incomplete decay was due to the formation of a new stable bound state below the threshold. In the third approach, we diagonalised the sub–system of the discrete states only and showed that the incomplete decay could also be regarded as being due to the suppression of the decay of the lower dressed state of this sub–system as it was pushed below the threshold at strong fields. An asymmetry in the Stark splitting of the photoelectron spectrum was found even under resonance conditions. This is thought to be due to the energy shift of the intermediate state induced by its interaction with the continuum. We showed that assumption regarding the diagonalisation of the intermediate bound state with the continuum is valid when the coupling between them is weak compared to the width of the continuum.

Further Work

Several extensions to the scattering problem are worth following up, in particular the exact role of the new bound states and their effect on the reflection and transmission coefficients. The wavefunctions calculated by our program would be useful in multiphoton ionisation calculations. The fact that in the high frequency regime, the

number of contributing channels is reduced means that a full three dimensional calculation may be feasible, at least far away from resonances. The role of the new bound states in three dimensions will be of particular interest.

Regarding the ionisation problem, the next stage is to include further states, both bound and continuum, in the system. Study of this problem is already in its early stages and interesting effects due to the counter rotating terms have been found.